Chemical-Scale Studies of the 5-HT$_3$ and D2 Dopamine Receptors
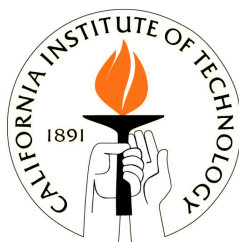
Thesis by

Kiowa San Bower

In Partial Fulfillment of the Requirements

for the Degree of

Doctor of Philosophy

California Institute of Technology
Pasadena, CA
2010

(Defended January 13, 2010)

Acknowledgements

I have truly enjoyed my time in graduate school, and there are many to thank who have helped along the way, contributing practically, intellectually, and emotionally, to make this the positive experience that it was. My advisor, Professor Dennis Dougherty has played a huge role in making graduate school a rewarding experience. His sharp insights and inquisitive intellect have been an invaluable resource and have cultivated my development as a scientist. Dennis creates a very positive research environment for his students and is truly interested in their well being. Much of this work was done in collaboration with Professor Henry Lester, who was really a coadvisor. Henry is a brilliant biologist and has somehow retained an unreasonable amount of information, which he often draws on to answer my questions and contribute to scientific discussion in group meetings. Henry takes a genuine interest in his students' development as scientists. Henry combines warmth and humor with a real demand for scientific rigor. I also have much thanks for my collaborator across the pond, Professor Sarah Lummis at the University of Cambridge. Sarah is an expert on the 5-HT$_3$ receptor and a very, very nice person. Sarah is also a data and publication machine, and along with a few members of her lab, was instrumental in the completion and publication of several projects. I would also like to thank my committee members, Peter Dervan, Robert Phillips, and Douglas Rees for their time and commitment to my education. All of my interactions with each of them has been both positive and helpful.

My experience as a graduate student has been enhanced immeasurably by the other members of the Dougherty lab, whom I have had the pleasure of working (and

playing) with all of these years. Each and every one of them has helped me along the way, and some have become genuine friends. I am immensely grateful for all of their help with experiments in lab, but my acknowledgments to individuals will lean toward the personal side, since that is what I will value and remember most.

Some individuals who are no longer members of the lab deserve special mention. The most recent to depart the lab, Katie McMenimen, was a true friend and shared with me a number of bottles of wine and conversations about relationships. Ariele Hanek was a super nice person and always full of energy. Both of these qualities are exemplified by her frequent baking of yummy goods for everyone in the lab to enjoy. Mike Torrice shared with me (and several others) the middle office bay for the last few years of my time there, and we also collaborated to produce a sweet paper on GPCRs. Mike was a delight to have in the bay. His humor was infectious, and his cynicism refreshing. Amy Eastwood left a year before me and I truly miss her presence. Amy is a very caring, and emotionally mature individual. We had many meaningful conversations and became true friends over the years. Eric Rodriguez took care of all of us—kind of like a parent does a child. What a mess we would have been without him changing our diapers. Steve Spronk was a genuine friend despite our very different worldviews. Our differences were also the source of many an engaging discussion. Joanne Xiu was a sweet, sweet woman. We became close sitting next to each other in the north bay and I truly regretted losing her company after moving to the middle bay. Lori Lee was a Dougherty old timer and one of my first real friends at Caltech. She showed me the ropes as well as some fun times. Before Lori was Ting-Wie Mu and Sarah May. Both of these individuals were

very helpful and very nice and were instrumental in my training as a fresh graduate student. James Peterson, Darren Beene, and Amanda Cashin also left the lab several years back, and were among the cooler peeps that I found a connection with at Caltech.

Several of the most recent arrivals to the Dougherty Lab are Noah Duffy, Margret Thompson, Ethan Van Arnam, and Ximena Da Silva Tavares Bongoll. I have had a chance to get to know each of them a little bit and found them to be kind, intelligent individuals, like most who join this group. I must however give special thanks to Ethan and Kristina, who took over the GPCR project and put up with my incomplete presence in lab as they were learning the ropes. Of course, I am sure that by now they are more accomplished experts on GPCRs than I ever was. Sean, who is more passionate about organic chemistry than anyone I have met, has been around a bit longer. Embarrassingly, I still never knew him very well, even though we coauthored a publication. We did however, have had some fun banter during lunch. I never had the chance to know Angela Blum or Kristin Gleitsman very well, but I do know them both to be very intelligent and driven individuals, and I am sure they will get far in science. Shawna Frazier divides her time between the Dougherty and Lester labs, but I have still had the chance to enjoy many an interesting conversation with her (and an occasional drink). She has proven to be both smart and patient, which are two important qualities for an electrophysiologist.

Three current members of the lab whom I was particularly close to are Nyssa Puskar, Jai Shanata, and Kay Walrati (Kay) Limapichat. They all joined the lab several years after I arrived, but I have had plenty of time to connect, and now consider them

close friends, and I definitely miss them now that I have moved away. Nyssa likes to dress up, and is also good at it. She accompanied me on many a fun night in the city and was often my ticket to admission to the poshest Hollywood clubs. Beyond the glamour and flashing lights, Nyssa is also a very compassionate, sincere, and smart woman, and we connected on a number of levels. Kay is a very unique and interesting individual. We became closest toward the end of my time at Caltech. I enjoyed talking with her and capturing her (sometimes jaded) perspective. Underneath a sometimes-bitter exterior is a really sweet person. Jai is a rare INFJ like myself but has many qualities that set him apart from most others I have met. He lives his life with great integrity and compassion for others, but amusingly, he sometimes masks his very caring nature with seemingly harsh and judgmental statements. He is a very generous person and offers to help others, even when he cannot really afford the time. His perspective on the world is unique and sometimes outrageous, but well reasoned and intelligent, so we have enjoyed many a deep philosophical discussion.

I have much to thank for my close friendship with Josh Klein, which began the same time as my career at Caltech. Josh and I share a passion for the outdoors, and had countless adventures together, hiking, mountain biking, and snowshoeing in the nearby San Gabriel Mountains. Josh was not only a good friend, but also an excellent wingman. In addition to many shared interests, Josh is an exceptional human being. Though he is a lethal weapon, you would never suspect it, as he has a very gentle and respectful nature. He is brilliant, dedicated, principled, and knowledgeable about many aspects of life. Our conversations were never dull. Other friends to thank include my very cool flatmates

Reid and Jen. They were a vivacious couple and I enjoyed the energy that they brought to the house. Ariane, Mark, Scott, Ma'ayan, Yoni, and Jeff were some of the coolest people to be found, and truly enriched my experience at Caltech.

Finally, I am grateful to my parents, who have always been so supportive and loving. My father, Rendell, and both of my mothers Stephanie and Lisa, I consider not just my parents but real friends. They are genuinely cool and I can talk with them about anything. I am very fortunate to be their son.
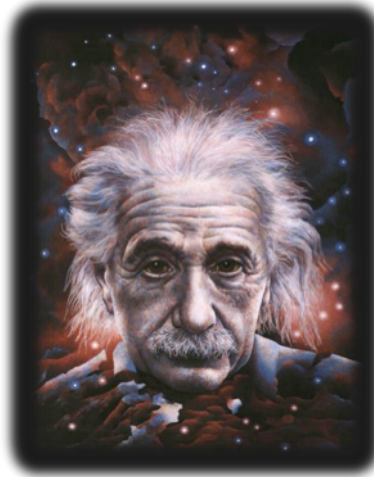
A human being is part of the whole called by us "universe", a part limited in time and space. We experience ourselves, our thoughts and feelings as something separate from the rest... a kind of optical delusion of consciousness. This delusion is a kind of prison for us, restricting us to our personal desires and to affection for a few persons nearest to us. Our task must be to free ourselves from the prison by widening our circle of compassion to embrace all living creatures and the whole of nature in its beauty. The true value of a human being is determined by the measure and the sense in which they have obtained liberation from the self. We shall require a substantially new manner of thinking if humanity is to survive. (Albert Einstein, 1954)

Abstract

During synaptic transmission in the central nervous system, neuroreceptors transduce a chemical signal into an electrical signal, a process that is mediated by both ligand-gated ion channels (LGICs) and G-protein coupled receptors (GPCRs). The work in this thesis examines structure-function relationships within these receptors, with a focus on elucidating the mechanism of molecular recognition during ligand binding. We utilize conventional and unnatural amino acid mutagenesis, structural derivatives of agonists, and homology models to identify specific interactions and the role of binding site residues in ligand binding and receptor activation. The technique of unnatural amino acid mutagenesis allows us to study these processes in greater detail than would otherwise be possible, even at the scale of a chemical bond.

Chapter 2 covers structure-function investigations of a ligand-gated ion channel, the 5-HT$_3$ receptor, with a goal of understanding agonist binding and receptor activation. The project examines residues in close proximity to the ligand-binding site and focuses on polar interactions with hydrophilic residues. We identify 5-fluorotryptamine (5-FT) as a partial agonist of the 5-HT$_3$ receptors and show that size and electronegativity are important at the 5' position for efficient channel opening. Our investigation of the compound 1-OT revealed it to be an agonist of equal potency to the native agonist (5-HT), demonstrating that the indolic proton of serotonin is not essential to its activation of the receptor. A study focusing on loop A residues led us to refine our homology model and propose that Glu129 faces into the binding pocket, where, through its ability to

hydrogen bond, it plays a critical role in ligand binding. Further studies of binding site residues identified an ionic interaction that likely participates in the conformational changes associated with receptor gating and characterized several other residues that play critical roles in receptor activation. Finally, we compare and contrast the behaviors of two structurally distinct agonist classes, 5-HT and its related structures, and *m*-chlorophenylbiguanide (*m*CPBG) and identify several residues that play critical roles in modulating agonist binding and gating in response to these agonists.

Chapter 3 describes a study examining the binding site and the mechanism of agonist activation of a GPCR, the D2 dopamine receptor. A number of aromatic amino acids thought to be near the agonist binding site were evaluated. Incorporation of a series of fluorinated tryptophan derivatives at a conserved tryptophan of the D2 receptor establishes a cation-π interaction between the agonist dopamine and this residue (W6.48), suggesting a reorientation of W6.48 on agonist binding, consistent with proposed "rotamer switch" models.

Finally, chapter 4 describes a project that seeks to extend the nonsense suppression methodology to include mammalian expression systems. Progress is made developing techniques for efficient transfection of cells in culture.

Table of Contents

List of Figures

List of Tables

Chapter 1

Introduction

Chemical-Scale Neuroscience

The human brain is arguably the most complex structure in nature. It is composed of approximately 10^{12} neurons, and each of these form an average of 10^3 connections or synapses. Overwhelming evidence coming from the field of neuroscience suggests that all that we know of an experience arises as a result of the activity of this vast network containing $\sim 10^{15}$ connections. With the development of sophisticated biochemical and imaging technologies, the last decade has seen unprecedented advances in neuroscience at both the molecular and systems level. Even with such advances, there still remains much more that we do not understand. Neurons function by transmitting electrical signals, but the communication between neurons most often involves chemical signals. When the electrical signal in a neuron reaches a synapse, it induces the release of neurotransmitters stored in synaptic vesicles. These molecules rapidly diffuse across the synaptic cleft and bind to receptors embedded in the membrane of the postsynaptic cell (figure 1.1).

a

Presynaptic
axon terminal

Synapse

Synaptic
vesicles

Neurotransmitter

Postsynaptic dendrite

Synaptic
Cleft

Na+   Na+   Na+

Synaptic
cleft

Receptors

Cytosol

Transmitter-gated
ion channels

b

Na+

100 Å
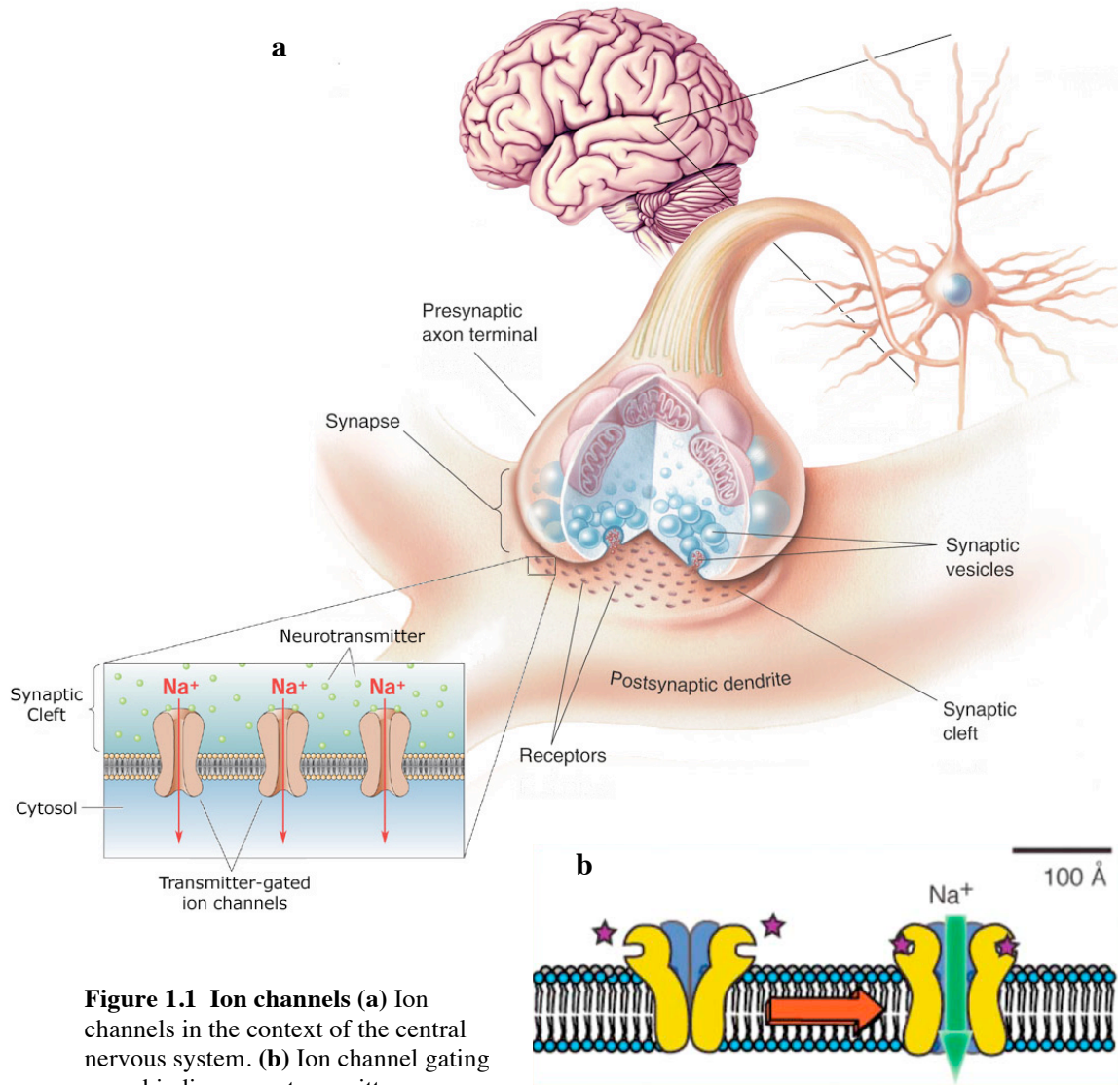
Figure 1.1 Ion channels (a) Ion channels in the context of the central nervous system. **(b)** Ion channel gating upon binding neurotransmitter.

Receptors in the nervous system fall into two main classes, the ligand-gated ion channels (LGICs) and the G-protein coupled receptors (GPCRs). LGICs mediate fast synaptic transmission. In these receptors, the binding event causes a conformational change in the receptor that opens a pore (gating), and permits the flow of ions through the channel down their electrochemical gradient. The flow of ions changes the potential across the postsynaptic membrane, and this voltage shift is summed with the inputs from other synapses. The sum of inputs (excitatory and inhibitory) determines the electrical

signal that will be passed on to the postsynaptic neurons of this cell. Thus the chemical signal of the neurotransmitter is converted back into an electrical signal. This process takes place on the millisecond timescale in LGICs, and is the basis of most information processing in the central nervous system(1). GPCRs also play a critical role in neuronal function, but their activation does not always result in the direct transmission of electrical signals. These receptors are also vitally important for many other biological processes such as vision, olfaction, autonomic function, and immune function. Because they act through second messenger pathways, their modulatory effect on cellular activity is on a longer timescale.

The goal of our chemical-scale studies is to understand the mechanism of molecular recognition during ligand binding as well the structure-function relationships during the process of receptor activation. Our primary method for studying receptors involves the mutation of one or more amino acids in the peptide sequence with the goal of changing the receptor's function. The determination of which mutations will be studied in the receptor is usually guided homology models constructed from crystal structures of closely related proteins. These models allow us to come up with hypotheses about receptor function at scales as small as the functional group of the amino acid side chain. Such hypotheses can be tested using electrophysiology to characterize functional changes resulting from induced mutations. Site-directed mutagenesis is a useful tool to explore and sometimes answer these questions, but the relatively small number of twenty naturally occurring amino acids imposes significant limitations on the structural and chemical diversity available with this method.

1.1 Unnatural Amino Acid Mutagenesis

Unnatural amino acid mutagenesis ("unnaturals") is a powerful tool that vastly expands the potential changes we can make to protein structure, and allows us to study LGICs at the chemical level. Potential amino acids to be incorporated are limited only by synthetic feasibility and ability to pass through a cell's translation machinery (figure 1.2). Figure 1.2 illustrating unnatural amino acid structures was adapted from England P.M., 2004 (2). The studies described in this work utilize unnatural amino acids that differ in subtle ways from natural amino acids. For example, incorporation of O-methylthreonine in the place of threonine removes the ability of the side chain to donate a hydrogen bond, while retaining its general shape and its ability to accept a hydrogen bond. Structure-function studies using conventional mutagenesis can provide us with information about which parts of a protein are important for function, but the use of unnaturals allows us to probe structure with much greater precision.
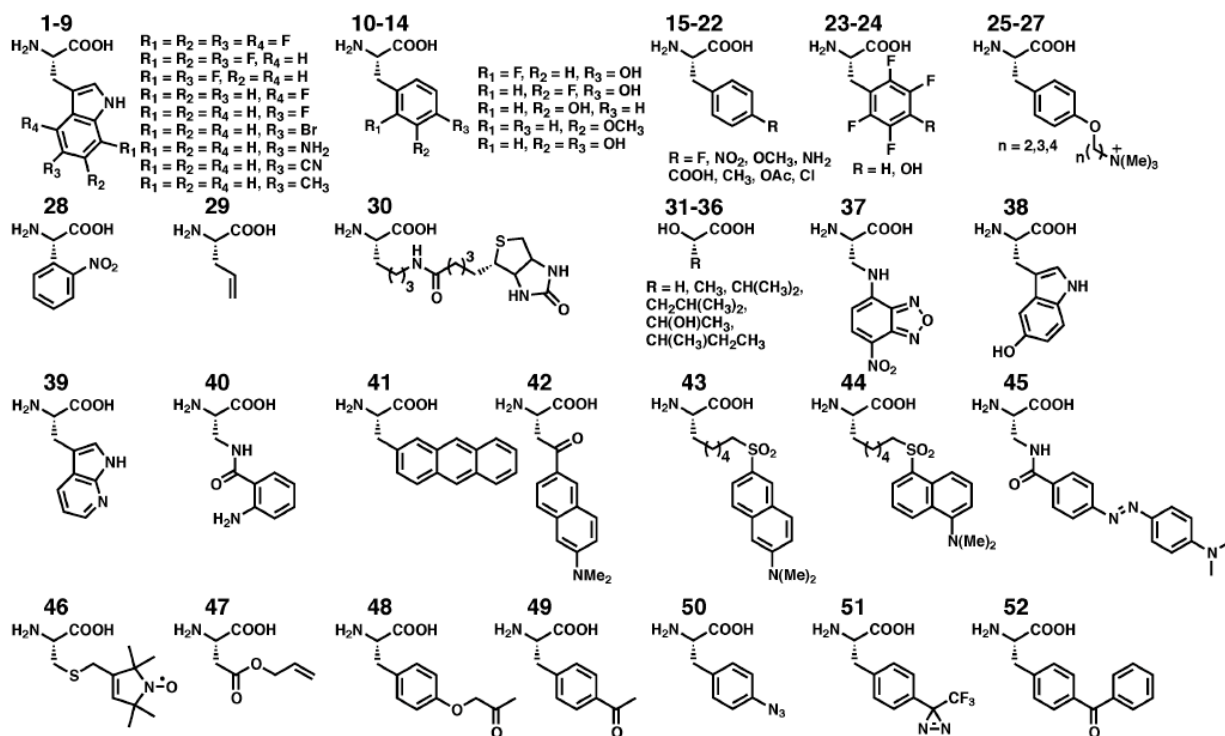
Figure 1.2 Unnatural Amino Acids. Significant diversity of structures available using unnatural methodology. Shown are many of the amino and hydroxy acids that have been successfully incorporated into proteins using nonsense suppression.

1.2 The Cation-π Interaction

The utility of unnatural amino acids is effectively illustrated by our studies of cation-π interactions within receptor binding sites. The cation-π interaction is an important and common interaction in biological systems. An analysis of protein data bank structures revealed that one in 77 amino acids is involved in a cation-π interaction and it is frequently found in the binding site of aminergic ligands (3,4).

Cations bind to the electron-rich π face of an aromatic ring through strong electrostatic interactions (3,5,6) (figure 1.3a). Studies of this interaction using conventional mutagenesis are hindered by a limited selection of residues for substitution.

For example if investigating a tryptophan site, the experimenter could substitute a different aromatic residue such as phenylalanine and also a nonaromatic hydrophobic residue such as leucine. If Phe caused little change in function, but Leu led to a large effect, these results would be consistent with the importance of aromaticity at this site. However, they would not be conclusive and there are alternative explanations. For example, the significant structural difference between Leu and Phe and not the loss of aromaticity may be the cause of the functional change.
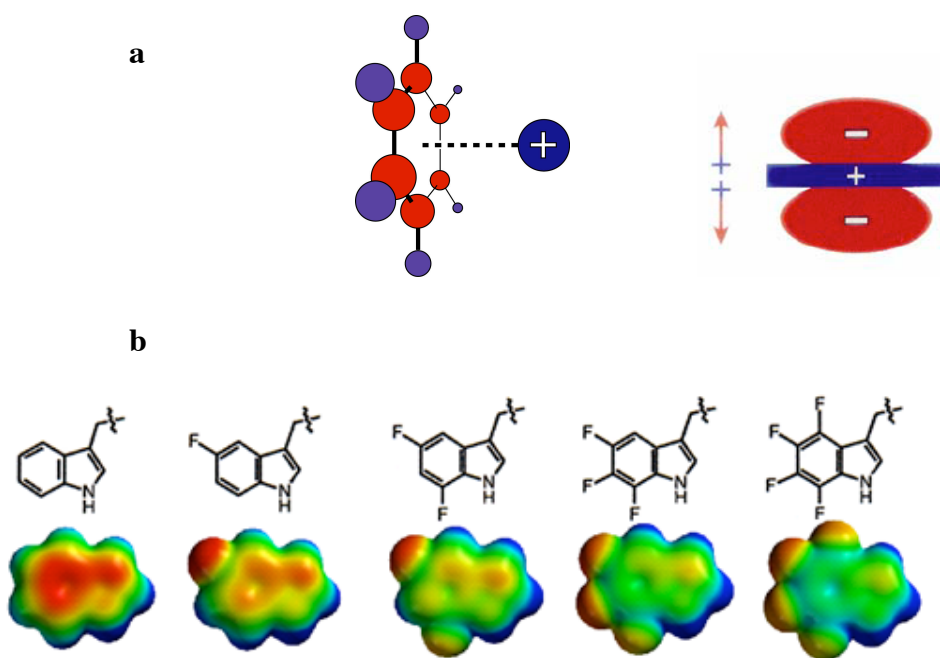
Figure 1.3. The cation-π interaction (a) A cation interacting with benzene. **(b)** Electrostatic potential surfaces of the fluorinated tryptophan series calculated using Spartan.

Unnatural amino acids provide a means to modulate the cation-π interaction without significantly altering the amino acid structure. This is accomplished by substituting the aromatic residue with fluorinated derivatives (figure 1.3b). The

electronegativity of fluorine shifts the partial negative charge present on the face of the aromatic ring towards the outside of the ring. The substitution of additional fluorines reduces the negative potential on the face of the ring in a stepwise manner and leads to a corresponding reduction of the cation-π binding ability. This reduced binding is illustrated by a change in the electrostatic potential surface from red (more favorable) to green (less favorable) (figure 1.3b). Thus, if we incorporate a series of fluorinated aromatic residues into a protein and observe a corresponding stepwise decrease in function, we have strong evidence for the presence of a cation-π interaction.

Our studies of the D2 dopamine receptor focus on identifying a cation-π interaction, but unnatural amino acids can be used to investigate a diverse set of interactions. For example our studies of the 5-HT$_3$ binding site used a different group of unnatural amino acids to investigate polar interactions such as hydrogen bonds. In general, substitution of unnatural amino acids provides more conclusive results about specific interactions than would be possible using conventional mutagenesis.

1.3 Nonsense Suppression

Nonsense suppression is an effective methodology developed to site-specifically incorporate unnatural amino acids into proteins (figure 1.4)(7-10). Using site-directed mutagenesis, an amber stop codon (TAG) is incorporated into the gene at the position coding for the amino acid of interest. mRNA is transcribed from the mutatant DNA *in vitro* and contains the corresponding UAG stop codon. A specially designed suppressor tRNA (tRNA$_{CUA}$) that recognizes the UAG codon is prepared separately and chemically

acylated with the desired unnatural amino acid. A solution containing both the mRNA and this acylated tRNA (aa-tRNA$_{CUA}$) is then introduced into a cell. In the absence of this specially designed aa-tRNA, translation of the mRNA would stop when the ribosome reaches the inserted stop codon, producing a "nonsense" protein. In this system, however, the aa-tRNA$_{CUA}$ recognizes the stop codon and suppresses the termination of translation. The ribosome incorporates the unnatural amino acid just as it would a natural aa-tRNA, and translation continues, producing a full-length protein with an unnatural amino acid at the intended specific site.
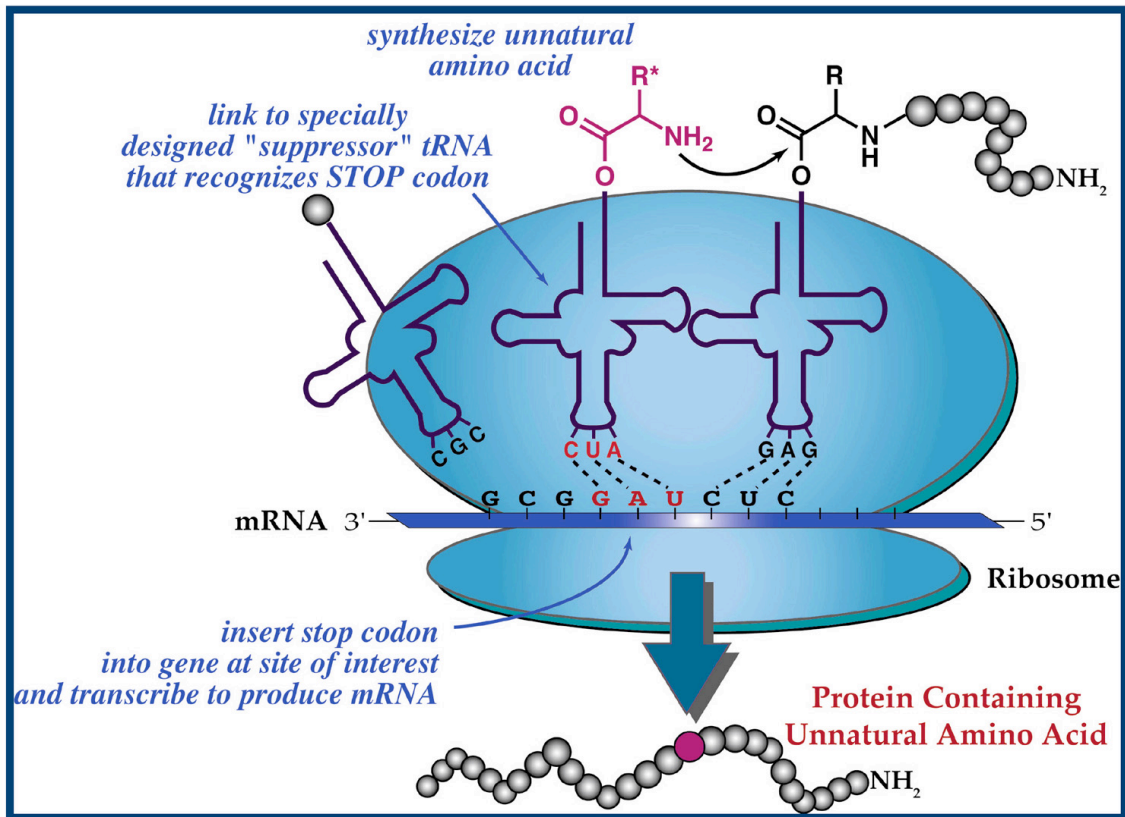
Figure 1.4. Unnatural amino acid mutagenesis by nonsense supression. Suppressor tRNA recognizes the UAG stop codon and the attached unnatural amino acid is incorporated at the site of interest by the ribosome.

Expression of the protein containing the unnatural amino acid begins with injection of a solution of the mRNA and tRNA into an oocyte using a micropipette. The techniques used to transfect cells in culture are described in chapter 4. Cells are incubated for ~1–2 days. During this time the protein is translated as described above, folded, and transported to the cell surface (figure 1.5). At this point electrophysiology can be used to characterize the effect on ion channel function that the structural perturbation of the unnatural amino acid has caused. Electrophysiology is an extremely sensitive technique, and this makes it an ideal assay to for our studies using unnatural amino acids. This is

because the aa-tRNA is a stoichiometric reagent, and the amount of mutant protein expressed in each cell is relatively small. Electrophysiology allows us to accurately record very small currents and thus measure changes in ion channel function even when very few channels are expressed.
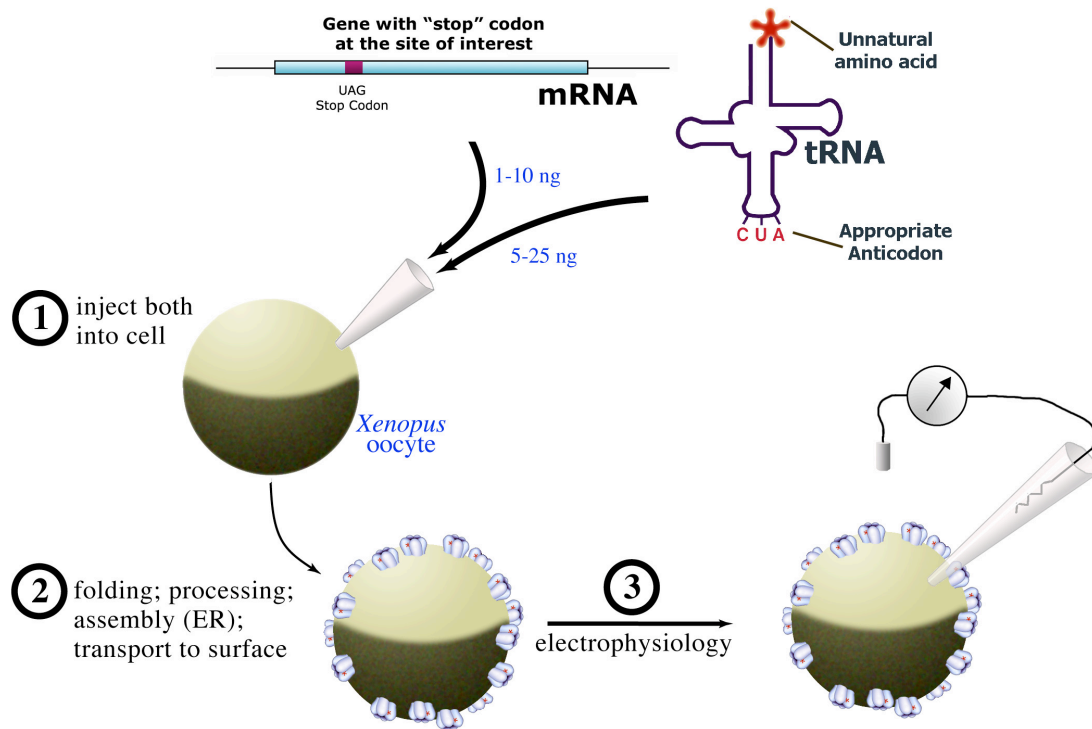
Figure 1.5 *In vivo* **nonsense suppression in oocytes**. mRNA with the stop codon and aminoacyl suppressor tRNA are injected into *Xenopus* oocytes. Cells are incubated 1-2 days and then assayed using electrophysiology.

1.4   Data Acquisition

One of the primary means used to obtain data regarding the effect of a mutation on receptor function is via a dose-response assay applied to cells using two-electrode

voltage clamp (TEVC). In TEVC, the voltage electrode measures the potential difference across the cell membrane while the current electrode connected via a feedback circuit applies a current to maintain the membrane potential at the value that is set by the experimenter. Application of agonist to the cell results in the opening of ion channels, which allows ions to flow across the cell membrane down their electrochemical gradient (figure 1.1b). To maintain the membrane potential at the predetermined value, the current electrode must inject current equal in magnitude to the current passing through the open ion channels. In this way we are able to precisely measure the current resulting from the open ion channels.

A dose-response relationship is measured by measuring the current induced by the application of varying concentrations of agonist (figure 1.6a). Normalized current response values are plotted with the agonist concentration on the x-axis (in logarithmic scale). Dose-response relations are most often characterized by their EC_{50}, which is defined as the concentration of agonist at which half-maximal response is elicited (figure 1.6b). EC_{50} is a composite value, measuring both ligand binding and channel gating, and should not be confused with K_d, which is a direct measure of ligand affinity.

a

b
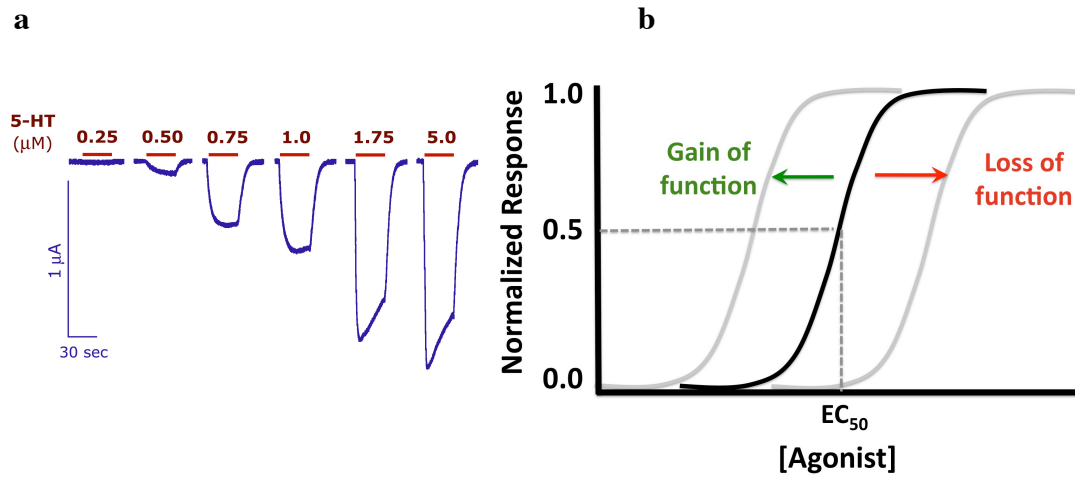
Figure 1.6 Electrophysiology assay. **(a)** Example current responses. Increasing concentrations of agonist leads to a greater number of open channels and an increase in measured current. **(b)** Currents are normalized and plotted agonist concentration (log scale). The EC_{50} is the concentration of agonist that elicits a half-maximal response. Mutations that make agonist binding or channel activation less favorable shift the curve to the right (increase EC_{50}). Mutations that are favorable to function shift the curve to the left (lower EC_{50})

1.5   Dissertation Summary

The following work is divided into three different chapters, each describing a project that focuses on a different membrane receptor. Chapter 2 covers structure-function investigations of the ligand-gated ion channel 5-HT$_3$ using both conventional and unnatural amino acid mutagenesis. The aim of this study is the elucidation of the mechanism of receptor activation by serotonin as well as several non-native agonists. The project probes the role that residues in close proximity to the ligand-binding site play in agonist binding and receptor activation and focuses on polar interactions with hydrophilic residues. Chapter 3 describes a study examines the mechanism of agonist activation the D2 dopamine receptor which is a GPCR. This project has a more specific aim of utilizing derivatives of aromatic residues to search for a presumed cation-π interaction between dopamine and one of the aromatic residues that make up the agonist-binding cleft. Finally, chapter 4 describes a project that seeks to extend the nonsense suppression methodology to include mammalian expression systems.

These studies utilize both conventional and unnatural amino acid mutagenesis, but the most compelling results often come from the use of unnaturals. With this technique we have been able to alter protein structure on the chemical scale and by looking at the effect that this change has on receptor function, identify specific interactions within the receptor or between the receptor and its ligand. The broad goal of these studies is to contribute to our basic understanding of receptor function and neuroscience, and we expect that these results will be of practical importance in the development of therapeutics that target these neuroreceptors.

1.6   References

1.   Kandel, E. R., Schwartz, J. H., and Jessel, T. M. (2000) *Principles of Neural Science*, 4th Ed., McGraw-Hill, New York, NY

2.   England, P. M. (2004) *Biochemistry* **43**(37), 11623-11629

3.   Gallivan, J. P., and Dougherty, D. A. (1999) *Proc. Natl. Acad. Sci. USA* **96**, 9459-9464

4.   Zacharias, N., and Dougherty, D. A. (2002) *Trends in Pharmacological Sciences* **23**(6), 281-287

5.   Dougherty, D. A. (1996) *Science* **271**(5246), 163-168

6.   Ma, J. C., and Dougherty, D. A. (1997) *Chem. Rev.* **97**(5), 1303-1324

7.   Bilgicer, B., and Kumar, K. (2003) *J. Chem. Ed.* **80**, 1275-1281

8.   Dougherty, D. A. (2000) *Curr Opin Chem Biol* **4**(6), 645-652

9.   Mendel, D., Cornish, V. W., and Schultz, P. G. (1995) *Annu Rev Biophys Biomol Struct* **24**, 435-462

10.   Petersson, E. J., Brandt, G. S., Zacharias, N. M., Dougherty, D. A., and Lester, H. A. (2003) *Methods Enzymol* **360**, 258-273

Chapter 2

Studies of the Ligand Binding Site

in the 5-HT$_3$ Receptor

2.1 Introduction

The 5-HT$_3$ receptor is a cation-selective Cys-loop receptor and has the endogenous agonist 5-hydroxytryptamine (5-HT) or serotonin. The Cys-loop family of ligand-gated ion channels is named for a conserved Cys-Xaa$_{13}$-Cys sequence, which forms a disulfide bond and thus a "loop" in the N-terminal domain (1). This family also includes the nicotinic acetylcholine (nACh), gamma-amino butyric acid (GABA), and glycine (Gly) receptors (1-6). Cys-loop receptors function as a pentameric arrangement of subunits, with each subunit having a large extracellular N-terminal region, four transmembrane helices (M1-M4) and an intracellular loop between M3 and M4 (figure 2.1). The binding site is located at the interface of two adjacent subunits and is formed by the convergence of three loops (A-C) from the principal subunit and another three loops (D-F) from the complementary subunit (7).
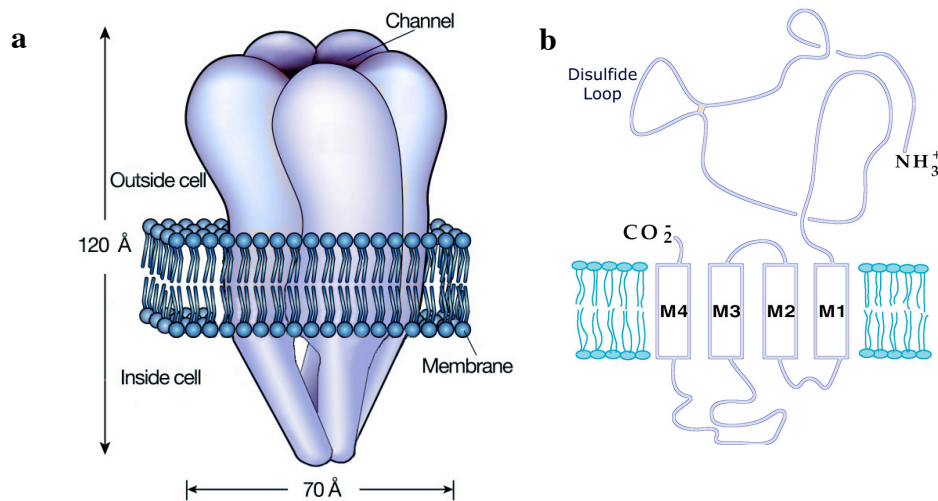
Figure 2.1. The 5-HT$_3$ receptor (**a**) The 5-HT$_3$ receptor like all cys-loop receptors has five homologous subunits. (**b**) Each subunit contains four transmembrane segments and an intracellular domain, which contains the ligand binding site.

Molecular details of the binding pocket have been extrapolated from the structure of the acetylcholine binding protein (AChBP), which is homologous to the extracellular domain of Cys-loop receptors, and a range of amino acid residues that are important for agonist and antagonist binding have been identified (8,9). Previous studies have established an important role for aromatic residues that are conserved across the Cys-loop family (Figure 2.2b), including a cation-π interaction between the positive charge of 5-HT and the side chain of Trp183 on loop B of the principal subunit (10).

The availability of the high-resolution structure of the acetylcholine binding protein (AChBP) has enabled the construction of a series of homology models of the extracellular domains of several Cys-loop receptors, including nACh, $GABA_A$ and $5\text{-}HT_3$ receptors (9,11-16) (Figure 2.2). While there are no crystal structures of the transmembrane region of Cys-loop receptors, cryoelectron microscopy data has been used to construct a refined 4 Å structure of the nAChR (17). This study provides valuable information regarding how subunits and domains are put together as well as the most detailed view to date of the transmembrane region. These models, especially of the extracellular domain, are supported by experimental data and by the recent structure determination of the extracellular domain of a nACh receptor α subunit (18). However, as homology models are inherently speculative, experimental validation of predictions based on these models are invaluable to the elucidation of the actual binding interactions between 5-HT and its receptor.
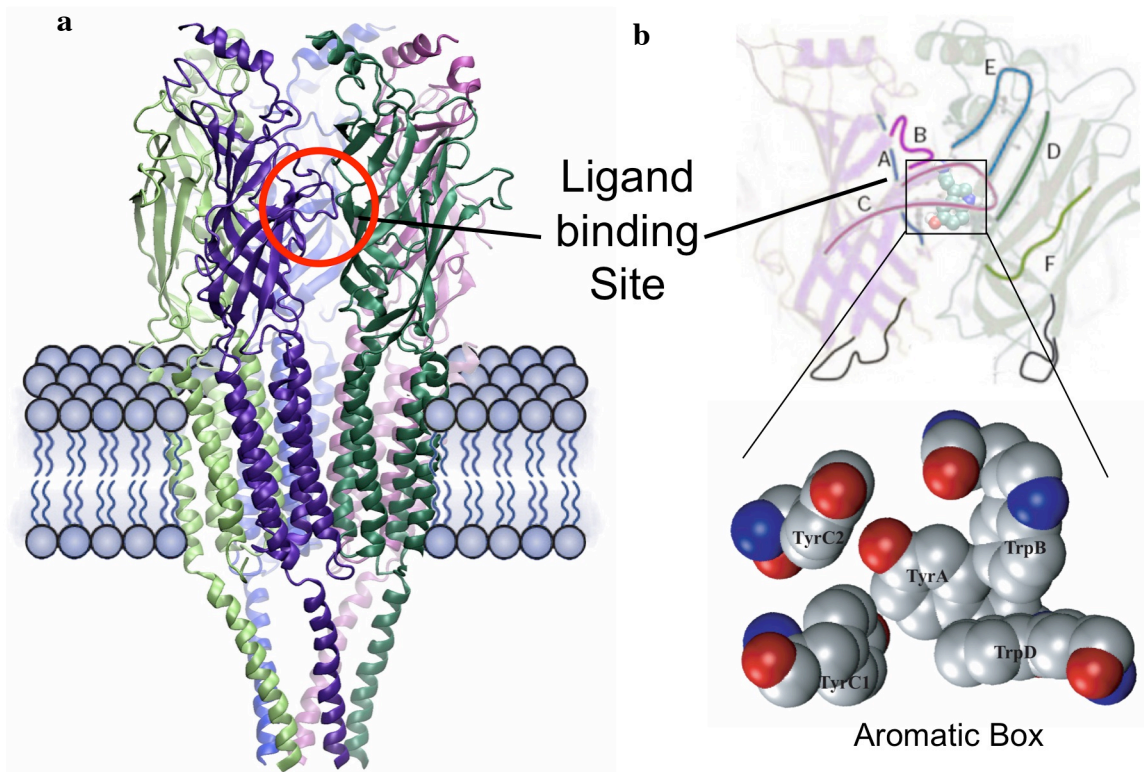
Figure 2.2. (**a**) Homology model of the 5-HT$_3$ receptor. The extracellular domain is based on the crystal structure of the acetylcholine binding protein (AChBP). (**b**) The ligand binding site is located at the interface of two subunits and formed by loops A-F. Within the ligand binding site is a core of conserved aromatic residues (Aromatic Box).

The relevance of 5-HT$_3$ receptor investigations

The 5-HT$_3$ receptor is an important model system for the study of structure-function relationships in the Cys-loop family of receptors and also holds direct medical significance. Because there is significant homology within the Cys-loop family (25%-30% conservation in amino acid sequence identity), studies on any receptor are informative about the function of the entire family (19). However, the 5-HT$_3$R has

particular relevance as a model system because it is a relatively early ancestor within this family (20,21). These receptors have maintained significant conservation of the ligand binding residues, especially considering the structural differences between 5-HT and the native agonists of other receptors. Two of the six residues on the principal face involved in ACh binding are completely conserved in the 5-HT$_3$R (7). In fact, many nAChR ligands including nicotine and ACh competitively antagonize 5-HT$_3$R currents (22). Similarly, 5-HT can interact with nACh, GABA$_A$, and glycine receptors (23-25). This pharmacological overlap reinforces the relevance that 5-HT$_3$ studies have to the understanding of other Cys-loop receptors. This fact, combined with the receptor's ancestry and ability to yield functional homomeric channels, makes a strong argument for use of the 5-HT$_3$ receptor as a model system for the elucidation of Cys loop receptor function (7).

The importance of 5-HT$_3$ receptors to medicine offers additional relevance to their investigation, especially studies relating to the understanding of ligand-receptor interactions. Peripheral 5-HT$_3$ receptors are thought to modulate pain as well as intestinal and cardiovascular functions (26). In the central nervous system, 5-HT$_3$Rs are important targets for the control of emesis induced post-operatively by chemotherapy and radiotherapy and in the palliative care of patients with multiple sclerosis (27). 5-HT acting through 5-HT$_3$ receptors may contribute to the mediation of inflammatory pain. Also, 5-HT$_3$ receptor antagonists have been shown to reduce secretion and motility in the gut and thus can be useful treatments for irritable bowel syndrome or other visceral pain disorders. Antagonists are also currently being investigated as possible treatments for

fibromyalgia and other rheumatic diseases (28). Study of the 5-HT$_3$ receptor can have relevance for the treatments for many diseases, including Alzheimer's disease, Parkinson's disease, ADHD, epilepsy, emesis associated with chemotherapy, nicotine addiction, schizophrenia, and anxiety (1).

Receptor-ligand interactions

Due to the difficulty acquiring such data, structural details of receptor-ligand interactions at the molecular level have only recently begun to emerge. The structure of AChBP has allowed the definition of the ligand binding domain of the 5-HT$_3$R in greater detail than had been possible before. Some important clues about the ligand interactions and orientation can be obtained from modeling studies such as that by Reeves and Lummit (7). In this study, a homology model of the 5-HT$_3$R binding site was created based upon the AChBP structure and then the agonist 5-HT was docked computationally. Such models offer insights into potential ligand-receptor interactions, though we recognize the importance of combining the insights that are obtained from homology and docking studies with experimental studies.

While many other small molecule neurotransmitters contain only two potential sites that can form hydrogen bonds, serotonin has three positions that have the potential to form hydrogen bonds with the ligand binding site (figure 2.3). The primary ammonium cation and the indolic amine group can act as
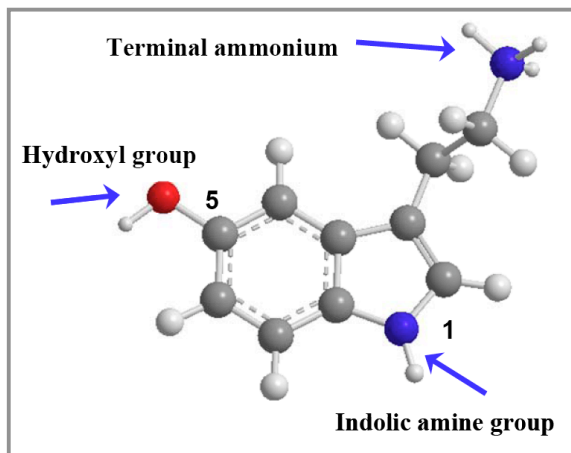
Figure 2.3. 5-HT chemical structure. Serotonin (5-HT) contains three sites with the potential to form hydrogen bonds.

hydrogen bond donors, and the hydroxyl group can act as both a hydrogen donor and an acceptor. A determination of the functional groups that hydrogen bond to 5-HT should help to fix the orientation of this agonist in the binding site with relative precision. This in turn could reveal information about other non-covalent interactions in the binding site.

Heteromeric 5-HT$_3$ Receptors

To date, two 5-HT$_3$R subunits have been investigated in detail; 5-HT$_{3A}$, and 5-HT$_{3B}$, and additional subunits have been proposed (7,19,29-31). The 5-HT$_{3A}$ subunit forms functional homooligomeric receptors, whereas 5-HT$_{3B}$ subunits are retained in the ER unless coexpressed with 5-HT$_{3A}$ subunits (32). The subunit stoichiometry for hetero-oligomeric 5-HT$_{3A/B}$ receptors has recently been revealed by atomic force microscopy to be 2A:3B in the arrangement B-B-A-B-A (33). The conductance of the heterooligomeric receptors is ~15 pS, whereas that of the homooligomeric complex is 30× smaller

(~0.5 pS). Thus, the incorporation of B subunits results in some changes in the biophysical characteristics of the receptor, but yet has little effect on the pharmacological profile (34-36).

Summary

We are interested in understanding the molecular details of ligand-receptor interactions in the 5-HT$_3$R. Homology models provide a useful starting point for structure-function studies. To confirm specific interactions, one must identify the particular residue that participates in an interaction and in addition show that the ligand and not another amino acid is the interacting partner. Conventional mutagenesis can provide useful information and help determine whether or not a residue is critical for ligand binding or other aspects of binding-site function. However, conventional mutagenesis often cannot address questions at the level of detail we are interested in. The goal of these studies is the elucidation of residues important for ligand binding and receptor activation, but more precisely we would like to determine the specific functional groups that participate in the ligand-receptor as well as intrareceptor interactions. One effective approach we utilize is the forward and reverse pharmacology method. This method complements the subtle modifications possible using unnatural amino acid mutagenesis with the use of a number of structural analogues of receptor ligands. Our results identify several important interactions and lead to a more complete and accurate model of agonist binding and activation the 5-HT$_3$ receptor.

2.2   5-Fluorotryptamine is a partial agonist at 5-HT$_3$ receptors

Reproduced in part from (37).

2.2.1 Results

5-HT$_3$ receptor antagonists have been suggested as potentially useful in treating inflammatory pain, anxiety, depression, schizophrenia, and drug abuse (26), and are currently in clinical practice for the treatment of irritable bowel syndrome and emesis (38-40). It is therefore not surprising that many 5-HT$_3$ receptor antagonists have been developed. There are, however, fewer 5-HT$_3$ selective agonists. 2-Me-5-HT and *m*CBPG have been widely used, and some novel compounds have been developed more recently such as benzoxazoles (41) and pyrroloquinoxaline-related compounds (42). Here we explore the agonist properties of a compound closely related to 5-HT, 5-fluorotryptamine (5-FT), at both 5-HT$_{3A}$ and 5-HT$_{3AB}$ receptors, and compare them to the properties of 5-HT, *m*CBPG and tryptamine (figure 2.4). We also explore several other 5-substituted tryptamine derivatives.

Effects of agonists on 5-HT$_3$ receptor mediated currents

Application of 5-HT to *Xenopus* oocytes expressing 5-HT$_{3A}$ or 5-HT$_{3AB}$ receptors produced concentration-dependent, rapidly activating, inward currents that desensitized over the time course of the application (figure 2.5a-b). Plotting current amplitude against a series of 5-HT concentrations revealed EC$_{50}$s of 1.4 μM and 3.2 μM with Hill slopes of 2.5 and 1.4 respectively (table 2.1).
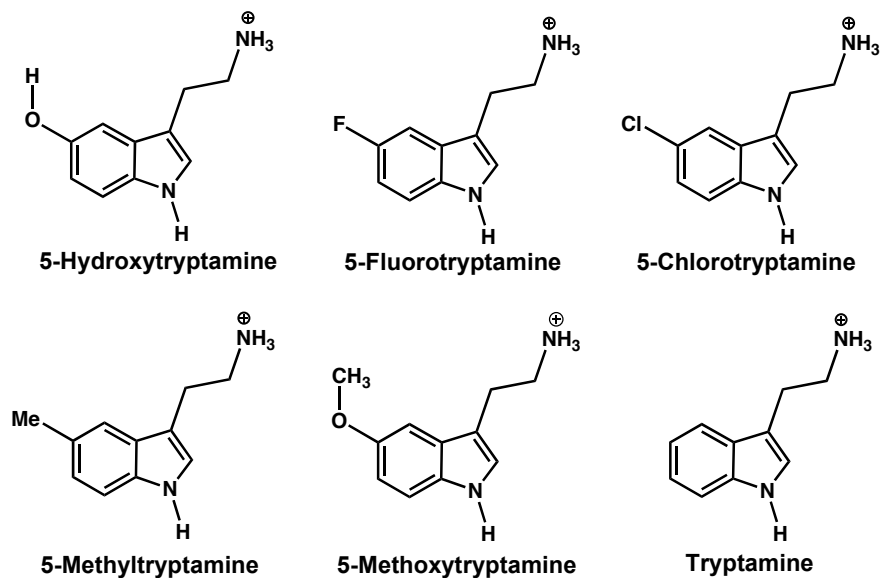
Figure 2.4 Structures of 5-HT agonists used in this study.

	pEC$_{50}$	EC$_{50}$ (µM)	n$_H$
A 5-HT	5.85 $\pm$ 0.10	1.4	2.5 $\pm$ 0.4
AB 5-HT	5.49 $\pm$ 0.03	3.2	1.4 $\pm$ 0.4
A 5-FT	4.80 $\pm$ 0.05	16	2.4 $\pm$ 0.5
AB 5-FT	4.57 $\pm$ 0.08	27	1.4 $\pm$ 0.3
A mCPBG	6.29 $\pm$ 0.04	0.5	2.3 $\pm$ 0.4
AB mCPBG	5.96 $\pm$ 0.06	1.1	1.6 $\pm$ 0.4
A Tryptamine	3.91 $\pm$ .03	113	2.5 $\pm$ 0.5
AB Tryptamine	4.22 $\pm$ .09	61	1.8 $\pm$ 0.5

Table 2.1. Functional parameters of A and AB receptors
Data = mean $\pm$ SEM, n=4-6

	5-FT	mCPBG	Tryptamine
A	0.64 $\pm$ 0.03	0.74 $\pm$ 0.07	0.15 $\pm$ 0.06
AB	0.45 $\pm$ 0.04	0.92 $\pm$ 0.09	0.14 $\pm$ 0.02

Table 2.2. Relative efficacy of partial agonists of A and AB receptors.
Data = mean $\pm$ SEM, n=5-9

Application of 5-FT to *Xenopus* oocytes expressing 5-HT$_{3A}$ or 5-HT$_{3AB}$ receptors also produced concentration-dependent, rapidly activating, inward currents, with EC$_{50}$s of 16 μM and 27 μM and Hill slopes of 2.4 and 1.4 respectively. A maximal concentration of 5-FT, however, did not elicit the same maximal currents as those obtained from 5-HT application in the same oocyte, indicating a partial agonist; 5-FT had a R$_{max}$ (I$_{max}$ drug / I$_{max}$ 5-HT) of 0.64 $\pm$ 0.03 for 5-HT$_{3A}$ receptors and R$_{max}$ of 0.45 $\pm$ 0.04 for 5-HT$_{3AB}$ receptors (table 2.2).

Application of *m*CPBG produced concentration-dependent, rapidly activating, inward currents, with EC$_{50}$s of 0.5 μM and 1.1 μM and Hill slopes of 2.3 and 1.6 for 5-HT$_{3A}$ or 5-HT$_{3AB}$ receptors, respectively. This compound had an R$_{max}$ of 0.74 $\pm$ 0.07 for 5-HT$_{3A}$ receptors and 0.92 $\pm$ 0.09 for 5-HT$_{3AB}$ receptors.

Application of tryptamine produced concentration-dependent, rapidly activating, inward currents, but here there was little desensitization over the time course of the application (figure 2.5a). Plotting current amplitude against a series of tryptamine concentrations revealed EC$_{50}$s of 113 μM and 61 μM with Hill slopes of 2.5 and 1.8 for 5-HT$_{3A}$ and 5-HT$_{3AB}$ receptors respectively. Tryptamine had an R$_{max}$ of 0.15 $\pm$ 0.06 for 5-HT$_{3A}$ receptors and an R$_{max}$ of 0.14 $\pm$ 0.03 for 5-HT$_{3AB}$ receptors.
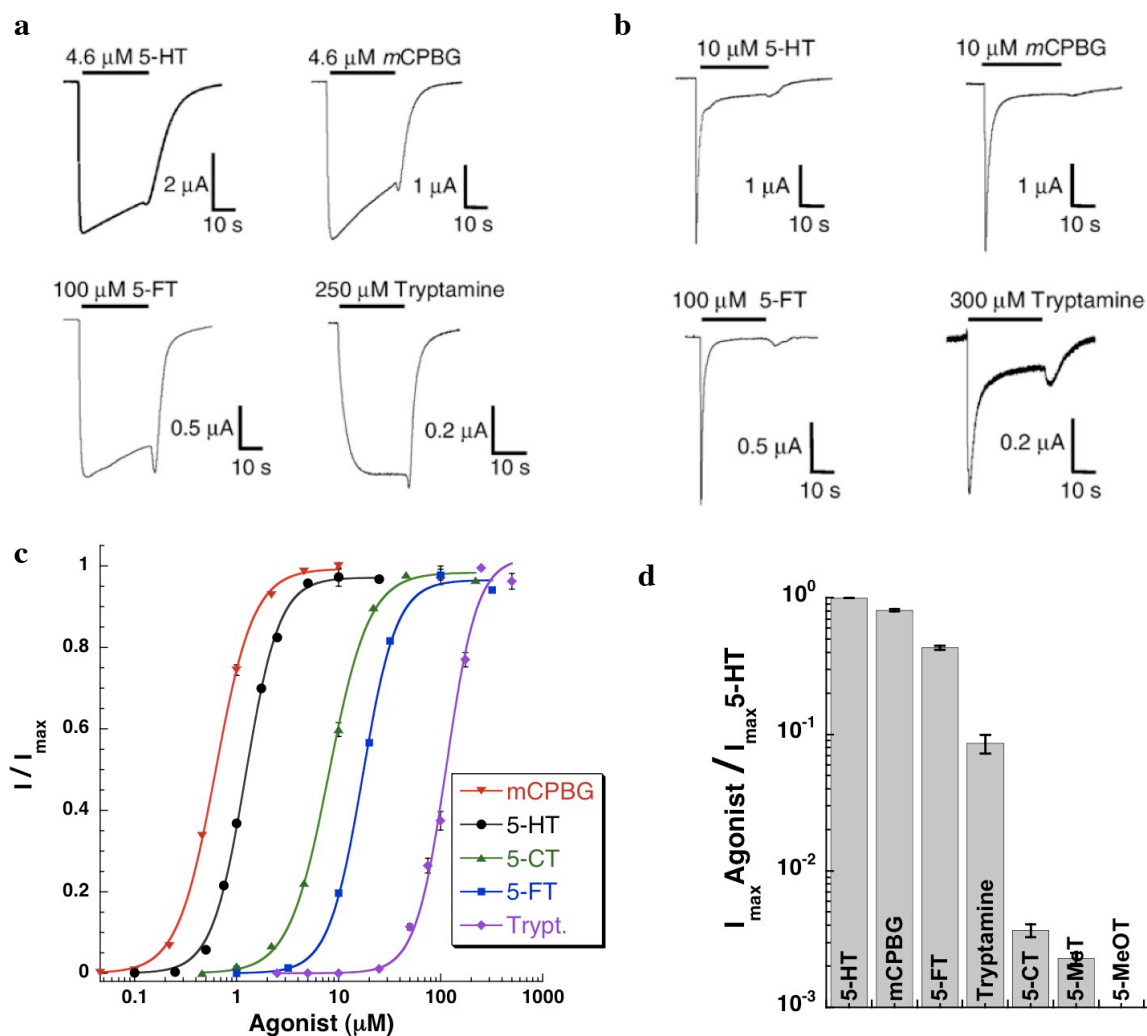
Figure 2.5. Properties of 5-HT$_{3A}$ and 5-HT$_{3AB}$ receptors expressed in *Xenopus* oocytes. Typical responses to maximal concentrations of 5-HT, mCPBG, 5-FT and tryptamine in **(a)** 5-HT$_{3A}$ and **(b)** 5-HT$_{3AB}$ receptors; **(c)** concentration-response curves in 5-HT$_{3A}$ receptors; **(d)** relative efficacies (R$_{max}$) of agonists compared to 5-HT.

5-Chlorotryptamine (5-ClT) was a very weak partial agonist of 5-HT$_{3A}$ receptors, with an R$_{max}$ of 0.0037; the size of the responses precluded data from 5-HT$_{3AB}$ receptors. Despite its low R$_{max}$, 5-ClT had an EC$_{50}$ (8.1 $\pm$ 0.3 μM, n=11) that was lower than that of 5-FT (16 μM).

5-Methyltryptamine (5-MeT) was also a very weak partial agonist at 5-HT$_{3A}$ receptors with an R$_{max}$ of 0.0023. Dose-response curves yielded an EC$_{50}$ of 60 $\pm$ 3 μM (n=3) indicating it was slightly more potent than tryptamine (EC$_{50}$ = 113 μM).

5-Methoxytryptamine (5-MeOT) was unable to activate 5-HT$_3$ receptors at concentrations up to 10 mM.

[^{3}H]granisetron binding studies

Saturation binding studies revealed no significant difference in the affinity (K$_d$) of [^{3}H]granisetron between 5-HT$_{3A}$ and 5-HT$_{3AB}$ receptors (0.42 $\pm$ 0.15 and 0.62 $\pm$ 0.21nM respectively, n=3). Competition binding studies using [^{3}H]granisetron revealed displacement of specific binding in a concentration dependent manner by all the ligands. K$_i$s (Table 2.3) revealed that 5-HT, *m*CPBG, 5FT and tryptamine did not substantially distinguish between 5-HT$_{3A}$ and 5-HT$_{3AB}$ receptors.

[^{3}H]granisetron competition studies using 5-ClT, 5-MeT and 5-MeOT on membranes from cells expressing 5-HT$_{3A}$ receptors revealed 5-ClT had a similar K$_i$ to 5-FT, which was ~10-fold more than the K$_i$ for 5-HT. Values for tryptamine, 5-MeT and 5-MeOT were ~50-, 100- and 300-fold greater than 5-HT respectively (table 2.3).

Competition radioligand binding studies on the mutant receptors N128A, T181A and E236A, revealed no significant changes in K$_i$ values compared to WT receptors for

either 5-FT or 5-HT (table 2.4). E129A and T179A mutant receptors had either no specific radioligand binding, or levels were too low to obtain accurate data as previously reported (43).

	A (K_i, µM)	AB (K_i, µM)
5-HT	0.11 ± 0.02	0.11± 0.03
mCPBG	0.010 ± 0.003	0.012 ± 0.004
5-FT	0.83 ± 0.17	1.8 ± 0.4
Tryptamine	4.8 ± 0.9	15.5 ± 3.5
5-Cl-tryptamine	2.7 ± 0.7	3.1 ± 1.1
5-Me-tryptamine	11.0 ± 0.9	7.7 ± 1.1
5-MeO-tryptamine	34.9 ± 3.0	21.7 ± 2.1

Table 2.3. Inhibition constants derived from [^{3}H] granisetron binding to 5-HT$_{3A}$ and 5-HT$_{3AB}$ receptors. Data = mean ± SEM, n=3-6.

	5-HT (K_i, µM)	5-FT (K_i, µM)
WT	0.11 ± 0.02	0.83 ± 0.17
N128A	0.21 ± 0.05	2.43 ± 0.47
T181A	0.19 ± 0.04	1.02 ± 0.34
E236A	0.20 ± 0.05	1.62 ± 0.41

Table 2.4. Mutant inhibition constants derived from [^{3}H] granisetron binding to mutant 5-HT$_{3A}$ receptors. Data = mean ± SEM, n=3-6.

2.2.2 Discussion

The data described here show that 5-FT is a partial agonist at both 5-HT$_{3A}$ and 5-HT$_{3AB}$ receptors, with an R$_{max}$ close to 0.5 and an EC$_{50}$ about 10-fold higher than 5-HT. Similarly, tryptamine is a partial agonist at both types of receptor, as previously reported for various native and recombinant 5-HT$_3$ receptors, including those natively expressed in N1E-115 cells, which may possess both 5-HT$_{3A}$ and 5-HT$_{3B}$ receptor subunits (44). Tryptamine has a lower potency than both 5-HT and 5-FT (EC$_{50}$ 10–100-fold higher) and a lower R$_{max}$, indicating the importance of the group at the 5 position of 5-HT. Further studies on other 5-substituted tryptamine derivatives confirm this hypothesis, and also reveal the importance of size and electronegativity at this location for efficient channel opening.

Subtle differences between 5-HT$_{3A}$ and 5-HT$_{3AB}$ receptors have been reported by a number of authors, and were also observed in the current study. Compared to the 5-HT$_{3A}$ receptor, responses from 5-HT$_{3AB}$ receptors are smaller and desensitize more rapidly; EC$_{50}$ and K$_d$ values differ by ~2-fold and there is an ~2-fold decrease in the Hill slope of the dose-response curves. There is also a difference in the efficacy of *m*CPBG, which acts as a partial agonist at 5-HT$_{3A}$ receptors, but a full agonist at 5-HT$_{3AB}$ receptors. This indicates gating characteristics of the two receptors are different, and indeed it has been established that the channel conductance is greatly increased in 5-HT$_{3AB}$ receptors (34).

Previous functional studies have revealed only small differences in the affinities (EC$_{50}$ and IC$_{50}$s) of A and AB receptors for a range of 5-HT$_3$ selective ligands (36), and

we observed a similar absence of selectivity for 5-HT, *m*CPBG, 5-FT and tryptamine in this study. These results are somewhat surprising, given that a recent study has suggested that in the heterologously expressed 5-HT$_{3AB}$ receptors the subunits are in the order BABBA (33), and, as agonist binding sites in Cys-loop receptors are constituted from two adjacent subunits, these data imply that binding interfaces would either be AB (most likely), BA, or BB (Figure 2.6a). Based on the sequence alignment (figure 2.6b), one would expect significant structural differences due to the different residues that would contribute to AA (required for the homopentameric 5-HT$_{3A}$ receptor) compared to AB/BA or BB binding sites. At present, we cannot explain why there are not larger changes in pharmacological characteristics of the AB receptor.

Figure 2.6. Subunit arrangement and sequence alignment for 5-HT$_{3AB}$ receptors. (a) Subunit arrangement of 5-HT$_{3AB}$ receptors with agonist shown in the presumed binding locations. **(b)** Alignment of 5-HT$_{3A}$ and 5-HT$_{3B}$ subunit sequences. Residues that have similar chemical properties are shown in grey. The binding loops that constitute the binding site are underlined.

The new data reveal some interesting features of the binding pocket. Tryptamine is ~100-fold less potent and much less efficacious than 5-HT (R_{max} = ~0.15), establishing the importance of the hydroxyl group. However 5-FT can significantly compensate for the lack of a hydroxyl; it is only 10-fold less potent than 5-HT and R_{max} = ~0.5. In our model of the binding pocket (8), the hydroxyl of 5-HT is located in a hydrophilic pocket constituted of Asn128, Glu129, Thr179, Thr181 and Glu236, and it has the potential to hydrogen bond with at least one of these residues (figure 2.7). Mutation of Asn128, Thr181 and Glu236 to Ala results in no significant changes to the 5-HT K_i, suggesting that Glu129 and Thr179 are the most likely residues to contribute to hydrogen bonds. However as these mutant receptors express poorly we could not prove this hypothesis. 5-FT can be located in a similar location to 5-HT, but we believe it is unlikely that F also forms hydrogen bonds here. Fluorine is the most electronegative element, and as such it is reluctant to donate a lone pair of electrons to a hydrogen bond donor. As a result, organic fluorine (fluorine bonded to a carbon) hardly ever accepts a hydrogen bond (45). Even without a hydrogen bond, however, it appears that an electronegative atom is more favorable than no substituent at all at this location.
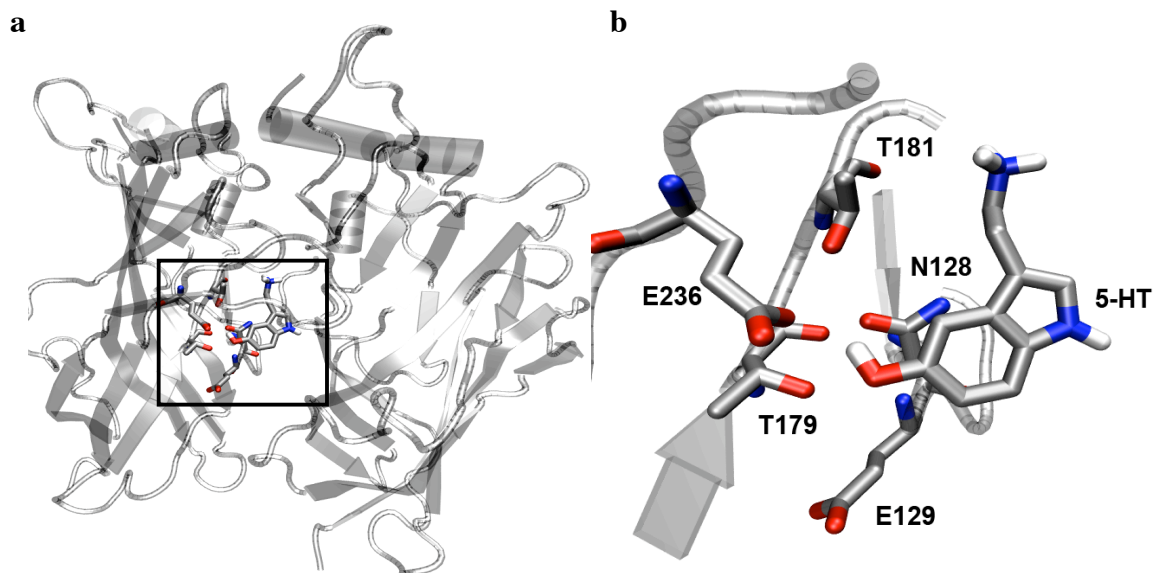
Figure 2.7. 5-HT docked into a homology of the 5-HT$_3$ receptor (Reeves et al. 2002). **(a)** Two subunits of the 5-HT3 receptor showing the location of the binding pocket (boxed) at their interface; **(b)** Enlarged image of the binding site showing the proximity of the hydroxyl group to the hydrophilic residues Asn128, Glu129 Thr179, Thr181 and Glu236.

To further explore this region of the binding site, we examined 5-ClT, 5-MeT and 5-MeOT in 5-HT$_{3A}$ receptors. 5-ClT was of similar potency to 5-FT in the functional assays (EC$_{50}$= 8 μM) but was much less effective in opening the channel (R$_{max}$ = 0.0037). 5-ClT and 5-FT bind to the receptor with similar affinities (K$_i$s are not significantly different), demonstrating there is no relationship between K$_i$ or EC$_{50}$ and R$_{max}$. Thus it appears that the atom at the 5 position of tryptamine plays a critical role in the conformational changes that result in channel opening. Since both 5-FT and 5-ClT present a relatively electronegative atom at this position, we propose that the increased steric size of Cl versus F contributes to decreased efficacy of 5-ClT. Sterics also rationalize the inefficacy of 5-MeOT, which has an electronegative element in the 5 position but is apparently too large. The data from 5-MeT also support the hypothesis that

size and polarity are important; Me is a similar size to Cl, but is nonpolar, and 5-MeT is less effective at opening the channel.

The data also show that for most agonists there is a direct relationship between EC_{50} and K_i, with EC_{50}s 13–50-fold higher than K_i. This is expected, as K_i values are considered to represent binding to a high affinity desensitized state. However, for 5-ClT and 5-MeT, which have very low efficacy, EC_{50} is less than 5-fold higher than K_i. This suggests that if agonist binding does not result in significant channel opening (R_{max} less than 0.01), then there may be no significant entry of receptors into a high-affinity state.

Partial agonists are increasingly being used to distinguish between binding and gating events at Cys-loop receptors, and 5-FT, with an R_{max} of ~0.5 will be a useful addition to the more usually used mCBPG (R_{max} = ~0.8) and 2-Methyl-5-HT (R_{max} = ~0.2). Partial agonists are also potentially useful as therapeutic agents. The most well-established role of 5-HT_3 receptors is in regulating gastrointestinal motility and the vomiting reflex, although they may play a role in many other neuronal functions. Currently, 5-HT_3 receptor antagonists are used clinically as antiemetics, and to treat irritable bowel syndrome (38-40). However, there is some evidence that these compounds also cause side effects in many patients, by inhibiting normal lower bowel function (46). Thus there has been an increased interest in 5-HT_3 receptor partial agonists, which might control gastroenteric motility without completely blocking 5-HT_3-sensitized nerve function (47,48). 5-HT_3 receptor agonists also have a potential therapeutic role through their modulation of acetylcholine release *in vivo* (49), making these compounds of

interest for the treatment of neurodegenerative and neuropsychiatric disorders in which cholinergic neurons are affected. Full 5-HT_3 receptor agonists, however, cause nausea and vomiting; thus partial agonists are potentially more useful for therapeutic applications in this area. Recently developed compounds, e. g., those described by Yoshida et al. (2004) are probably potentially more useful as therapeutics than 5-FT, but a comparison of their actions compared to 5-FT may clarify details of their mode(s) of action.

In conclusion we have shown that 5-FT is a partial agonist at both homomeric 5-HT_{3A} and heteromultimeric 5-HT_{3AB} receptors. The data have also revealed that the atom in the 5' location of 5-HT plays an important role both in receptor binding and in subsequent channel gating.

2.3 1-oxo-5-hydroxytryptamine and Fluorinated 5-HT Analogues

2.3.1 1-OT Results and Discussion

Reproduced in part from (50).

While it is quite clear that the 5' hydroxyl plays an important role in agonist binding an activation, very little is known about the role of the protic indole nitrogen of 5-HT. As part of our efforts to map out the binding of 5-HT we became curious as to whether the protic indole nitrogen of 5-HT forms a hydrogen bond with the receptor as part of its binding interaction. A valuable probe of this putative interaction would be the benzofuran analog of 5-HT, in which an aprotic oxygen replaces the indole nitrogen.

This molecule, which we name 1-OT (1-oxo-5-hydroxytryptamine) (figure 2.7), has been synthesized once before (51), but it has never been explicitly tested on any of the known 5-HT receptors (52). In considering this molecule for our own studies, we felt that the published synthesis (10 steps and <3% yield) was cumbersome, and we chose to pursue a novel synthetic strategy that could provide more ready access to 1-OT. A successful synthetic strategy was developed and carried out by Sean Kedrowski, and the details of this synthesis have been published (50).

The pharmacology of 1-OT on the 5-HT$_3$ receptor proved very interesting, as its EC$_{50}$ value is nearly idential to that of the native agonist, (1.7 versus 1.2 μM, respectively; figures 2.8 and 2.9). Furthermore, 1-OT is essentially a full agonist, with an

efficacy that is $94 \pm 4\%$ of 5-HT. Surprisingly, the indole NH is not required for effective receptor activation. This result was unexpected because there is the potential for this group to be used to make a specific interaction that could distinguish 5-HT from other similar molecules. As was made clear in section 2.2, removing hydrogen bonding function at the 5' position has large effects on agonist EC_{50} and relative efficacy. The varient with the smallest effect (5-FT) still had an EC_{50} that shifted more than 10-fold and an efficacy 30% that of 5-HT.
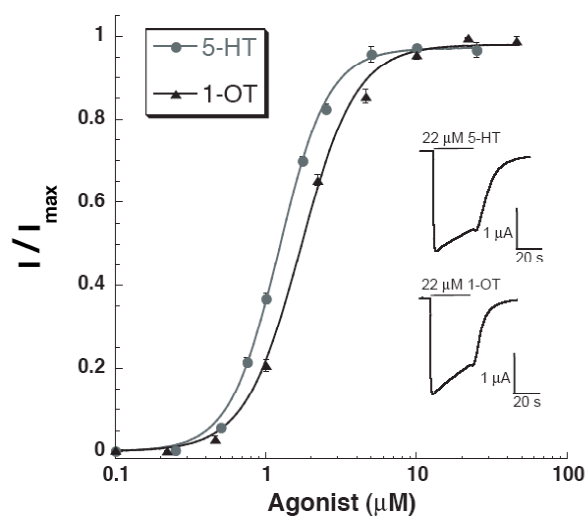
Figure 2.8. Dose-response curves for 5-HT and 1-OT with sample current traces inset.
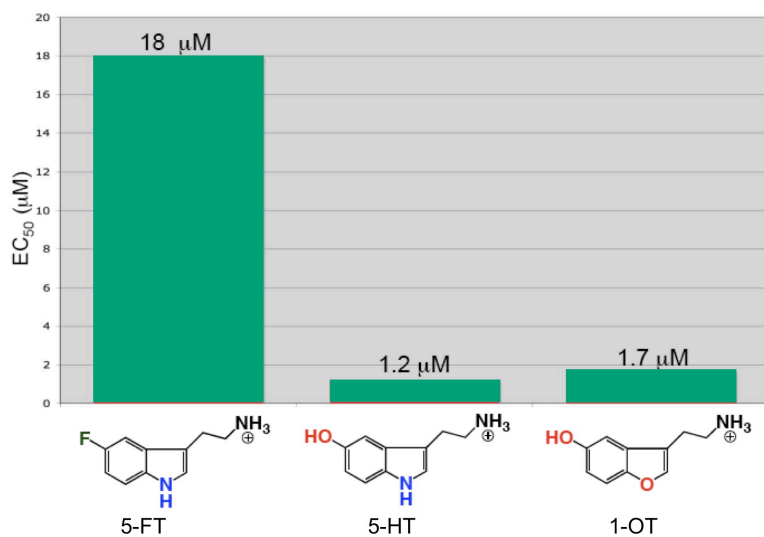
Figure 2.9. Plots illustrating relatively small EC_{50} shift of 1-OT.

In conclusion, we have established an efficient new route to 1-oxo-5-hydroxytryptamine, the benzofuran analog of serotonin. We have further shown that this molecule is a competent agonist of the 5-HT$_3$ receptor, suggesting that the indole nitrogen of 5-HT does not donate a hydrogen bond to the receptor. The increased availability of 1-OT afforded by the synthetic route developed in this study will enable similar investigations to elucidate agonist binding in the other six classes of 5-HT receptors. In addition, this route should be easily modifiable to synthesize more substituted 1-OT derivatives for further elucidation of 5-HT receptor binding sites.

2.3.2 Fluorinated 5-HT Analogues

As part of our study exploring the mechanism of 5-HT activation of the 5-HT$_3$ R, we examined two 5-HT analogues with fluorine replacing hydrogen at either the 6 or the 4 and 6 positions (figure 2.10). Because of the electron-withdrawing effect of fluorine, the hydroxyl group on these compounds is more electron deficient and has a lower pKa. This should make the group a better hydrogen bond donor, and might be expected to lower the EC$_{50}$ value. Furthermore, characterization of a series of 5-HT derivatives with zero, one, and two fluorines might reveal a stepwise shift in EC$_{50}$ that could be used to identify a specific interaction with the 5-HT hydroxyl.

5-HT
pKa 10.7

6-Fluoro-serotonin
pKa 9.1

4,6-Fluoro-serotonin
pKa 8.0
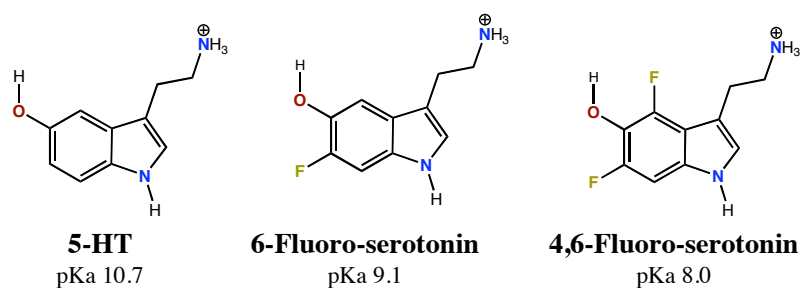
Figure 2.10. Structures of the 5-HT and two fluorinated analogues used in our studies.

The dose-response relationships of both fluorinated 5-HT compounds were measured using wild-type 5-HT$_3$. The EC$_{50}$ of 6-fluoro-serotonin (1.1 ± 0.1μM) is not significantly different from that of serotonin, while the EC$_{50}$ of 4,6-fluoro-5-HT (2.1 ± 0.1 μM) is two-fold larger than serotonin. This is a shift in the opposite direction from what is predicted based upon changes to the hydrogen bond donating ability of the hydroxyl group. Because fluorine is almost isosteric with hydrogen, it is most likely that this effect is a result of differences in electrostatics.

The orientation and binding mode of 5-HT offer at least one explanation for the rightward shift in EC$_{50}$. In the docked model, the "4" position is on the side of serotonin involved in the majority of interactions, while the "6" position is left free and exposed to solvent (figure 2.11). If this model is correct, the higher EC$_{50}$ observed in the 4,6-fluoro-serotonin (4,6-F-5HT) could be due to a repulsive interaction between the fluorine at the '4' position and one of the residues on this face of the binding pocket. Experiments with 4-fluoro-serotonin would be an informative test of this hypothesis.
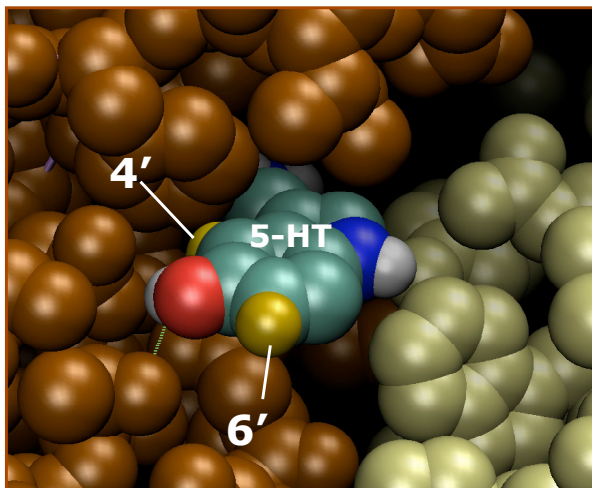
Figure 2.11. The homology model displayed in 'spacefill' illustrates one possible explanation for the unexpected higher EC_{50} observed from 4,6 fluroro-5-HT compared to 6-fluroro-5-HT. The 4' position appears much more likely to interact with the residues in the binding site (and thus to affect EC_{50}).

While the differences in EC_{50} between different fluorinated analogues were subtle, the measured difference in receptor kinetics were much more pronounced. The desensitization resulting from the application of 4,6-F-5HT was 10-fold faster than that from the application of either 5-HT or 6-F-5HT (figure 2.12). (The equation used to determine τ is, $Ae^{(-t/\tau)} + C$). These results indicate that the fluorine at the 4' position interacts with the receptor directly and are consistent with the unexpected rightward shift in EC_{50} for 4,6-F-5HT. They also indicate that the residue participating in this interaction could be linked closely to the mechanism of receptor desensitization. Our results are particularly interesting because such effects on desensitization are rarely, if ever, induced by agonists (53).
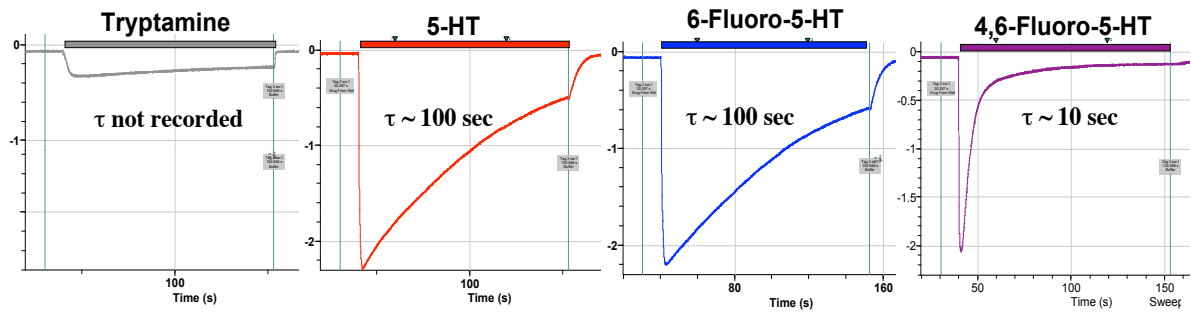
Figure 2.12. Differences in activation and desensitization kinetics induced by serotonin and several analogues. This data suggest that the presence of fluorine at the 4' position leads to changes in gating, either directly or indirectly.

2.4 A Hydrogen Bond in Loop A Is Critical for Binding and Function of the 5-HT$_3$ Receptor.

Reproduced in part from (54).

2.4.1 Loop A Introduction

Studies in nACh, GABA$_A$, and 5-HT$_3$ receptors indicate that loop A makes an important contribution to receptor function (43,55-58). The loop A residues Asn128, Glu129, and Phe130 are conserved in all known 5-HT$_{3A}$ and 5-HT$_{3B}$ receptor subunits (Figure 2.13), and it is therefore likely that these residues are important for receptor binding and/or gating. The structure of AChBP indicates that only a single loop A residue contributes to the binding pocket, but determining the precise 5-HT$_3$ receptor residue in the equivalent location is not straightforward, as loop A exemplifies a region where the alignment of subunit residues with AChBP is difficult. A model of the 5-HT$_3$ receptor binding pocket predicts that the side chain of Asn128 faces into the binding pocket and interacts with 5-HT via a hydrogen bond (15), but a later study indicates that Asn128 does not participate in ligand binding (43). This study suggested a new orientation with Glu129 replacing Asn128 in the binding pocket, but did not provide any experimental evidence from Glu129 mutant receptors to support this hypothesis. Phe130 has also been previously proposed as a ligand binding residue, as its substitution with Asn created receptors that respond to ACh (58); however a more recent study (43) indicates that this is unlikely as substitutions at this site create receptors that are more sensitive both to 5-HT and non-specific agonists such as ACh, which will activate 5-HT$_3$ receptors at high concentrations (>1 mM). In this study we have therefore concentrated on Asn128 and Glu129, substituting them with a range of natural and unnatural amino acids (figure 2.14)

to probe potential interactions with 5-HT. The data suggest that Glu129 is directly involved in ligand binding by participating in a critical hydrogen bond with the hydroxyl group of 5-HT, thus providing the first direct evidence that the revised model may be correct.
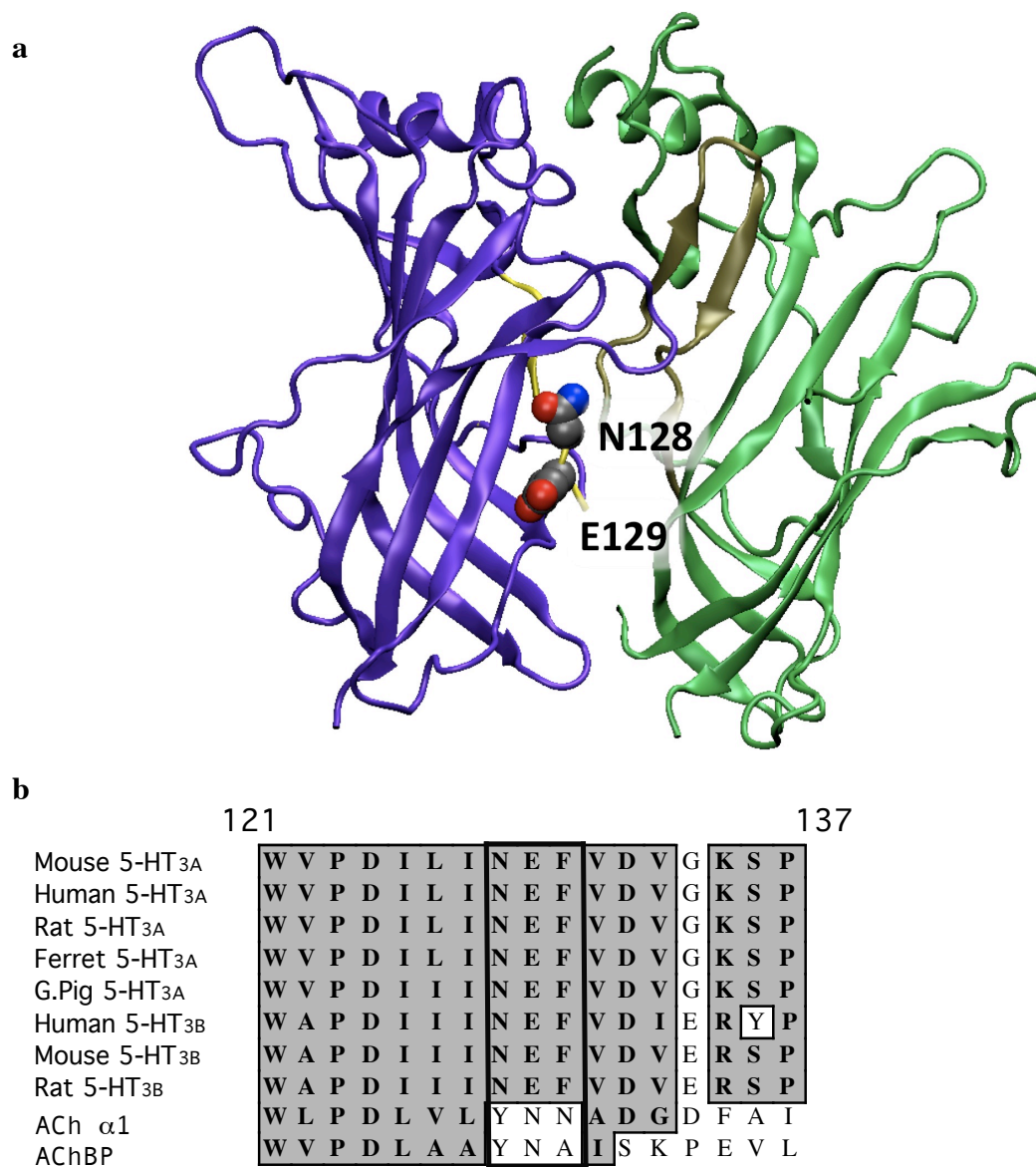
Figure 2.13. (a) Model of two adjacent subunits of the 5-HT₃ receptor based on Reeves et. al., 2003 showing the positions of loop A (in yellow) and residues Asn128 and Glu129 (space fill). (**b**) **Alignment of the binding loop A region from various 5-HT₃ₐ and 5-HT₃ᴮ receptor subunits, the *Torpedo* nACh receptor α1 subunit and AChBP**. Binding loop A was originally defined as equivalent to W121-N128 (Joshi et. al., 2006), but recent data suggest it may be longer (present study and Shapira et. al., 2003). Residues with similar chemical properties are in grey. The Asn, Glu and Phe residues conserved in all 5-HT₃ receptor subunits are boxed. Numbering is from the mouse 5-HT₃ₐ receptor subunit.
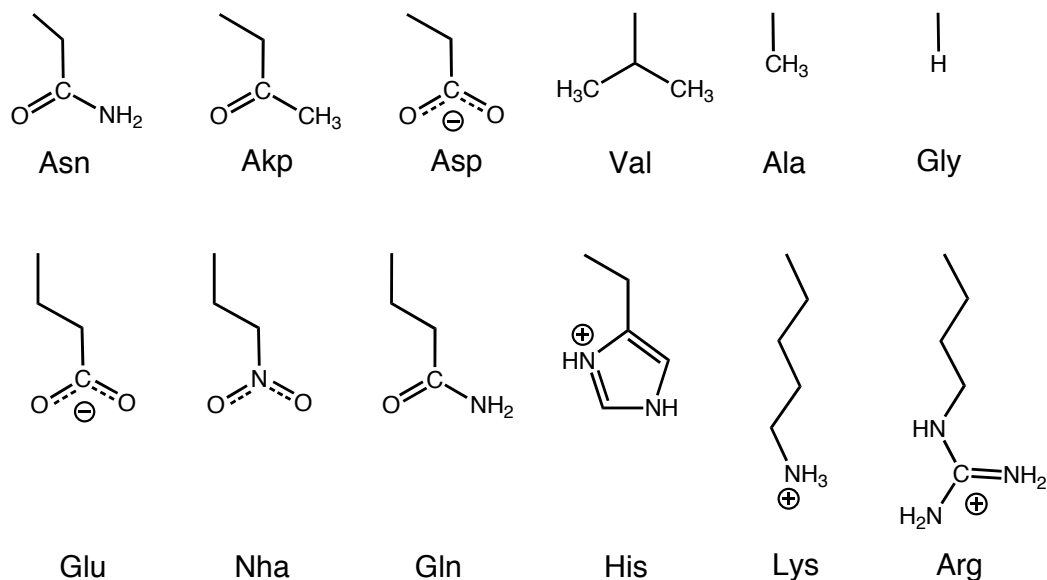
Figure 2.14. (a) Structures of the side chains of the natural and unnatural amino acids used in these studies. Akp = 2-amino-4-ketopentanoic acid; Nha = nitrohomoalanine.

2.4.2 Results

Wild-type (WT) 5-HT$_{3A}$ receptors displayed large, rapidly activating and desensitizing currents (figure 2.15) with an EC$_{50}$ of 1.2 μM for 5-HT (pEC$_{50}$ = 5.93 ± 0.01, n=10). Only homomeric 5-HT$_{3A}$ receptors were examined in this study. The partial agonists *m*-chlorophenylbiguanide (*m*CPBG), 5-FT and tryptamine had EC$_{50}$s of 0.47, 18 and 120 μM respectively (tables 2.4-2.5, figure 2.16). *m*CPBG was almost as efficacious as 5-HT at these receptors, with an R$_{max}$ of 0.81 ± 0.02 (n= 14). The R$_{max}$ for 5-FT was 0.44 ± 0.02 (n=19). However, for tryptamine the R$_{max}$ was only 0.09 ± 0.01 (n=8); these small currents precluded systematic data recording in a number of experiments.
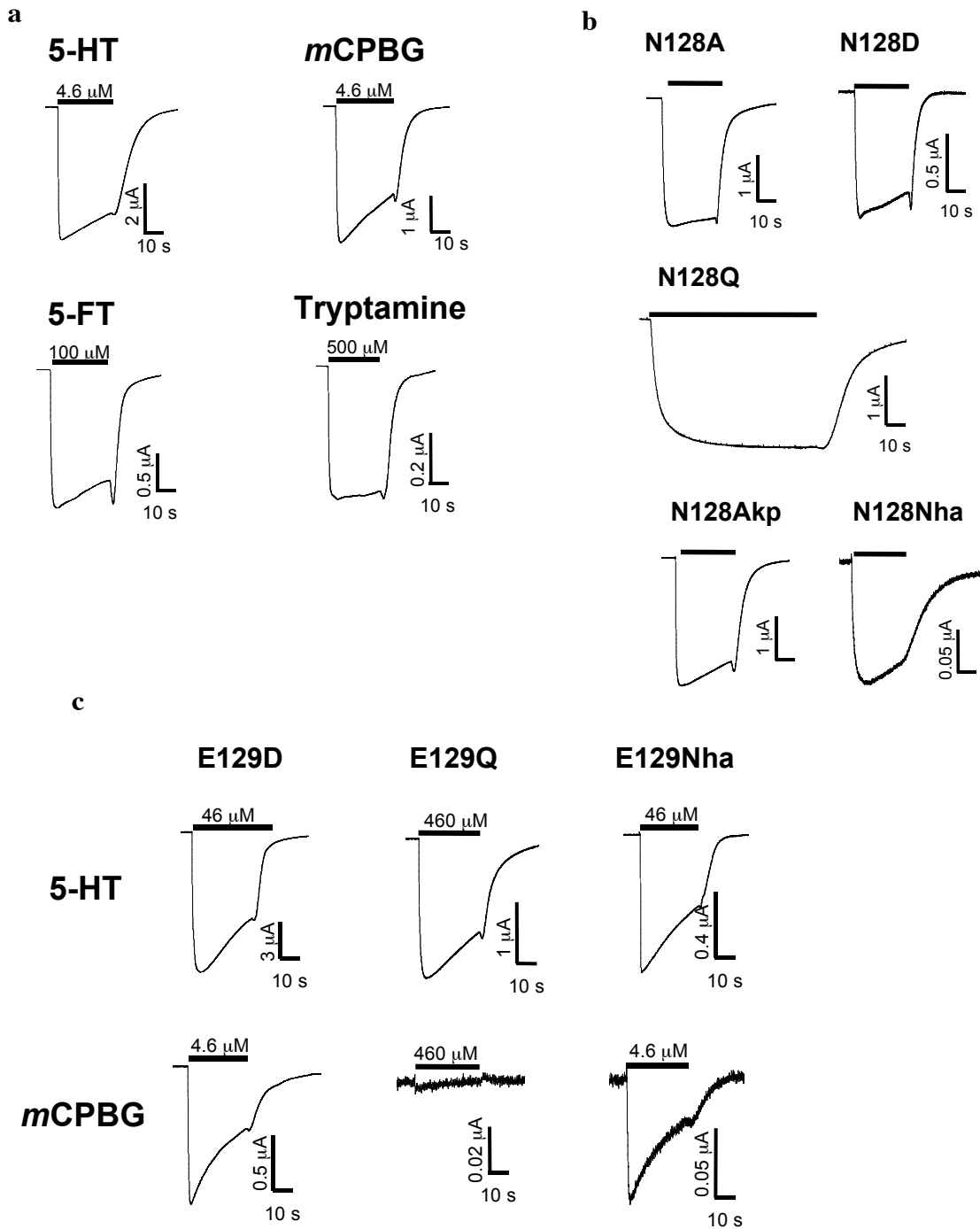
Figure 2.15. Examples of current traces. (**a**) Typical responses to maximal concentrations of 5-HT, *m*CPBG, 5-FT and tryptamine from the same oocyte expressing WT 5-HT₃ receptors; (**b**) typical 5-HT responses of oocytes expressing Asn128 mutant receptors; [5-HT] = 22 μM, except N128Q (200 μM) and N128-Nha (48 μM); (**c**) typical 5-HT and *m*CPBG responses from oocytes expressing Glu129 mutant receptors.

Receptor	5-HT pEC$_{50}$	5-HT EC$_{50}$, µM	nH	mCPBG pEC$_{50}$	mCPBG EC$_{50}$, µM	nH
WT	5.93 ± 0.01	1.2	2.54 ± 0.15	6.33 ± 0.02	0.47	2.03 ± 0.23
N128A	5.44 ± 0.03	3.6	1.34 ± 0.13*	5.95 ± 0.02	1.1	1.33 ± 0.08
N128D	5.51 ± 0.01	3.1	1.63 ± 0.08*	6.56 ± 0.03	0.27	1.54 ± 0.15
N128E	5.68 ± 0.04	2.1	1.48 ± 0.18*	6.56 ± 0.03	0.28	1.81 ± .019
N128Q	4.64 ± 0.03*	23	2.11 ± 0.29	5.52 ± 0.18*	3.0	2.41 ± 0.16
N128R	SR	SR	SR	5.14 ± 0.02*	7.3	1.93 ± 0.16
N128K	4.47 ± 0.03*	34	2.13 ± 0.38	5.41 ± 0.03*	3.9	1.43 ± 0.16
N128V	7.04 ± 0.02*	0.091	3.18 ± 0.60	7.13 ± 0.02*	0.074	5.07 ± 0.85*
N128-Akp	5.33 ± 0.01*	4.6	1.49 ± 0.06*	ND	ND	ND
N128-Nha	SR	SR	SR	5.55 ± 0.02*	2.8	2.18 ± 0.23
E129A	NR	NR	NR	NR	NR	NR
E129D	5.73 ± 0.03	1.9	1.81 ± 0.16*	6.60 ± 0.10	0.25	1.19 ± 0.31
E129G	NR	NR	NR	NR	NR	NR
E129H	4.85 ± 0.09*	14	1.07 ± 0.24*	6.43 ± 0.04	0.37	1.63 ± 0.20
E129K	NR	NR	NR	NR	NR	NR
E129N	4.25 ± 0.02*	56	1.17 ± 0.07*	6.21 ± 0.05	0.62	1.25 ± 0.19
E129Q	3.93 ± 0.01*	120	1.55 ± 0.07*	NR	NR	NR
E129-Nha	5.45 ± 0.04	3.5	1.18 ± 0.12*	6.25 ± 0.07	0.56	1.91 ± 0.60

Table 2.5. 5-HT and mCPBG EC$_{50}$ values and Hill coefficients for N128 and E129 mutant receptors Data = Mean ± SEM, n = 3-16. NR = no response; SR = small (<100 nA) responses, ND = not determined; * Significant difference p < 0.05 and for pEC$_{50}$ > 3-fold different to WT.

Receptor	5-FT pEC$_{50}$	EC$_{50}$, µM	nH	Tryptamine pEC$_{50}$	EC$_{50}$, µM	nH
WT	4.75 ± 0.02	18	2.71 ± 0.24	3.93 ± 0.01	120	2.86 ± 0.14
N128A	5.00 ± 0.06	10	2.34 ± 0.75	4.04 ± 0.03	91	2.90 ± 0.68
N128D	4.75 ± 0.02	18	2.61 ± 0.28	SR	-	-
N128E	4.86 ± 0.02	14	1.97 ± 0.18	4.23 ± 0.03	59	2.90 ± 0.53
N128Q	4.03 ± 0.05*	94	2.38 ± 0.58	3.62 ± 0.02	240	3.10 ± 0.39
E129D	5.08 ± 0.04	8.3	1.95 ± 0.30	SR	-	-
E129N	4.93 ± 0.04	12	1.25 ± 0.13*	SR	-	-

Table 2.6. 5-FT and tryptamine EC$_{50}$ values and Hill coefficients for N128 and E129 mutant receptors. Data = Mean ± SEM, n = 3-13. SR = small (<100 nA) responses. * Significant difference p < 0.05, and for EC$_{50}$ >3-fold different to WT.
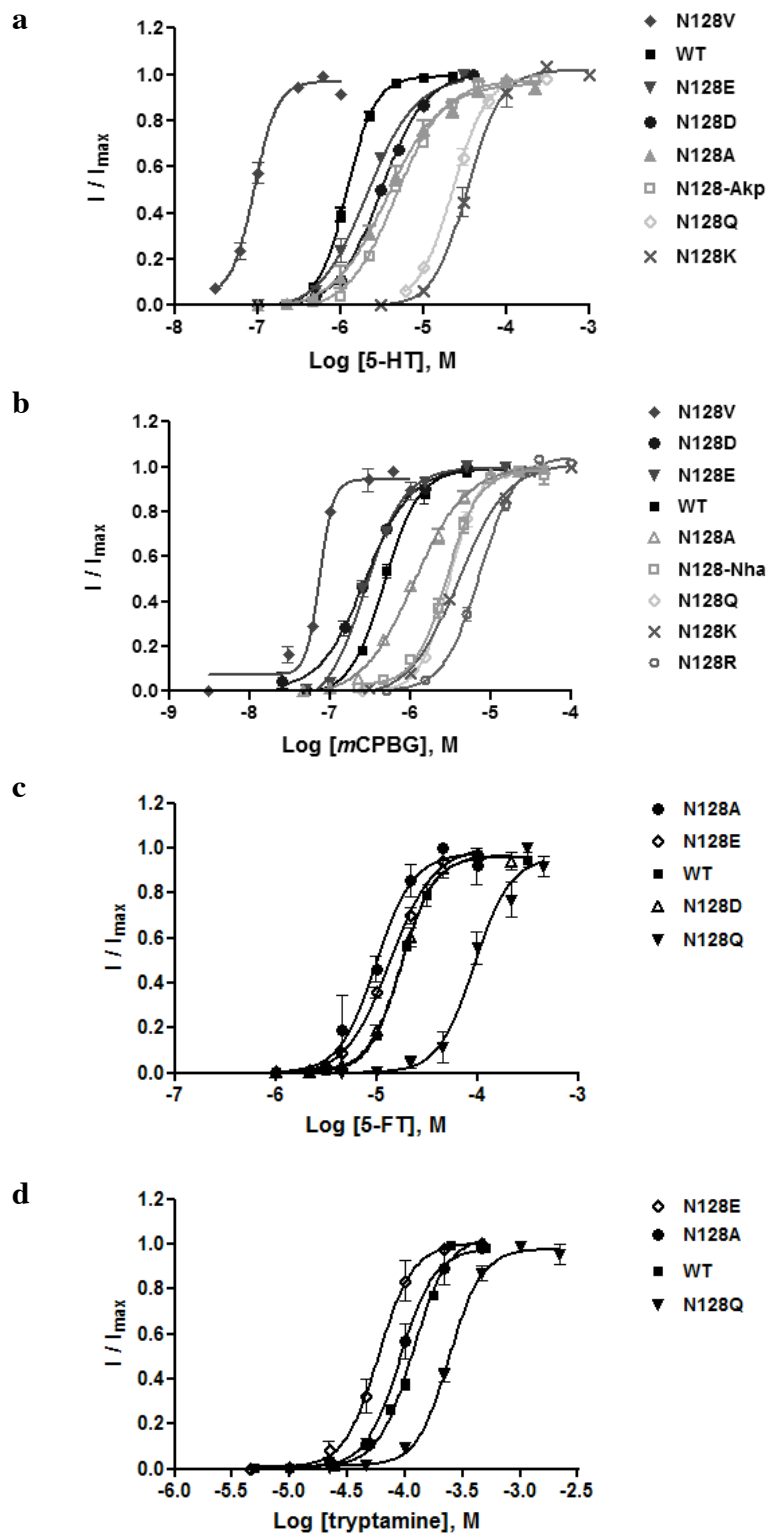
Figure 2.16 a-d. Concentration-response data for wild-type (WT) and mutant 5-HT$_3$ receptors. Data = mean ± SEM. Parameters of the fitted curves are shown in Tables 2.5 and 2.6.
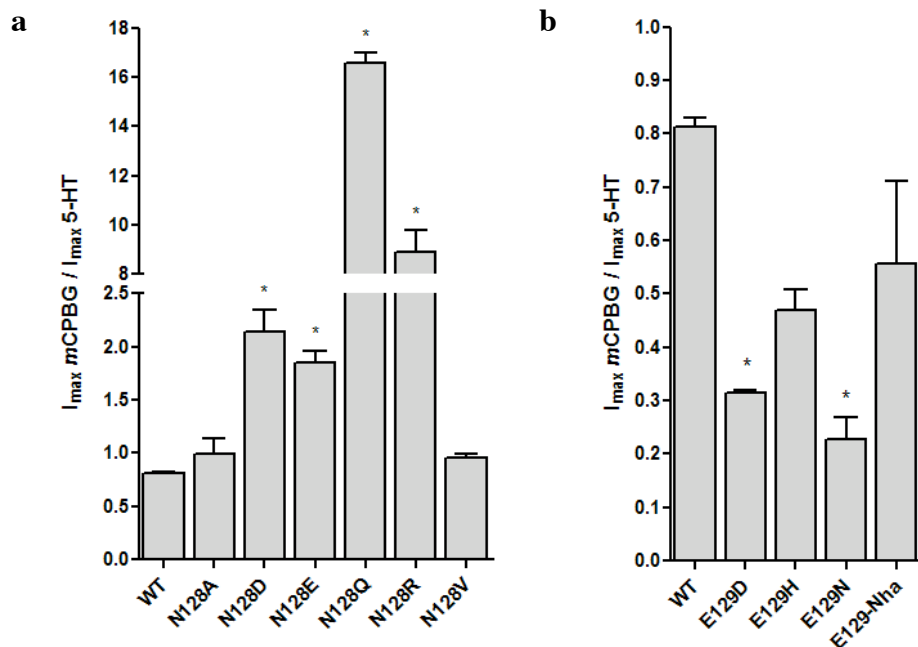
Figure 2.17. Relative efficacy (R_{max}) of *m*CBPG at WT and (a) N128 and (b) E129 mutant receptors. Data = mean $\pm$ SEM, n $\geq$ 3. Note the substantial change in the range of efficacies in Part B versus Part A. * = significantly different to WT, $p < 0.05$.

Asn128 mutants

Replacement of Asn128 with Asp, Glu, Ala and the unnatural amino acid Akp resulted in no or small changes in 5-HT, *m*CPBG and 5-FT EC_{50} values, although Hill coefficients for 5-HT were reduced (tables 2.4-2.5, figure 2.16). In contrast, replacement with Gln or Lys resulted in significant increases in EC_{50} values for 5-HT, *m*CPBG and 5-FT, while replacement with Val significantly decreased the EC_{50}. There were no changes in Hill coefficients for these 3 mutants (tables 2.4–2.5). For the N128R mutant the efficacy of 5-HT appeared significantly reduced (Figure 2.17a), but responses to 5-HT were too small to allow a determination of EC_{50}. Most of the mutations (all except Ala and Val) also resulted in changes to *m*CPBG R_{max} values; these were increased 2-19-fold compared to WT (figure 2.17). There were also changes in the current profile for some mutants: N128V and N128Q substitution resulted in an apparent slower activation rate

and no obvious desensitization in the continued presence of 5-HT (figure 2.15b). A

detailed kinetic analysis of these changes would require single channel analyses, which

are not possible with these receptors (<1pS conductance), but the clear changes in the

macroscopic data between WT and mutant receptors are consistent with changes to

receptor activation and desensitization.

Glu129 mutants

E129D, E129N and E129Q showed robust responses to 5-HT (figure 2.15c).

E129H responses were small and only measurable if recorded >72 h post-injection.

E129G and E129K mutants failed to respond to high concentrations (100 μM) of either 5-

HT or *m*CPBG. The unnatural amino acid Nha, which is isoelectronic and isosteric to

Glu, but which lacks charge, had an EC_{50} for 5-HT similar to WT, as did E129D. Overall

EC_{50} values for 5-HT were in the rank order WT $\leq$ E129D $\leq$ Nha < E129H < E129N <

E129Q (figure 2.16b). Hill coefficients of all the functional mutants were reduced

compared to WT (tables 2.4-2.5). Interestingly, E129Q mutant receptors failed to be

activated by *m*CPBG; instead *m*CPBG acted as an antagonist and was able to block 5-

HT-induced currents, as previously reported (55). In our study, *m*CPBG blocked 100 μM

5-HT-induced currents with an IC_{50} of 0.63 μM (pIC_{50} = 6.20 $\pm$ 0.04 M, n=5; figure 2.18).

Furthermore, 5-FT, another partial agonist of 5-HT$_3$ receptors (37) also became an

antagonist, blocking 100 μM 5-HT-induced currents with an IC_{50} of 13 μM (pIC_{50} = 5.26

$\pm$ 0.06, n=3; figure 2.18). Like *m*CPBG, this compound failed to activate E129Q mutant

receptors on its own.
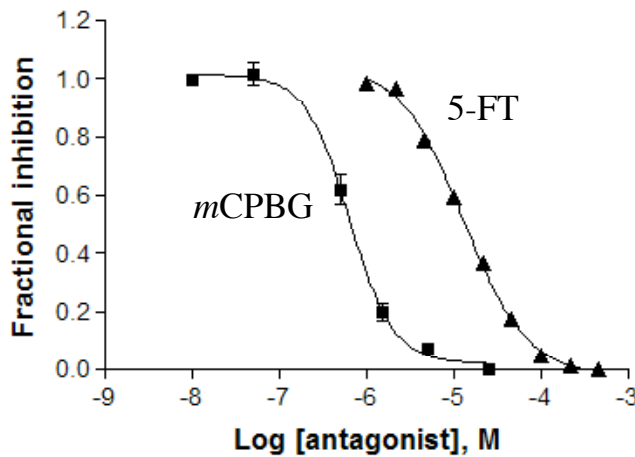
Figure 2.18. *m*CPBG and 5-FT are antagonists at E129Q receptors. Concentration response data showing inhibition of the 100 μM 5-HT-induced response. Each agonist was co-applied with 5-HT. Responses are normalized to the response to 5-HT alone. Data = mean $\pm$ SEM, n = 3-6.

We also tested whether granisetron could inhibit 5-HT-induced responses from these mutant receptors. At E129D receptors, 10 nM granisetron was able to block 80 $\pm$ 5% (n=3) of the response to an EC_{50} concentration of 5-HT, and 96 $\pm$ 3% at 100 nM, and recovery from granisetron block was complete in < 3 min, compared with > 15 min at WT receptors. Granisetron was less potent at E129N receptors, where 100 nM granisetron did not block the response to an EC_{50} concentration of 5-HT.
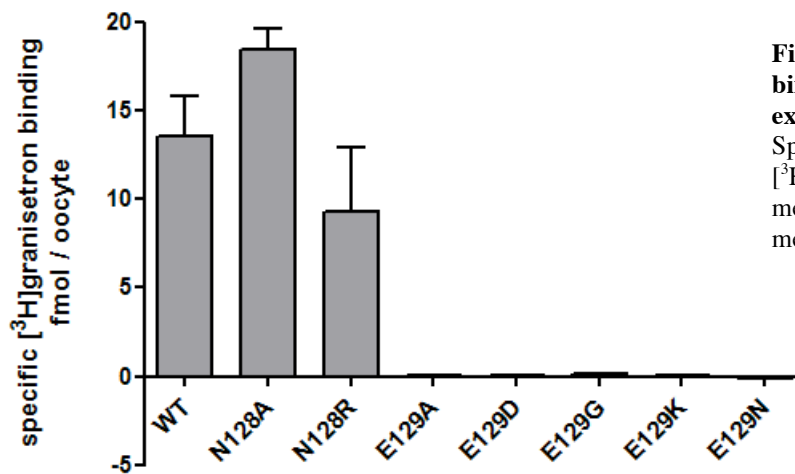
Figure 2.19. Antagonist binding to 5-HT$_3$ receptors expressed in oocytes. Specific binding of 0.5 nM [^{3}H]granisetron to oocyte membrane samples. Data = mean $\pm$ SEM, n = 4.

Binding data

Both Asn128 and Glu129 mutant receptors have been previously examined

expressed in HEK cells (43). For Asn128 mutant receptors there was no significant differences in [³H]granisetron binding affinity for any substitution studied, while no specific binding was observed for any Glu129 mutant receptor, at concentrations up to 20 nM. In the current study we examined single point [³H]granisetron binding to solubilized oocyte preparations. No specific radioligand binding was observed at 0.5 nM [³H]granisetron for E129A, E129G and E129K mutant receptors, while levels of binding in Asn128 receptors were similar to WT receptors (figure 2.19). These data suggest that Glu129 substitutions ablate high affinity antagonist binding, but at least some substitutions permit agonist binding, as large (> 5 μA) responses to 5-HT and *m*CPBG were observed for E129D and E129N receptors.

2.4.3 Discussion

The data described here support a modified 5-HT$_3$ receptor homology model (43), in which Glu129, rather than Asn128, faces into the binding pocket. The data indicate a critical hydrogen bond between Glu129 and the hydroxyl of 5-HT, which places this residue firmly in the binding pocket. Asn128 may play a role in receptor gating, but the data show that it is not directly involved in binding ligands, as previously proposed (15).

Loop A was identified as a region that contributes to ligand binding in nACh receptors many years ago; affinity labeling with [³H]ACh mustard indicated the positive charge of ACh was positioned near the loop A residue Tyr93 (59). There was also evidence for a contribution from neighboring Asn94 (60), and a detailed functional analysis of Asp97 has led to the proposal that loop A could be compared to a latch, which

holds the channel closed in the absence of agonists, and reduces the probability of channel opening (57). More recent studies, in particular the high resolution structure determination of AChBP, confirm the importance of the loop A Tyr at position 89, (equivalent to Tyr93 in nAChR) which is in close contact with bound ligands (61). The aligned Tyr is also important in $GABA_A$ receptors; Tyr97 in the β2 subunit has recently been shown to make a cation-π interaction with GABA (62). It was therefore not surprising that the aligning residue in the 5-HT_3 receptor, Asn128, was considered to be important. Homology modeling identified it as the only loop A residue in the binding pocket, and predicted a hydrogen bond between Asn128 and 5-HT (15). However, experimental studies have cast some doubt on this conclusion, as changing Asn128 did not affect [^{3}H]granisetron binding affinity (43).

Our new data, incorporating both natural and unnatural amino acids at this position, provide a detailed analysis of the role of Asn128, and strongly suggest that Asn128 has its most significant role in the conformational change that results in receptor gating. All Asn128 mutant receptors showed changes in their functional characteristics (figure 2.15b), but these were particularly evident in N128Q receptors. Gln has similar chemical properties to Asn, yet this mutation markedly slows apparent current activation, increases the relative efficacy (R_{max}) of the partial agonist *m*CPBG, and eliminates receptor desensitization (figures 2.15 and 2.17). Changes in current activation and R_{max} strongly suggest effects on receptor opening, and, while desensitization is not well understood, it is known to be influenced by channel opening and closing rates, and the rates of conformational changes to and from the desensitized state. These observations

therefore all suggest that Asn128 has a role in facilitating transitions between conformational states rather than direct effects on ligand binding. In the new model this residue is close to loop B, especially Thr179, and both these residue contribute to a complex network of hydrogen bonds that could potentially be involved in the conformational change that results in receptor gating.

Receptors with substitutions at Glu129 have, in the past, been insufficiently characterized due to problems with low expression (43,55). In this study, these problems have been largely overcome by the use of *Xenopus* oocytes as expression hosts. Large responses to 5-HT and the partial agonists *m*CPBG and 5-FT were measured with mutants of Glu129 that did not previously display measurable currents when expressed in HEK293 cells. Interestingly, only the Glu129 mutant receptors where Glu was replaced with residues that have the ability to accept a hydrogen bond responded robustly to 5-HT application, suggesting that this property is critical for 5-HT binding. Previous ligand docking data has indicated that the hydroxyl of 5-HT is located in this region of the binding pocket, and in the new model this hydroxyl would donate a hydrogen bond to Glu129; more specifically one of the side chain oxygens (Os) of Glu129 would interact with the hydrogen of the 5-HT 5-hydroxyl (figure 2.20). Note that an ionic interaction involving Glu129 is not supported by our data with the unnatural amino acid Nha. This amino acid is structurally similar to Glu: the nitro group is planar, like the carboxylate, and the two N-O bonds are of equal length, as are the C-O bonds in carboxylate. Two resonance structures are possible (as with carboxylate) but in a nitro group the nitrogen (N) carries a positive charge and the Os share a negative charge—thus overall the group

is neutral, in contrast to the negative charge on a carboxylate; a nitro group could therefore not contribute to an ionic bond. As there was no significant increase in EC_{50} when Nha was substituted for Glu, it shows that an ionic bond is not formed here. Nha could, however, still form a hydrogen bond as each O in the nitro group has two lone pairs of electrons (as does the carboxylate), which can serve as hydrogen bond acceptors.
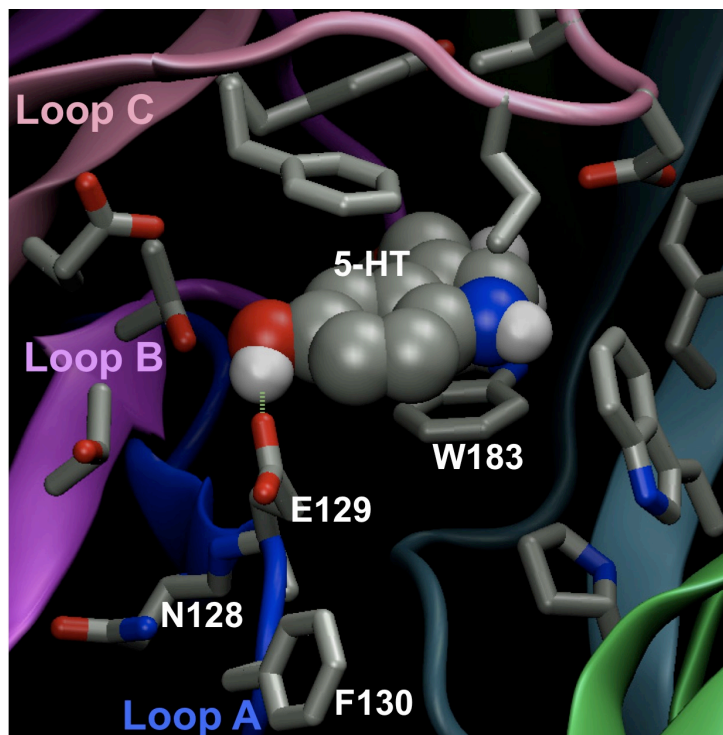
Figure 2.20. The new model of 5-HT$_3$ receptor binding site, showing 5-HT hydrogen bonded to Glu129. This model is that described by Sullivan *et al*. 2006, where a single amino acid gap was inserted into the 5-HT$_{3A}$ receptor subunit sequence (accession number: Q6J1J7) following V131 (WVPDILINEFV-DVG). The new model of the complete mouse 5-HT$_{3A}$ receptor extracellular domain was then built using *L. stagnalis* AChBP (accession number P58154, PDB ID 1I9B) as a template. The locations of Asn128, Glu129 and Trp183 relative to 5-HT are shown. The proposed H-bond between Glu129 and the hydroxyl group of 5-HT is shown in green.

Interestingly, mutations at Glu129 have no effect on the EC_{50}s of the partial agonists *m*CPBG or 5-FT (figure 2.21). This might be expected with *m*CBPG, which has a distinct structure to 5-HT and is unlikely to interact with identical binding site residues, but the only difference between 5-HT and 5-FT is the group at the 5 position. The OH of

5-HT is a good hydrogen bond donor and a moderately good hydrogen bond acceptor; however the F of 5-FT cannot donate a hydrogen bond and is a very poor hydrogen bond acceptor. Thus if 5-FT binding in the same orientation as 5-HT, which seems likely, it is probable that there is no hydrogen bond here with Glu129, a hypothesis that is supported by the data. The lack of this bond may be the reason why 5-FT only acts as a partial agonist.
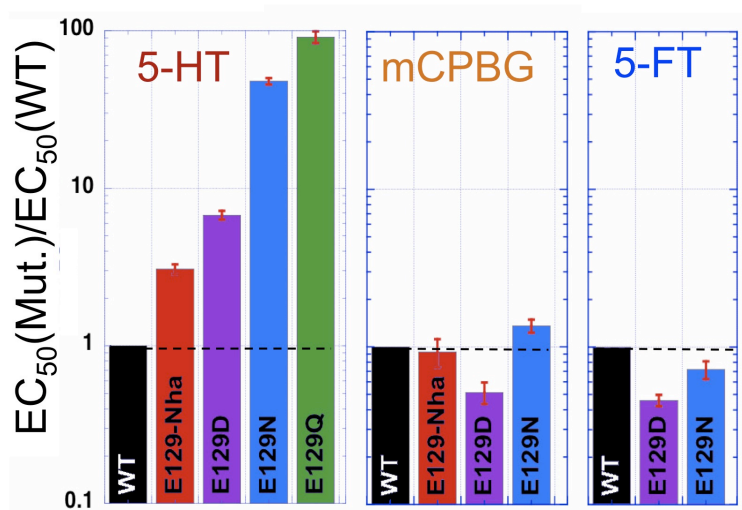
Figure 2.21. Comparison between agonists on the effect of mutation at Glu 129. *m*CPBG and 5-FT, which lack hydroxyl groups show little change in EC_{50}.

If Glu129 interacts directly with 5-HT, then it must face into the binding site and could interact with antagonists. Our, and previous, data support this proposal: there is no specific [³H]granisetron binding to Glu129 mutant receptors in either HEK cells or oocyte membranes in the usual subnanomolar range (13). Interestingly, though, granisetron does appears to be able to bind to E129D mutant receptors at higher concentrations, as 10 nM granisetron inhibited ~80% of 5-HT-induced currents (WT IC_{50} = 0.2 nM; (63)). Combined with the fact that E129D mutant receptors recover more quickly than WT receptors from granisetron inhibition, these data suggest that E129D mutant receptors have a higher dissociation rate constant for granisetron. Such an explanation is consistent with previous equilibrium radioligand binding studies, where an

~100-fold decrease in the granisetron K_d was reported (9).

Our data also reveal small but significant changes in relative efficacies for *m*CPBG at functional Glu129 mutant receptors, indicating there may also be a role for this residue in the conformational changes leading to receptor gating. These changes are opposite to those we observed with Asn128. We do not yet understand what this implies, although it may be related to the different roles of the 2 residues and/or distinct mechanisms of action or critical binding residues used by different agonists. In support of this latter hypothesis, a similar study on a series of loop C residues, which are also proposed to play a role in binding and/or gating, revealed increases in *m*CPBG efficacy but decreases in the efficacy of another partial agonist, 2-methyl-5-HT, in the same mutant receptors (64). In our study, the conversion of *m*CPBG from a partial agonist to an antagonist at E129Q mutant receptors could reflect a change in affinity of *m*CPBG for certain conformational states of the receptor only (e.g., a reduction in affinity of the open state but not the closed state). This would correspond to the 'K' phenotype of allosteric receptor mutants described by Galzi et al. (65).

The importance of Glu129 suggests it may be equivalent to Tyr93 in the nACh receptor, which has also been proposed to play a role in both binding and function. Mutating Tyr93 results in a rightward shift of the dose-response curve (66), mainly because of slower ligand-association and channel-opening rate constants (67). Similarly, the equivalent residue in the $GABA_A$ receptor, β_2Tyr97, which directly contacts GABA through a cation-π interaction (62), may also be involved in gating; mutation to Cys

causes spontaneous activation (56). Aligning Glu129 and Tyr93 requires that a space be inserted in the conserved WxPDxxxN domain in loop A of the nACh receptor. This sequence is critical for locating the B loop in the nACh receptor through interactions involving Asp89 (68). More recent data, however, show that in non-ACh receptors the xxxN portion of this region may not be critical; in the $GABA_A$ receptor, for example, two amino acid 'spaces' must be inserted in the 'xxx' tract to allow β_2Tyr97 to contribute to the binding pocket. We therefore propose that Glu129 is equivalent to Tyr93, and faces into the binding pocket, where it forms a hydrogen bond with the 5-OH group of 5-HT.

2.5 Structure-function Studies on the 5-HT$_3$ Receptor Ligand binding Site Reveal Polar Residues Critical for Receptor Activation and Identify an Intersubunit Salt Bridge

2.5.1 Polar Residues Introduction

Here, we investigate the function of polar residues in the ligand binding region of the 5-HT$_3$ receptor using a recently refined homology model to guide the effort (54). The polar residues that are the focus of this study are located in the region adjacent to and just outside of the highly conserved aromatic box (figure 2.22b). Previous data have shown that many of these residues modulate the binding of 5-HT and the gating of the receptor (e.g., Arg92, Glu129, Asp229, Glu236, and Thr181) (43,54,55,69-71). Recently, we found that mutations to Glu129 that eliminated its ability to act as a hydrogen bond acceptor increased the EC$_{50}$ of the 5-HT$_3$ receptor by as much as 100-fold for 5-HT but not 5-HT analogs that could not act as hydrogen bond donors (54). In this study, we expanded our investigation to other polar residues in the 5-HT$_3$ binding site with the goal of elucidating the specific roles that these other residues play in agonist binding and receptor activation.
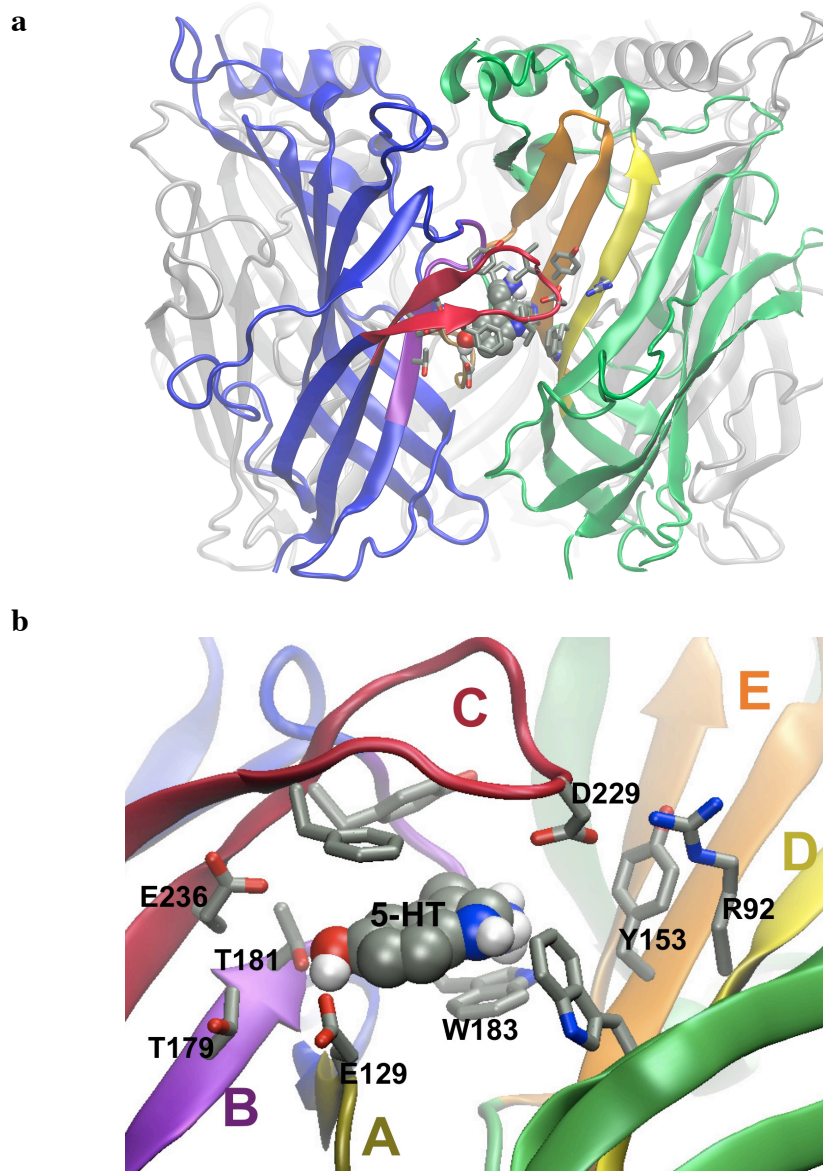
Figure 2.22. Homology model of the 5-HT₃ receptor. (**a**) The ligand binding site is formed by loops (various colors) at the interface of two adjacent subunits shown in blue and green. (**b**) The ligand binding site showing the side chains of residues examined in this study.

As in earlier studies, we utilize both conventional and unnatural mutagenesis so as to make use of the full range potential changes to amino acid functionality that are

available. Most unnaturals used in this study introduce subtle changes to amino acid structure and facilitate our understanding of the contributions of an amino acid with greater precision (figure 2.23c). Using these tools, we have been able to characterize the role of several polar residues in close proximity to the agonist-binding site. In particular, we identify an ionic interaction that likely participates in conformational changes associated with receptor gating. We also characterize several other residues that play critical roles in receptor activation. Last, we have compared and contrasted the behaviors of two structurally distinct agonist classes, serotonin (5-HT) and its related structures, and m-chlorophenylbiguanide (mCPBG) (figure 2.23a, b) and identified several residues that play critical roles in modulating agonist binding and gating in response to these agonists.

2.5.2 Results

Application of 5-HT to *Xenopus* oocytes expressing wild-type (WT) 5-HT_{3A} receptors resulted in rapidly activating inward currents with an EC_{50} of 1.2 μM and a Hill coefficient of 2.5. Only homomeric 5-HT_{3A} receptors were examined in this study. The recently characterized partial agonist 5-FT (5-fluorotryptamine) is an analogue of 5-HT in which the OH of the indole ring is replaced with F(37) (figure 2.23b). 5-FT had an EC_{50} of 16 μM with a Hill coefficient of 2.4 for WT 5-HT_3. The relative efficacy (ε) of an agonist is defined as the ratio of the maximum response of that agonist to that of 5-HT. The efficacy (relative to 5-HT) of 5-FT is 0.44. The partial agonists mCPBG and m-chlorophenylguanide (mCPG) induced kinetically similar responses with EC_{50}s of 0.62 μM and 3.7 μM and Hill coefficients of 2.3 and 1.8, respectively. mCPBG has a relative

efficacy close to that of 5-HT in WT receptors (ε = 0.81) while *m*CPG is somewhat less efficacious (ε = 0.55).

a

5-hydroxytryptamine   5-fluorotryptamine   *m*-chlorophenylbiguanide   *m*-chlorophenylguanide

b

5-HT   mCPBG

c

Glu   Nha   Gln   Asp   Asn   Arg

Thr   aThr   Omt   Val   Ser   Ala
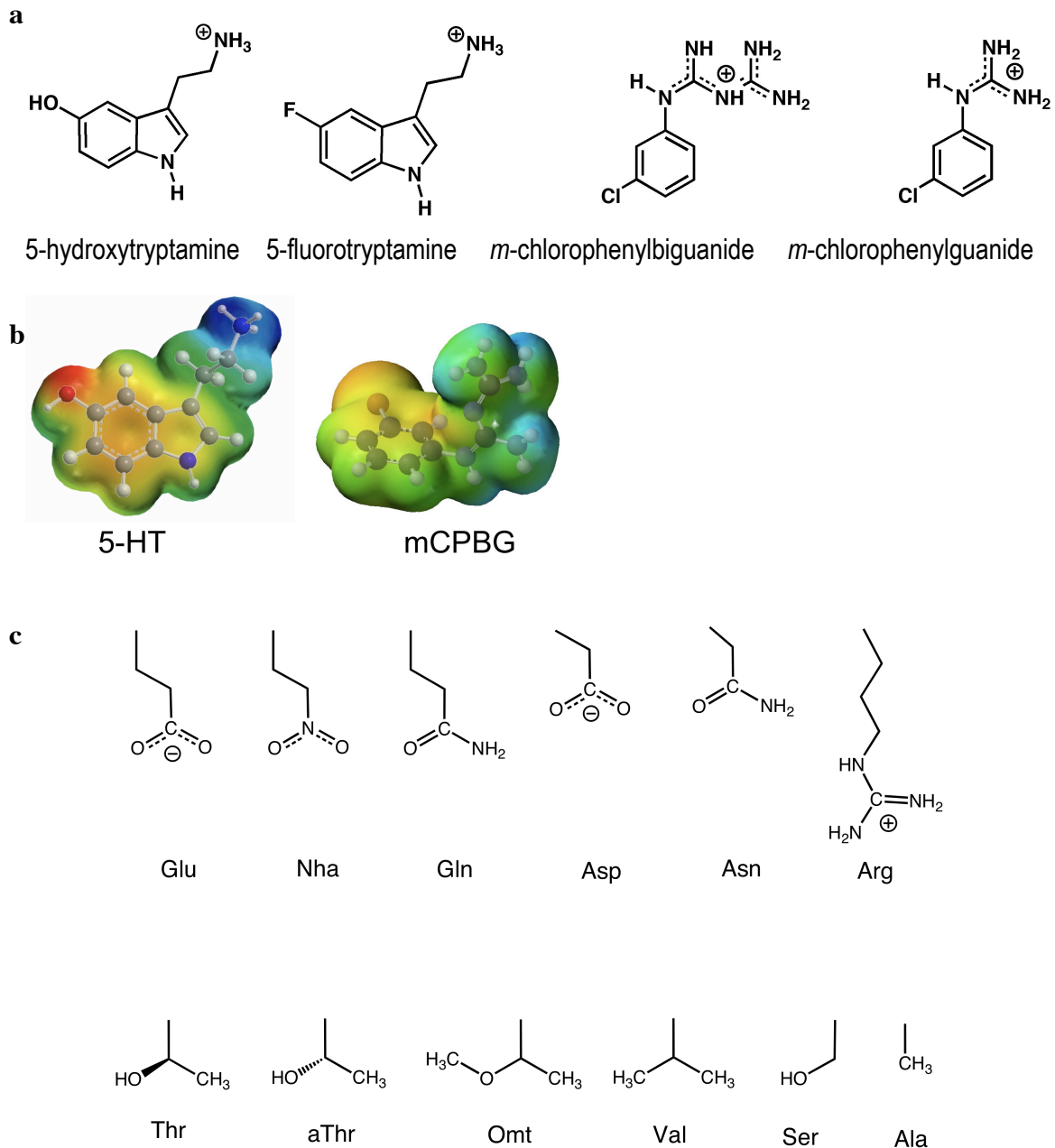
Figure 2.23. (a) Structures of agonists used in this study. **(b)** Electrostatic potential surface representations of 5-HT *m*CPBG illustrating the more diffuse positive charge of the biguanide moiety. **(c)** Side chains of conventional and unnatural mutations.

Asp229•••Arg92

In the homology model (figure 2.22b), the side chain of Asp 229 extends from the end of loop C and is in close proximity to Arg 92 on loop D of the adjacent subunit. To test for the importance of a potential ionic interaction, a classical charge-reversal experiment was performed. Using 5-HT as an agonist, some charge-reversal mutations gave nonfunctional receptors, but all mutants gave significant responses to *m*CPBG. The D229R mutation led to a 138-fold increase in EC_{50} compared to wild type; R92D led to a 35-fold increase. The EC_{50} of the double mutant D229R/R92D, however, increased EC_{50} only 24-fold. A standard mutant cycle analysis gives a coupling parameter, Ω, of 0.005, and a coupling interaction energy, $\Delta\Delta G_{int} = RT\ln(\Omega)$ of -3.1 kcal/mol.

The charge-conserving substitution D229E produced receptors with WT EC_{50}s and no shift in the relative efficacy of the partial agonists *m*CPBG or 5-FT (figure 2.24d). Substitution with nitrohomoalanine (Nha), which is isoelectronic and isosteric with glutamate but has a neutral charge, produced an 8-fold increase in EC_{50}. D229A and D229N were the most disruptive, increasing the EC_{50} 26-fold and 75-fold respectively, while D229Q raised EC_{50} only 4-fold. Smaller shifts in EC_{50} were observed for the partial agonists *m*CPBG and 5-FT than were observed for 5-HT, though the trends were the same.

The relative efficacy of *m*CPBG remained unchanged with the Glu, Gln, and Nha mutations but *increased* for D229A and D229N (to 1.4 and 4.6 respectively). These shifts may reflect a decrease in function for 5-HT rather than an increase for *m*CPBG. The

relative efficacy of 5-FT for charge-neutralizing mutations showed an opposite trend from that of *m*CPBG. D229Q and D229Nha showed a reduction in efficacy from 0.44 to 0.08 and 0.05, respectively. D229N and D229A did not give measureable responses to high concentrations (up to 2 mM) 5-FT.

Figure 2.24. Relative efficacies of *m*CPBG, calculated by dividing the maximum current induced by *m*CPBG by the maximum current induced by 5-HT applied to the same cell. N=5−15

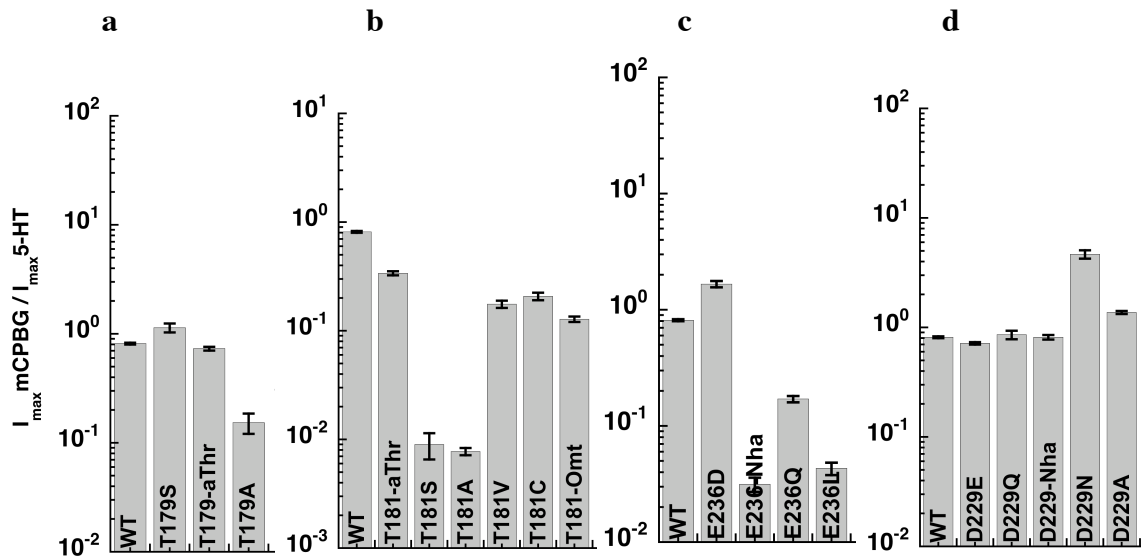| Receptor	5-HT EC$_{50}$ (µM)	n$_H$	mCPBG EC$_{50}$ (µM)	n$_H$	I$_{max}$ mCPBG/5-HT	I$_{max}$ 5-FT/5-HT
WT	1.2 ± 0.1	2.5 ± 0.1	0.62 ± 0.02	2.3 ± 0.1	0.81 ± 0.02	0.44 ± 0.04
T179-aThr	7.0 ± 0.3	2.0 ± 0.1	0.43 ± 0.02	3.1 ± 0.2	0.73 ± 0.03	-
T179S	2.4 ± 0.3	0.98 ± 0.1	0.66 ± 0.04	1.5 ± 0.1	1.1 ± 0.1	-
T179-Omt	1.1 ± 0.2	1.3 ± 0.2	-	-	-	-
T179A	2.1 ± 0.2	1.6 ± 0.2	1.1 ± 0.1	1.4 ± 0.1	0.15 ± 0.04	-
T179V	19 ± 1	1.7 ± 0.1	NR	-	-	-
T181-aThr	5.3 ± 0.2	2.5 ± 0.2	8.5 ± 0.3	1.7 ± 0.1	0.34 ± 0.02	0.052 ± 0.006
T181S	14 ± 2.0	1.4 ± 0.2	1.1 ± 0.1	1.6 ± 0.1	0.01 ± 0.01	< 0.002
T181-Omt	58 ± 4	2.7 ± 0.1	17 ± 2	1.8 ± 0.2	0.13 ± 0.02	-
T181A	25 ± 2	1.8 ± 0.1	2.4 ± 0.1	1.8 ± 0.1	0.01 ± 0.01	< 0.002
T181V	29 ± 3	1.8 ± 0.3	54 ± 5	2.9 ± 0.7	0.18 ± 0.02	0.021 ± 0.004
T181C	43 ± 5	1.8 ± 0.3	-	-	0.21 ± 0.02	-
E236V	NR	-	14 ± 1	2.2 ± 0.2	-	
E236D	15 ± 1	1.7 ± 0.2	0.48 ± 0.05	1.4 ± 0.2	1.7 ± 0.1	0.09 ± 0.02
E236-Nha	29 ± 2	1.2 ± 0.1	3.3 ± 0.2	1.7 ± 0.1	0.03 ± 0.01	NR
E236L	42 ± 3	2.1 ± 0.1	65 ± 5	2.1 ± 0.1	0.04 ± 0.01	NR
E236Q	100 ± 5	2.4 ± 0.2	61 ± 2	2.4 ± 0.1	0.17 ± 0.02	NR
E236N	NR	-	9.6 ± 0.5	2.0 ± 0.2	-	-
E236A	NR	-	NR	-	-	-
D229E	1.1 ± 0.1	2.4 ± 0.3	0.22 ± 0.02	2.1 ± 0.2	0.72 ± 0.02	0.69 ± 0.06
D229Q	4.2 ± 0.2	2.4 ± 0.2	1.8 ± 0.1	1.8 ± 0.2	0.86 ± 0.08	0.079 ± 0.008
D229-Nha	9.5 ± 0.3	1.8 ± 0.1	2.0 ± 0.1	1.9 ± 0.1	0.81 ± 0.04	0.054 ± 0.007
D229N	90 ± 4	1.9 ± 0.2	6.3 ± 0.3	1.9 ± 0.2	4.6 ± 0.5	NR
D229A	31 ± 1	2.0 ± 0.1	2.4 ± 0.1	2.3 ± 0.1	1.4 ± 0.1	NR
D229R	> 1000	-	86 ± 1	3.2 ± 0.2	-	-
R92A	11 ± 1	2.3 ± 0.2	-	-	-	0.15 ± 0.05
R92D	> 500	-	22 ± 1	2.9 ± 0.2	-	-
Y153F	27 ± 1	3.0 ± 0.2	1.8 ± 0.1	2.3 ± 0.2	0.42 ± 0.03	0.005 ± 0.002
Y153-4FPhe	28 ± 2	1.6 ± 0.1	0.52 ± 0.03	1.5 ± 0.1	2.6 ± 0.4	NR
D229A-R92A	77 ± 2	2.1 ± 0.1	0.84 ± 0.02	2.1 ± 0.1	2.1 ± 0.1	NR
D229A/Y153F	240 ± 10	2.2 ± 0.2	NR	-	34 ± 4	NR
R92A/Y153F	57 ± 2	2.0 ± 0.1	0.7 ± 0.03	1.9 ± 0.1	1.3 ± 0.1	NR
R92D/D229R	NR	-	15 ± 1	1.9 ± 0.1	-	NR
W183-4FW	3.6 ± 0.1	2.4 ± 0.2	0.47 ± 0.03	1.5 ± 0.1	0.11 ± 0.01	-
W183-5FW	5.9 ± 0.4	1.5 ± 0.2	5.8 ± 0.1	2.1 ± 0.1	-	-
W183-5BrW	73 ± 2	1.8 ± 0.1	20 ± 2	2.5 ± 4	0.65 ± 0.03	-
W183-F2W	19 ± 2	2.5 ± 0.2	2.8 ± 0.1	1.9 ± 0.1	0.39 ± 0.02	-
W183-F3W	240 ± 10	ND	9.7 ± 0.3	2.4 ± 0.1	0.51 ± 0.09	-
W183-F4W	-	-	7.3 ± 0.3	2.1 ± 0.2	-	-

Table 2.7. 5-HT and *m*CPBG EC$_{50}$ values and Hill coefficients for the majority of residues examined in this study. Data = mean ± SEM, n = 4–18. NR = no response detected.

Thr 181

Substitution of Thr by *allo*-threonine (aThr), where the stereochemistry at the beta-carbon is reversed by exchanging the positions of the OH and CH_3 groups (Fig 2.23c), increased the EC_{50} ~5-fold for 5-HT (Table 2.6). Mutation to Ser, which removes the CH_3 group but retains the hydroxyl, caused an 11-fold increase in the EC_{50}. When Thr was substituted with O-methylthreonine (Omt), we observed a 48-fold increase in EC_{50}. Incorporation of Omt results in replacement of the OH group with OCH_3, so the ability to accept a hydrogen bond is retained while the ability to donate a hydrogen bond is eliminated. A study of $5-HT_3$ expressed in HEK cells showed T181A led to a 6-fold increase in 5-HT $EC_{50(71)}$. We observed a more substantial shift of 21-fold for this mutation and similar shifts for T181V, and T181C (24-, and 36-fold respectively).

Mutations at Thr181 were more deleterious to activation of the receptor by *m*CPBG, compared to 5-HT. For this agonist, substitution by aThr and Omt led to 14- and 27-fold increases in EC_{50}, respectively. Val, which is sterically similar to Thr, increased the EC_{50} 87-fold. When the conventional mutants, T181A and T181S, were exposed to *m*CPBG, almost no activity was observed. However, the IC_{50} of *m*CPBG for either conventional mutant was similar to its EC_{50} for the WT receptor, suggesting that *m*CPBG essentially acted as a competitive antagonist. When the mutant receptors are expressed at very high levels (on the order of 100 μA of current in response to saturating 5-HT rather than the usual 2-10 μA), a small amount of receptor activation can be observed, and these *m*CPBG-induced currents have a relative efficacy of <0.01 as

compared to 5-HT (figure 2.24b). The EC_{50} values measured from the mCPBG-induced currents were close to that of WT receptors.

Application of 1 mM 5-FT to T181A and T181S mutants yielded a response less than 0.2% of that of 5-HT. Co-application of 5-FT was able to block 5-HT responses with an IC_{50} similar to the 5-FT EC_{50} indicating that, like mCPBG, 5-FT also acts as a competitive antagonist at these two mutant receptors. The more subtle aThr mutation diminished the relative efficacies of mCPBG and 5-FT to 0.34 and 0.05, respectively, levels that would be considered indicative of functional receptors.

Thr179

Overall, Thr179 is less sensitive to mutation than Thr181. The T179A, T179S, and T179Omt mutants display negligible shifts in EC_{50} (table 2.6). However, the Ala and Ser mutants displayed significantly slower kinetics of channel activation and an absence of desensitization (figure 2.25).
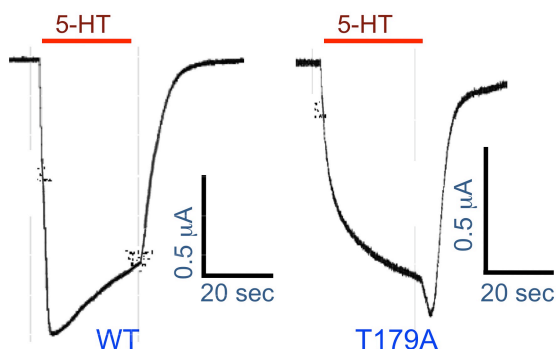
Figure 2.25. Example traces illustrating the slow kinetics of activation and lack of desensitization observed in the T179A and T179S mutants.

The relative efficacy of *m*CPBG for the T179A mutant was diminished to 0.15 (figure 2.24a). Mutation to aThr produces a 6-fold increase in EC_{50} for 5-HT but has no effect on *m*CPBG activation. T179V, which essentially replaces the hydroxyl with a methyl group, causes a 16-fold increase in 5-HT EC_{50} and a complete lack of response from *m*CPBG; *m*CPBG acts as a competitive antagonist for the T179V mutant.

Glu236

Receptor function was significantly compromised by any substitution at Glu236. The conventional mutations E236D and E236Q led to EC_{50} increases of 12- and 83-fold respectively. The substitution of the neutral but isosteric Nha, produced a 24-fold increase in EC_{50}.

*m*CPBG was less sensitive than 5-HT to changes at Glu236. E236D had a WT EC_{50} for *m*CPBG while the charge neutralizing E236Nha resulted in only a 5-fold increase in EC_{50}. The relative efficacy of *m*CPBG for E236D was unaffected while it diminished to 0.03 for E236Nha (figure 2.24c). The mutations E236N and E236V showed robust responses to *m*CPBG, but were not activated by high (2 mM) concentrations of 5-HT.

Tyr153

Previous studies have identified Tyr153 as playing a role in activation by 5-HT, serving as a hydrogen bond acceptor(72). As observed previously, we saw a 4-fold

reduction in the rate of receptor activation and large increases in 5-HT EC_{50} for the mutation Y153-4F-Phe and Y153F (23- and 24-fold respectively).

mCPBG was not as sensitive to mutations at this position. Y153-4F-Phe had a WT EC_{50} and a relative efficacy of 3.0 compared to 5-HT. Y153F led to a 3-fold increase in EC_{50} and a relative efficacy of 0.5. This mutation also gave a 3-fold increase in 5-FT EC_{50} but the relative efficacy was reduced to less than 0.01 that of 5-HT.

In the homology model, this residue is in close proximity to R92 so double mutant cycle analysis was performed on the two positions. The R92A mutation caused a 10-fold shift in EC_{50}, while the double mutant R92A/Y153F caused a 48-fold shift. For this mutant cycle, $\Omega = 0.23$, and the coupling interaction energy, $\Delta\Delta G_{int} = RTln(\Omega) = -0.9$ kcal/mol.

Trp183

Previous studies showed that progressive fluorination of Trp183 led to a systematic increase in 5-HT EC_{50}, establishing a cation-π interaction between the ammonium of 5-HT and the aromatic side chain of Trp183[10]. Interestingly, we now find that fluorination of Trp183 did not produce any clear trend in mCPBG EC_{50}. Introduction of fluorine at the 5 position increased the EC_{50} by 10-fold but fluorination at additional positions did not produce a continued increasing trend in EC_{50}. To better understand the cause of the shift from 5-F-Trp, we tested the effect of moving the

fluorine to the 4 position. The EC_{50} for 4-F-Trp was close to the WT value. To test the effect of steric differences we incorporated Trp with the larger substituent Br at the 5 position. This mutation led to a 32-fold increase in EC_{50}. The smaller agonist mCPG is less responsive to subtle changes at Trp183, but the difference between substitution at the 5 position vs. the 4 position persisted.

The efficacies of both *m*CPBG and mCPG are influenced by substitutions on the indole ring. There is some indication that, again, the 5 position is more perturbing than the 4 position, but the trend is not as clear as with the EC_{50} values.

Other Residues

Several other residues in the proximity of the binding site were examined and were found to be insensitive to mutation. Minor effects on receptor function were observed for the mutants Y73F (5-fold increase), P155V (no shift), K224M (3-fold increase), N232A (no shift), and K238M (2-fold increase).

2.5.3 Discussion

In the present work, we have performed mutational analysis at several sites in and around the putative ligand binding site of the 5-HT_3 receptor, using the agonist 5-HT and three partial agonist—5-FT, *m*CPBG, and *m*CPG. Our structure-function investigation found several polar residues that were very sensitive to subtle perturbations in structure.

For several mutations, the effects on receptor function differed between agonists. In particular, it appears that each of these residues plays an important role in receptor function, but that their roles often differ between 5-HT and *m*CPBG.

Salt Bridge between Asp 229 and Arg92

Previous studies have suggested that Asp229 plays an agonist-specific role in 5-HT$_3$ activation (64). To elucidate the role of Asp 229 and the differing effects that mutations at this position have on particular agonists, we characterized the substitutions Glu, Gln, Asn, and Nha. Mutation of D229 to Glu has only minor effects on the EC$_{50}$ and relative efficacy of the three agonists examined in this study (table 2.6, figure 2.24d). This might be expected, as Glu is the residue common at this site in other species. Mutations that neutralize charge such as Gln, Asn, or Nha all diminish receptor function but have a greater effect on the EC$_{50}$ of 5-HT than that of *m*CPBG. The wild type behavior of the Glu mutant allows a more meaningful interpretation of the unnatural amino acid Nha, which is isosteric and isoelectronic to Glu (figure 2.23c). The substantial increase in EC$_{50}$ seen with Nha indicates a clear role for charge at this position.

In the homology model, Asp229 is positioned at the most distal portion of loop C and is in close proximity (3.2 Å) to Arg92 on the opposite subunit. The possibility of a salt bridge has been proposed previously(71). To investigate the possibility of this salt bridge between these residues, we performed a charge-reversal experiment. The double mutant D229R/R92D did indeed recover function compared to either of the single

mutations, and mutant cycle analysis revealed an interaction energy of 3.1 kcal/mol. This value is within the predicted range for an ionic interaction and strongly supports the presence of an ion pair as suggested in the homology model. We propose that this ionic interaction plays an important role in the transition between closed and open states in the 5-HT$_3$R. The model used in this study is based on the structure of AChBP, which is proposed to be similar to the open or desensitized state of the nAChR(73). A recent study of the closed state (agonist unbound) of the nAChR found that Loop C points away from the center of the receptor(17). It is thought that subsequent to ligand binding, the C-loop closes over the binding pocket, a movement that may initiate receptor gating (figure 2.26). Because Asp229 is located at the end of loop C, it is expected that this residue would move significantly during the transition between closed and open states of the receptor. The increase in EC$_{50}$ observed in Asp229 mutants is consistent with a destabilization of an ionic interaction present in the open state of the receptor. While *m*CPBG was somewhat less affected by the charge reversal mutations, the EC$_{50}$ shifts of the E, Q, Nha, N, and R mutations follow the same trends. Thus, while the salt bridge may play a less significant role in the gating pathway of *m*CPBG, our results suggest that the formation of the ion pair is a general mechanism of receptor activation.
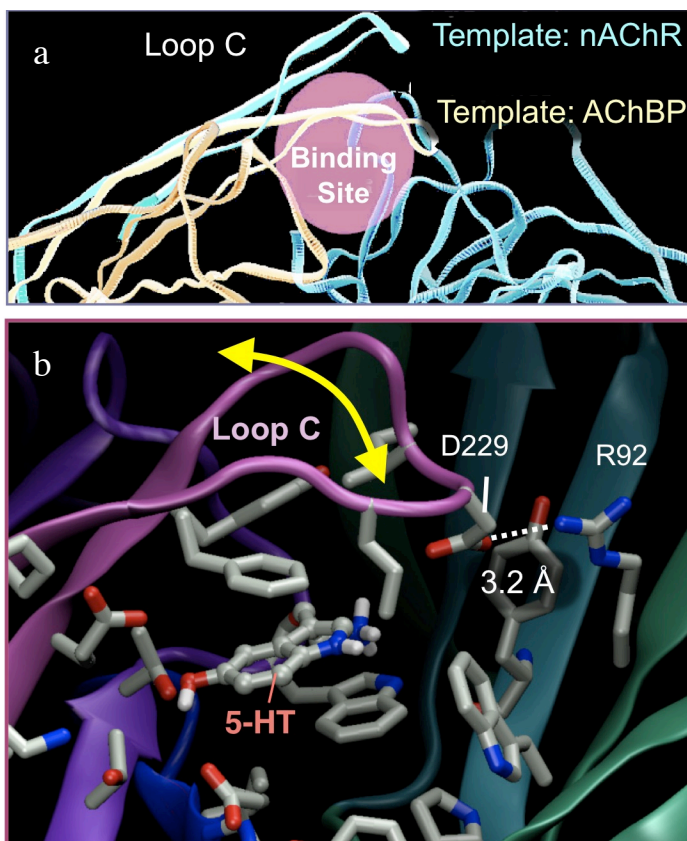
Figure 2.26. Model of 5-HT and the proposed movement of loop C during receptor gating. (**a**) Light blue: Ligand unbound structure based on nAChR with loop C positioned a greater distance from the binding site. Yellow: Ligand bound structure based on AChBP with loop C positioned close to binding site and the other subunit. Adapted from Jackson et. al., 1995.

(**b**) Movements proposed in (a) imposed upon our homology model illustrating the potential importance of interaction between D229 and R92 during the gating transition.

For each of the charge-reversal mutations, the response to agonists showed desensitization rates ~10-fold faster than wild type (figure 2.27). This observation is consistent with a destabilization of the open state in the mutant receptors, because this change would shift the equilibrium toward the desensitized state. While this shift could also be observed from a stabilization of the desensitized state, the large increases in EC_{50} in these mutations argues that a change in the open state is much more likely.
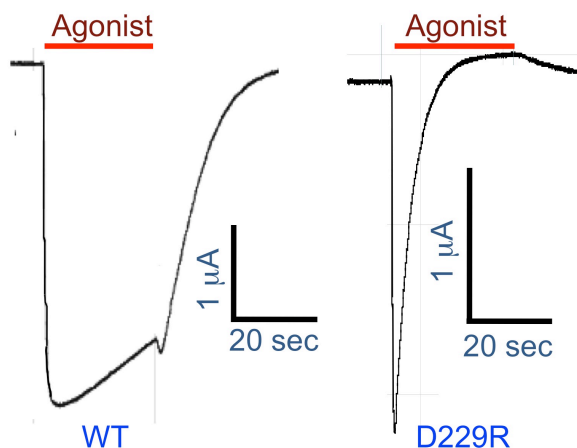
Figure 2.27. Example traces illustrating the 10-fold increase in apparent desensitization rate observed from charge reversal mutations.

Thr181 Plays an Essential Role in the Activation by Both 5-HT and mCPBG

Thr181 is located between Trp183 and β-strand 7 on loop B, which has been shown to be critical for 5-HT_3 receptor function. The side chain two residues in the C-terminal direction (Trp 183) plays a critical role in binding 5-HT through a cation-π interaction, and it could initiate the structural changes that are transmitted via β-strand 7 to the transmembrane domain in response to agonist binding (71).

Our results support a vital role for Thr181 in the activation by both 5-HT and *m*CPBG. Introduction of Omt, which retains only the ability to accept a hydrogen bond, causes 20–30 fold increases in the EC_{50} of both agonists (table 2.6). This indicates that the side chain of Thr181 likely acts as a hydrogen bond donor. Not only must the OH of Thr181 be present, but also it must be positioned properly. Swapping the OH and CH_3 groups of the side chain (aThr) increased EC_{50}, while deleting the CH_3 entirely (Ser) increased EC_{50} further. This could indicate that the increased rotational flexibility associated with the Ser side chain is deleterious to receptor function.

Taken together, the results suggest that Thr181 is a critical site that is sensitive to mutation. The OH is essential and likely involved in donating a hydrogen bond. In considering the homology model (figure 2.22b), the OH of 5-HT is, in principle, a potential hydrogen-bonding partner for Thr181. However, the significant effects on EC_{50} for mCPBG (which cannot accept a hydrogen bond) on activation kinetics, and on relative efficacies in general suggest an important role in gating rather than direct binding to agonist. Possible binding partners include the carboxylate of Glu236 and the backbone carbonyl of Ala235. Both of these potential interacting partners are on loop C, and the fact that this loop is believed to move significantly during the gating process is consistent with a role for Thr181 in gating.

A nearby threonine, Thr179, is conserved in all 5-HT_3 subunits, but not in the Cys-loop family as a whole. This residue aligns with Lys145 in nAChR, which is believed to play a role in coupling binding to gating interactions in the binding site (74).

It would appear that polarity is a key factor for Thr179. Hydrogen bond donation is ruled out by the near wild-type behavior of Omt. The increase that aThr causes for 5-HT, but not mCPBG EC_{50}, suggests that mispositioning the polar OH group of Thr179 is deleterious for 5-HT more so than for mCPBG. The strong effect of the T179V mutation, both in raising EC_{50} for 5-HT and in converting mCPBG into an antagonist, further shows that polar character at this site is essential for proper receptor function. Substitution with

residues of smaller volume at Thr179 causes a significant slowing in 5-HT activation kinetics (figure 2.25), but does not significantly change the EC_{50} of either 5-HT or *m*CPBG. This suggests that both the opening and closing rate constants are slowed (larger activation barrier), and that this residue is involved in the transition between open and closed states.

Tyr153 MayPparticipate in the Ion-pair Interaction

In the homology model, the side chain of Tyr153 is located on Loop E and is positioned close to both Asp229 and Arg92 (figure 2.22b). It was previously suggested that Tyr153 either accepts a hydrogen bond from the indole nitrogen of 5-HT, or from Arg92(72). However, we have recently shown that the indole nitrogen is not important for activation of the receptor(50). Mutant cycle analysis of the Y153A and R92A mutations gives a coupling parameter of 0.23, and a coupling interaction energy of -0.9 kcal/mol, suggestive of a modest interaction between these two residues. Considering previous evidence that Tyr153 acts as a hydrogen bond acceptor, it seems likely that Tyr153 accepts a hydrogen bond from Arg92, and participates in its role in receptor gating. Tyr153 mutations cause relatively large shifts in 5-HT EC_{50} and 5-FT efficacy while producing only small shifts in EC_{50} and efficacy of *m*CPBG. These results suggest that this residue plays a role in receptor activation that is specific to tryptamine agonists.

Glu236 is a Gating Residue

Glu236 aligns with Asp200 in the α subunit of the nAChR, which has been proposed to play an important role in gating (74). Previous studies of Glu236 in the 5-HT$_3$ receptor suggested that the residue interacts with bound ligand and is important for receptor function (69). The large effect of the Nha mutation on 5-HT EC$_{50}$ indicates that charge plays a critical role at this position. Glutamine is the conventional neutralizing mutation used to study the role of charge, but along with neutralizing the charge, these mutations replace a hydrogen bond accepting O with an NH$_2$ group, and this introduces the potential for an electrostatic clash. This is the likely explanation for the further increase in EC$_{50}$ of Gln compared to Nha. The smaller but still substantial 12-fold shift of E236D suggests that correct positioning of the carboxylic moiety is also important.

The charge neutralizing mutations E236Nha and E236Q decrease the relative efficacy of *m*CPBG, while the hydrophobic mutation E236V decreases the relative efficacy of 5-HT, essentially turning it into a competitive antagonist. Charge-neutralizing mutations also cause 5-FT to become a competitive antagonist, with IC$_{50}$ values similar to the EC$_{50}$ in wild-type receptors. For the wild-type receptor 5-FT has an EC$_{50}$ of 16 μM. These changes in the relative efficacy of partial agonists, as well as slower activation kinetics, indicate that mutations at E236 profoundly affect gating, while modestly perturbing affinity.

Large shifts in efficacy are evident for several agonists and several mutations at Glu236. Moreover, since, for a receptor that is activated by two molecules of agonist, EC_{50} tracks roughly with the square root of efficacy, much (if not all) of the changes seen in EC_{50} with Glu236 mutants can be ascribed to large changes in efficacy. We conclude that Glu236 plays an important role in receptor gating.

Trp183 Does Not Make a Cation-π Interaction to mCPBG

Previous studies established a cation-π interaction between the ammonium group of 5-HT and the indole ring of Trp183 (10). Here we have evaluated whether a comparable cation-π interaction contributes to the binding of *m*CPBG through incorporation of a series of fluorinated tryptophan residues. The lack of any clear trend in EC_{50} strongly suggests that there is no cation-π interaction with this residue. This result is particularly interesting because a cation-π interaction is critical for activation by 5-HT, and begs the question: What are the critical interactions between *m*CPBG and the 5-HT$_3$ receptor?

Comparison of 5-F-Trp and 4-F-Trp provides further evidence that *m*CPBG does not participate in a cation-π interaction with Trp183. These residues are essentially identical in their cation-π binding ability, and while they give the same 5-HT EC_{50} values, they show an almost 10-fold difference in *m*CPBG EC_{50}. All the fluorinated residues used in this study have fluorine at the 5 position except 4-F-Trp, and show a

~10-fold shift in EC_{50}. We conclude that mCPBG is sensitive to steric interactions at the 5 position of the indole ring of Trp183.

Differences among Agonists

The majority of mutations that produced a shift in the EC_{50} of mCPBG also led to shifts in its efficacy relative to 5-HT, helping to confirm that the residues investigated play at least some part in the gating pathway. For the partial agonist 5-FT, we did not observe a shift in the EC_{50} greater than 4-fold, however, the relative efficacy often decreased significantly more than mCPBG and sometimes became so inefficacious it behaved as a competitive antagonist. 5-FT is a less efficacious partial agonist than mCPBG ($R_{max} < 0.5$), and large EC_{50} shifts from gating are not expected for agonists with a gating equilibrium constant close to 1 (75). Comparing the mutations at Thr181, the pattern of relative efficacy shifts for mCPBG mirrors that of 5-FT, suggesting that this residue plays a general role in receptor gating. This is in contrast to the relative efficacy shifts observed at Asp229, where the two patterns differed significantly and suggest that this residue plays a more vital role in the activation of tryptamine-like agonists.

Almost invariably, mutations to the sites examined in this study led to increases in the EC_{50} of both 5-HT and mCPBG, but the magnitude of the effect often differed between these two agonists. This is most apparent with Trp183, which we determined does not participate in a cation-π with mCPBG as has been demonstrated previously with 5-HT. In addition to Trp183, 5-HT was also more sensitive to changes at Glu236, Y153,

and Asp229, while *m*CPBG was more sensitive to changes at Thr181. Such differences could be the result of the residues being in direct contact with agonists of differing structure, but our results, especially the large shifts in relative efficacy, argue that these residues (excluding Trp183) are involved in the gating pathway. We conclude that the observed differences between the two agonists results from the existence of two substantially different gating mechanisms that utilize the residues in the binding site vicinity in qualitatively different ways.

2.5.4 Conclusions

Our investigations of the 5-HT$_3$ receptor binding site were guided by a homology model that assisted the formulation of testable hypotheses regarding the role of specific residues in receptor function. Utilizing a combined approach of conventional mutagenesis, unnatural amino acid mutagenesis, and a variety of ligand derivatives, we were able to gain important insights into the mechanism of agonist binding and receptor activation. Some experimental results confirmed elements of the initial homology model, while other results were used to refine the model. The structure-function investigations guided changes to the sequence alignment and agonist orientation as well as sidechain and agonist conformations. The model proposed in section 2.5 (figure 2.22) is well supported by our experimental evidence as well as previous studies on the 5-HT$_3$R and other homologous receptors. Our results illustrate the important and sometimes critical roles that many of the proximal binding site residues play in agonist activation of the 5-HT$_3$ receptor and offer evidence for several specific interactions within the receptor and between the receptor and agonist. The agonist-specific effects of the binding site

mutations provide further evidence that different gating pathways are utilized by 5-HT and *m*CPBG. Information about agonist differences provides useful guidance for the development of small molecule therapies that target the 5-HT$_3$ receptor, and the studies of key binding site residues will also further the understanding of other members Cys-loop receptor family.

2.6 Materials and Methods

Materials

All cell culture reagents were obtained from Gibco BRL (Paisley, U.K.), except fetal calf serum, which was from Labtech International (Ringmer, U.K.). [³H]granisetron (63.5 Ci mmol^{-1}) was from PerkinElmer (Boston, Massachusetts, USA). 5-FT, 5-chlorotryptamine (5-ClT), 5-methyltryptamine (5-MeT), 5-methoxytryptamine (5-MeT) and tryptamine were from Sigma-Aldrich (Poole, Dorset, U.K.). All other reagents were of the highest obtainable grade.

Cell culture and Oocyte Maintenance

Human embryonic kidney (HEK) 293 cells were maintained in DMEM:F12 (Dulbecco's Modified Eagle Medium : Nutrient Mix F12 (1:1)) with GlutaMAX containing 10% fetal calf serum at 37°C and 7% CO_2 in a humidified atmosphere. *Xenopus laevis* oocyte positive females were purchased from NASCO (Fort Atkinson, Wisconsin, USA) and maintained according to standard methods (76). Harvested stage V-VI *Xenopus* oocytes were washed in six changes of ND96 (96 mM NaCl, 2 mM KCl, 1 mM $MgCl_2$, 1.8 mM $CaCl_2$, 5 mM HEPES, pH 7.5), defolliculated in 1.5 mg mL^{-1} collagenase Type 1A for approximately 2 h. Enzyme treatment was terminated by washing in six changes of ND96 and oocytes were stored in ND96 containing 2.5 mM sodium pyruvate, 50 mM gentamicin and 0.7 mM theophylline.

Mutagenesis and Receptor Expression

Mouse 5-HT$_{3A}$ (accession number: AY605711) or 5-HT$_{3B}$ (kindly provided by Ewen Kirkness) subunit cDNAs were cloned into pGEMHE for oocyte expression (77). Mutagenesis reactions were performed using the Kunkel method and confirmed by DNA sequencing. cRNA was *in vitro* transcribed from linearised (NheI) plasmid cDNA template using the mMessage mMachine T7 kit (Ambion, Austin, Texas, USA). Stage V and VI oocytes were injected with 50–100 ng cRNA, and recorded from 1 to 4 days post-injection. The unnatural amino acids nitrohomoalanine (Nha), 2-amino-4-ketopentanoic acid (Akp), allothreonine (aThr), O-methoxythreonine (Omt), and all substituted analogues of Trp and Phe were incorporated using nonsense suppression as previously described (72). For expression in HEK 293 cells, 5-HT$_3$ receptor subunit cDNAs were cloned into pcDNA3.1 (Invitrogen, Paisley, UK.). Mutagenesis reactions were performed using the Kunkel method and confirmed by DNA sequencing. Cells were transfected using calcium phosphate precipitation at 80%–90% confluency (78). Following transfection, cells were incubated for 3–4 days before assay.

Synthesis of tRNA and dCA Amino Acids

This was as described previously (72). Briefly, unnatural amino acids were chemically synthesized as nitroveratryloxycarbonyl (NVOC)-protected cyanomethyl esters and coupled to the dinucleotide dCA, which was then enzymatically ligated to 74-mer THG73 tRNA$_{CUA}$ as detailed previously (79). Immediately prior to coinjection with cRNA, aminoacyl tRNA was deprotected by photolysis (80). Typically 5 ng total cRNA was injected with 25 ng of tRNA-aa in a total volume of 50 nl. For a control cRNA was

injected with THG 74-mer tRNA (no unnatural amino acid attached) and with THG 74-mer ligated to dCA.

Characterization of Mutant Receptors

Agonist-induced currents were recorded at 22–25 ºC from individual oocytes either using conventional two-electrode voltage clamp electrophysiology or the higher-throughput automated OpusXpress system (MDS Axon Instruments) (figure 2.28); these two systems gave the same results. 5-HT, *m*-chlorophenylbiguanide (*m*CPBG), 5-fluorotryptamine (5-FT) and tryptamine were stored as 20-100 mM aliquots at -20 ºC, diluted in Ca-free ND96 buffer (96 mM NaCl, 2 mM KCl, 1 mM $MgCl_2$, 5 mM HEPES, pH 7.5). Glass microelectrodes were backfilled with 3 M KCl and had a resistance of ~1 MΩ. The holding potential was -60 mV.

Figure 2.28. The Opus Express system used for most experiments requiring two-electrode voltage clamp electrophysiology.

Data obtained from dose-response experiments were normalized by dividing the peak current at each concentration by the largest peak current observed for a particular oocyte. Normalized data were then plotted as a dose-response curve with the agonist concentration on the x-axis plotted on a logarithmic scale. To determine EC_{50} values, concentration-response data were fitted to the four-parameter logistic equation, $I = I_{min} + (I_{max} - I_{min})/(1+10^{(\log(EC50-[A])nH)})$, where I_{max} is the maximal response plateau, I_{min} is the minimum response plateau, $[A]$ is the log concentration of agonist and nH is the Hill coefficient, using PRISM v4.03 software (GraphPad, San Diego, CA). The value 'n' is

the Hill coefficient. This parameter gives information about the cooperativity of binding. In Cys-loop receptors, which have at least two agonist binding sites, the Hill coefficient is usually greater than one, indicating cooperative binding.

Relative efficacies of the partial agonists mCPBG, 5-FT and tryptamine are reported as $R_{max} = I_{max}drug/I_{max}5$-HT. One-way ANOVAs were performed with Dunnett's post test to determine statistical significance. Data are quoted as mean $\pm$ SEM (n) unless otherwise stated.

Drug Dilutions

All drug dilutions were prepared in the appropriate buffer from stock solutions (figure 2.29). For dose-response experiments, 1 ml of each drug solution was applied to the cells in a total of 30 seconds. Between 9 and 14 concentrations of agonist were used for dose-response experiments depending upon several factors including previous information about EC_{50}, the required accuracy of measurement, and oocyte health.
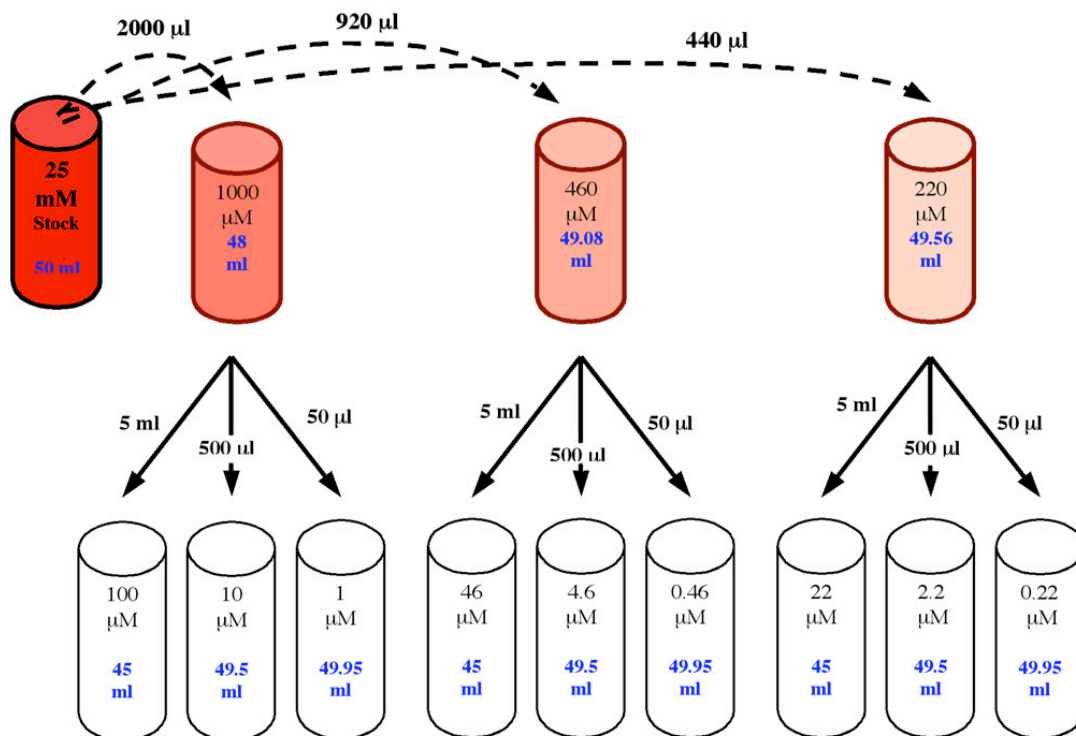
Figure 2.29. Dilution protocol used to make drug solutions for dose-response experiments.

[³H]granisetron Binding to Oocytes

For single point radioligand binding assays, 20-40 oocytes were homogenized in 200 μl 10 mM HEPES (pH 7.4) containing protease inhibitors (1 mM EDTA, 50 μg/ml soybean trypsin inhibitor, 50 μg/ml bacitracin, 0.1 mM PMSF) and 1% Triton X-100. Following a 10 min incubation at room temperature, oocyte yolk proteins were pelleted by centrifugation at 13,000 g for 10 min. The supernatant was retained, avoiding the uppermost lipid layer. Single point assays were performed in 500 μl 10 mM HEPES pH 7.4 containing 25 μl oocyte preparation and 0.5 nM [³H]granisetron (63.5 Ci/mmol; Perkin Elmer). Non-specific binding was determined using 10 μM quipazine (Tocris). Tubes were incubated at 4°C for 1 h before bound radioligand was harvested by rapid

filtration onto GF/B filters pre-soaked in 0.3% polyethylenemine. Filters were then washed with two 3 ml washes of ice-cold HEPES buffer and left in 3 ml scintillation fluid (Ecoscint A; National Diagnostics) for at least 4 h before scintillation counting to determine amounts of membrane-bound radioligand.

Radioligand Binding in HEK 293 Cells

Radioligand binding was undertaken in HEK 293 cells which provide an established and robust method of studying ligand binding. Methods were as previously described (81), with minor modifications. Briefly, transfected HEK 293 cells were washed twice with phosphate buffered saline (PBS) at room temperature and scraped into 1 ml of ice-cold HEPES buffer (10 mM, pH 7.4) containing the following proteinase inhibitors (PI): 1 mM EDTA, 50 µg ml^{-1} soybean trypsin inhibitor, 50 µg/ml bacitracin and 0.1 mM phenylmethylsulphonyl fluoride. After thawing, they were washed with HEPES buffer, resuspended, and 50 µg of cell membranes incubated in 0.5 ml HEPES buffer containing 0.5 nM [^{3}H]granisetron (a concentration approximately equivalent to the K_d); non-specific binding was determined using 10 µM quipazine. Competition binding was performed using ligand concentrations from 0.1 µM to 10 mM. Reactions were incubated for at least 1 h at 4°C and terminated by vacuum filtration using a Brandel cell harvester onto GF/B filters pre-soaked in 0.3% polyethyleneimine. Radioactivity was determined by scintillation counting using a Beckman LS6000SC (Fullerton, California, USA). Competition binding data were analyzed by iterative curve fitting (GraphPad Prism v3.02, GraphPad Software, San Diego, California, USA), according to the equation:

$$y = B_{\min} + \frac{B_{\max} - B_{\min}}{1 + 10^{[L] - \log IC_{50}}} \quad ,$$

where $B_{\min}$ is the lowest total binding, $B_{\max}$ is the maximum specific binding at equilibrium, $[L]$ is the concentration of competing ligand, and IC_{50} is the concentration of competing ligand that blocks half of the specific bound radioligand. K_i values were estimated from IC_{50} values using the Cheng-Prusoff equation:

$$K_i = \frac{IC_{50}}{1 + [L] / K_d} \quad ,$$

where K_i is the equilibrium dissociation constant for binding of the unlabeled antagonist, $[L]$ is the concentration of radioligand, and K_d is the equilibrium dissociation constant of the radioligand.

Modeling

The modeling was performed as described previously (43). Briefly, an alignment of the mouse 5-HT$_{3A}$ receptor extracellular domain (accession number: Q6J1J7) with the *Lymnaea stagnalis* AChBP (accession number P58154) was performed using ClustalX and then modified by the insertion of a single amino acid gap in the AChBP sequence following D85 (WVPD-LAAYNAISKP) and a single amino acid gap in the 5-HT$_3$ receptor subunit sequence following V131 (WVPDILINEFV-DVG). The new model of the 5-HT$_3$ receptor extracellular domain based on the AChBP structure (PDB ID 1I9B) was then built using MODELLER 6v2 (82) as described previously (15).

2.7 References

1. Lester, H. A., Dibas, M. I., Dahan, D. S., Leite, J. F., and Dougherty, D. A. (2004) *Trends Neurosci* **27**(6), 329-336

2. Corringer, P. J., Le Novere, N., and Changeux, J. P. (2000) *Annu Rev Pharmacol Toxicol* **40**, 431-458

3. Hucho, F., and Weise, C. (2001) *Angew. Chem. Int. Ed.* **40**, 3100-3116

4. Jackson, M. B., and Yakel, J. L. (1995) *Annu Rev Physiol* **57**, 447-468

5. Lummis, S. C. (2004) *Biochem Soc Trans* **32**(Pt3), 535-539

6. Ranganathan, R., Cannon, S. C., and Horvitz, H. R. (2000) *Nature* **408**(6811), 470-475

7. Reeves, D. C., and Lummis, S. C. (2002) *Mol Membr Biol* **19**(1), 11-26

8. Reeves, D. C., Sayed, M. F., Chau, P. L., Price, K. L., and Lummis, S. C. (2003) *Biophys J* **84**(4), 2338-2344

9. Thompson, A. J., Price, K. L., Reeves, D. C., Chan, S. L., Chau, P. L., and Lummis, S. C. (2005) *J Biol Chem* **280**(21), 20476-20482

10. Beene, D. L., Brandt, G. S., Zhong, W., Zacharias, N. M., Lester, H. A., and Dougherty, D. A. (2002) *Biochemistry* **41**(32), 10262-10269

11. Brejc, K., van Dijk, W. J., Klaassen, R. V., Schuurmans, M., van Der Oost, J., Smit, A. B., and Sixma, T. K. (2001) *Nature* **411**(6835), 269-276

12. Cromer, B. A., Morton, C. J., and Parker, M. W. (2002) *Trends Biochem Sci* **27**(6), 280-287

13. Le Novere, N., Grutter, T., and Changeux, J. P. (2002) *Proc Natl Acad Sci U S A* **99**(5), 3210-3215

14. Maksay, G., Bikadi, Z., and Simonyi, M. (2003) *J Recept Signal Transduct Res* **23**(2-3), 255-270

15. Reeves, D. C., Sayed, M. F., Chau, P. L., Price, K. L., and Lummis, S. C. (2003) *Biophys J* **84**(4), 2338-2344

16. Schapira, M., Abagyan, R., and Totrov, M. (2002) *BMC Struct Biol* **2**, 1

17. Unwin, N. (2005) *J Mol Biol* **346**(4), 967-989

18. Dellisanti, C. D., Yao, Y., Stroud, J. C., Wang, Z. Z., and Chen, L. (2007) *Nat Neurosci* **10**(8), 953-962

19. Dougherty, D. A., and Lester, H. A. (2001) *Nature* **411**(6835), 252-253, 255

20. Changeux, J. P., Bessis, A., Bourgeois, J. P., Corringer, P. J., Devillers-Thiery, A., Eisele, J. L., Kerszberg, M., Lena, C., Le Novere, N., Picciotto, M., and Zoli, M. (1996) *Cold Spring Harb Symp Quant Biol* **61**, 343-362

21. Ortells, M. O., and Lunt, G. G. (1995) *Trends Neurosci* **18**(3), 121-127

22. Gurley, D. A., and Lanthorn, T. H. (1998) *Neurosci Lett* **247**(2-3), 107-110

23. Blanton, M. P., McCardy, E. A., Fryer, J. D., Liu, M., and Lukas, R. J. (2000) *Eur J Pharmacol* **389**(2-3), 155-163

24. Maksay, G. (1998) *Neuropharmacology* **37**(12), 1633-1641

25. Ye, J. H., Hunt, T., Wu, W. H., and McArdle, J. J. (1997) *Eur J Pharmacol* **337**(1), 87-94

26. Greenshaw, A. J., and Silverstone, P. H. (1997) *Drugs* **53**(1), 20-39

27. Macleod, A. D. (2000) *J Pain Symptom Manage* **20**(5), 388-391

28. Costall, B., and Naylor, R. J. (2004) *Curr Drug Targets CNS Neurol Disord* **3**(1), 27-37

29. Davies, P. A., Pistis, M., Hanna, M. C., Peters, J. A., Lambert, J. J., Hales, T. G., and Kirkness, E. F. (1999) *Nature* **397**(6717), 359-363

30. Maricq, A. V., Peterson, A. S., Brake, A. J., Myers, R. M., and Julius, D. (1991) *Science* **254**(5030), 432-437

31. Niesler, B., Frank, B., Kapeller, J., and Rappold, G. A. (2003) *Gene* **310**, 101-111

32. Boyd, G. W., Doward, A. I., Kirkness, E. F., Millar, N. S., and Connolly, C. N. (2003) *J Biol Chem* **278**(30), 27681-27687

33. Barrera, N. P., Herbert, P., Henderson, R. M., Martin, I. L., and Edwardson, J. M. (2005) *Proc Natl Acad Sci U S A* **102**(35), 12595-12600

34. Davies, P. A., Pistis, M., Hanna, M. C., Peters, J. A., Lambert, J. J., Hales, T. G., and Kirkness, E. F. (1999) *Nature* **397**(6717), 359-363.

35. Dubin, A. E., Huvar, R., D'Andrea, M. R., Pyati, J., Zhu, J. Y., Joy, K. C., Wilson, S. J., Galindo, J. E., Glass, C. A., Luo, L., Jackson, M. R., Lovenberg, T. W., and Erlander, M. G. (1999) *J Biol Chem* **274**(43), 30799-30810.

36. Brady, C. A., Stanford, I. M., Ali, I., Lin, L., Williams, J. M., Dubin, A. E., Hope, A. G., and Barnes, N. M. (2001) *Neuropharmacology* **41**(2), 282-284.

37. Bower, K. S., Price, K. L., Sturdee, L. E., Dayrell, M., Dougherty, D. A., and Lummis, S. C. (2008) *Eur J Pharmacol* **580**(3), 291-297

38. Sanger, G. J., and Nelson, D. R. (1989) *Eur J Pharmacol* **159**(2), 113-124

39. Butler, A., Hill, J. M., Ireland, S. J., Jordan, C. C., and Tyers, M. B. (1988) *Br J Pharmacol* **94**(2), 397-412

40. Camilleri, M., Northcutt, A. R., Kong, S., Dukes, G. E., McSorley, D., and Mangel, A. W. (2000) *Lancet* **355**(9209), 1035-1040

41. Yoshida, S., Shiokawa, S., Kawano, K., Ito, T., Murakami, H., Suzuki, H., and Sato, Y. (2005) *J Med Chem* **48**(22), 7075-7079

42. Campiani, G., Cappelli, A., Nacci, V., Anzini, M., Vomero, S., Hamon, M., Cagnotto, A., Fracasso, C., Uboldi, C., Caccia, S., Consolo, S., and Mennini, T. (1997) *J Med Chem* **40**(22), 3670-3678

43. Sullivan, N. L., Thompson, A. J., Price, K. L., and Lummis, S. C. (2006) *Mol Membr Biol* **23**(5), 442-451

44. van Hooft, J. A., and Vijverberg, H. P. (1996) *Br J Pharmacol* **117**(5), 839-846

45. Dunitz, J. D. (2004) *Chembiochem* **5**(5), 614-621

46. Talley, N. J. (1992) *Aliment Pharmacol Ther* **6**(3), 273-289

47. Sato, Y., Yamada, M., Yoshida, S., Soneda, T., Ishikawa, M., Nizato, T., Suzuki, K., and Konno, F. (1998) *J Med Chem* **41**(16), 3015-3021

48. Sato, Y., Imai, M., Amano, K., Iwamatsu, K., Konno, F., Kurata, Y., Sakakibara, S., Hachisu, M., Izumi, M., Matsuki, N., and Saito, H. (1997) *Biol Pharm Bull* **20**(7), 752-755

49. Consolo, S., Bertorelli, R., Russi, G., Zambelli, M., and Ladinsky, H. (1994) *J Neurochem* **62**(6), 2254-2261

50. Kedrowski, S. M., Bower, K. S., and Dougherty, D. A. (2007) *Org Lett* **9**(17), 3205-3207

51. Hallmann, G. H., K. (1963) *Annalen Der Chemie-Justus Leibig* **662**, 147

52. Pinder, R. M., Green, D. M., and Thompson, P. B. (1971) *J Med Chem* **14**(17), 626-628

53. Lummis, S. C. (2005) Personal Communication.

54. Price, K. L., Bower, K. S., Thompson, A. J., Lester, H. A., Dougherty, D. A., and Lummis, S. C. (2008) *Biochemistry* **47**(24), 6370-6377

55. Boess, F. G., Steward, L. J., Steele, J. A., Liu, D., Reid, J., Glencorse, T. A., and Martin, I. L. (1997) *Neuropharmacology* **36**(4-5), 637-647

56. Boileau, A. J., Newell, J. G., and Czajkowski, C. (2002) *J Biol Chem* **277**(4), 2931-2937

57. Chakrapani, S., Bailey, T. D., and Auerbach, A. (2003) *J Gen Physiol* **122**(5), 521-539

58. Steward, L. J., Boess, F. G., Steele, J. A., Liu, D., Wong, N., and Martin, I. L. (2000) *Mol Pharmacol* **57**(6), 1249-1255

59. Cohen, J. B., Sharp, S. D., and Liu, W. S. (1991) *J Biol Chem* **266**(34), 23354-23364

60. Sullivan, D. A., and Cohen, J. B. (2000) *J Biol Chem* **275**(17), 12651-12660

61. Celie, P. H., van Rossum-Fikkert, S. E., van Dijk, W. J., Brejc, K., Smit, A. B., and Sixma, T. K. (2004) *Neuron* **41**(6), 907-914

62. Padgett, C. L., Hanek, A. P., Lester, H. A., Dougherty, D. A., and Lummis, S. C. (2007) *J Neurosci* **27**(4), 886-892

63. Paul, M., Callahan, R., Au, J., Kindler, C. H., and Yost, C. S. (2005) *Anesth Analg* **101**(3), 715-721, table of contents

64. Suryanarayanan, A., Joshi, P. R., Bikadi, Z., Mani, M., Kulkarni, T. R., Gaines, C., and Schulte, M. K. (2005) *Biochemistry* **44**(25), 9140-9149

65. Galzi, J. L., Edelstein, S. J., and Changeux, J. (1996) *Proc Natl Acad Sci U S A* **93**(5), 1853-1858

66. Aylwin, M. L., and White, M. M. (1994) *FEBS Lett* **349**(1), 99-103

67. Akk, G., Zhou, M., and Auerbach, A. (1999) *Biophys J* **76**(1 Pt 1), 207-218

68. Cashin, A. L., Torrice, M. M., McMenimen, K. A., Lester, H. A., and Dougherty, D. A. (2007) *Biochemistry* **46**(3), 630-639

69. Schreiter, C., Hovius, R., Costioli, M., Pick, H., Kellenberger, S., Schild, L., and Vogel, H. (2003) *J Biol Chem* **278**(25), 22709-22716

70. Thompson, A. J., Chau, P. L., Chan, S. L., and Lummis, S. C. (2006) *Biophys J* **90**(6), 1979-1991

71. Thompson, A. J., Lochner, M., and Lummis, S. C. (2008) *Biophys J*

72.   Beene, D. L., Price, K. L., Lester, H. A., Dougherty, D. A., and Lummis, S. C. (2004) *J Neurosci* **24**(41), 9097-9104

73.   Grutter, T., and Changeux, J. P. (2001) *Trends Biochem Sci* **26**(8), 459-463

74.   Mukhtasimova, N., Free, C., and Sine, S. M. (2005) *J Gen Physiol* **126**(1), 23-39

75.   Colquhoun, D. (1998) *Br J Pharmacol* **125**(5), 924-947

76.   Goldin, L. R. (1992) **207**, 267-279

77.   Liman, E. R., Tytgat, J., and Hess, P. (1992) *Neuron* **9**(5), 861-871

78.   Jordan, M., Schallhorn, A., and Wurm, F. M. (1996) *Nucleic Acids Res* **24**(4), 596-601

79.   Nowak, M. W., Kearney, P. C., Sampson, J. R., Saks, M. E., Labarca, C. G., Silverman, S. K., Zhong, W., Thorson, J., Abelson, J. N., Davidson, N., Schultz, P. G., Dougherty, D. A., and Lester, H. A. (1995) *Science* **268**(5209), 439-442

80.   Kearney, P. C., Nowak, M. W., Zhong, W., Silverman, S. K., Lester, H. A., and Dougherty, D. A. (1996) *Mol Pharmacol* **50**(5), 1401-1412

81.   Lummis, S. C., Sepulveda, M. I., Kilpatrick, G. J., and Baker, J. (1993) *Eur J Pharmacol* **243**(1), 7-11.

82.   Sali, A., and Blundell, T. L. (1993) *J Mol Biol* **234**(3), 779-815

Chapter 3

Probing the Binding Sites of GPCRs Using Unnatural Amino Acids: The Role of the Cation-π Interaction

Reproduced in part from (1)

3.1 Introduction

G-protein-coupled receptors (GPCRs) represent the largest family of transmembrane receptor proteins in the human genome and constitute a prominent class of targets for the pharmaceutical industry(2-4). These receptors share a topology consisting of seven transmembrane helices. In 2007, of 324 molecular drug targets, 25% of approved pharmaceuticals targeted GPCRs(5). This large proportion is due in part to the number and diversity of cellular pathways linked to GPCR activation. These receptors can be activated by a diverse array of stimuli such as neurotransmitters, peptides, odorants, proteins, lipids, and photons. The signaling pathways activated are involved in processes such as vision, olfaction, taste, memory, drug addiction, and the regulation of cardiac function (3, 6, 7). Accordingly, they have been studied extensively throughout academia and industry, utilizing the full range of chemical, biochemical, and biophysical techniques.

GPCR signaling begins with an extracellular stimulus such as ligand binding. The binding of ligand induces a conformational change in the transmembrane helices and shifts the equilibrium from the inactive to the active receptor conformation. In the active conformation, the intracellular face of the receptor binds heterotrimeric G-proteins (α, β, and γ subunits)(8). The binding of G-protein facilitates the exchange of GDP for GTP in the Gα subunit and dissociation from the G$\beta\gamma$ subunits. The dissociated Gα and G$\beta\gamma$ subunits can then each act on numerous different cellular pathways. There are several different Gα subfamilies, and each one acts on different effectors. G$_s$ activates adenyl

cyclase, G_i inhibits adenyl cyclase (AC), G_q modulates phospholipase C (PLCβ), $G_{12/13}$

mediates Rho GTPase activity, and $G_{i/o}$ gates G-protein activated inward rectifying

potassium channels (GIRKs) and inhibits AC (9). Hydrolysis of GTP within the Gα

subunit leads to reassociation of the Gα and Gβγ subunits and the termination of G

protein signaling (figure 3.1).

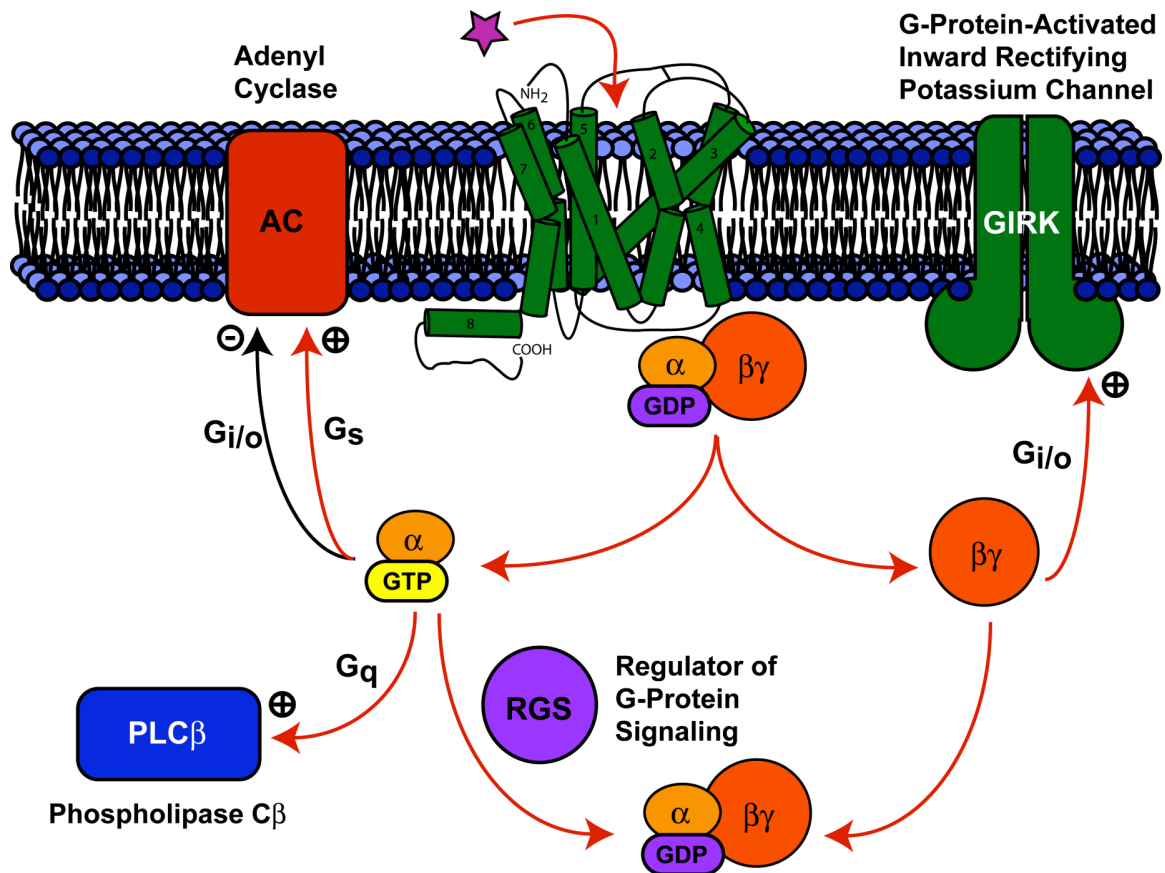**Figure 3.1**. GPCR signaling (figure courtesy of Dr. Michael Torrice).

The aminergic class of GPCRs respond to the monoamine neurotransmitters, such

as epinephrine, acetylcholine, serotonin, and dopamine. These receptors belong to class

A, which also includes rhodopsin and the olfactory receptors. In recent years the field

has been energized by several high-resolution crystal structures of mammalian GPCRs

that build on the earlier, highly informative structural studies of rhodopsin and bacteriorhodopsin (10-15).

The ligand binding site of aminergic GPCRs is a crevice formed between the seven transmembrane helices (16, 17) (figure 3.2). Key elements of this site include a cluster of conserved aromatic residues and a highly conserved Asp on TM3, D3.32. This numbering uses the one-letter amino acid code, the helix number (1-7), and a residue index number. To index each residue of a helix, the most conserved residue in the helix is denoted as 50 and all other residues are numbered N-terminal to C-terminal accordingly. For example, D3.32 refers to an Asp residue on TM3, 18 residues in the N-terminal direction from the highly conserved Arg residue, R3.50. It is generally accepted that the negative charge of D3.32 interacts with the positively charged amine group of the aminergic ligands. Indeed, the 3 crystal structures of adrenergic receptors show the ligand interacting directly with D3.32(12-14).
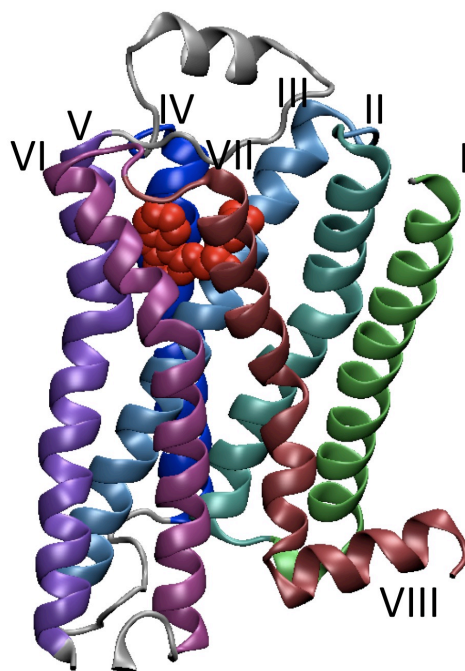

Figure 3.2. Structure of the β2AR. TM helices are labeled I through VIII. Bound inverse agonist Carazolol shown in red.

In receptors that bind catechol-containing agonists (dopamine and epinephrine) there is a set of conserved Ser residues on TM5 (S5.46 and S5.43). The hydroxyls of these serines are proposed to hydrogen bond with the two hydroxyls of the catechol moiety.

The structural snapshots provided by crystallography greatly enhance our understanding of specific receptors, but also raise many new issues. Key among these is the extent to which the information from available structures can be extrapolated to the hundreds of other GPCRs. In addition, a key goal in the study of GPCRs—and all receptors—is a description of the interconversions among several structural states that underlie the protein's biological function. It can be a challenging task to deduce a signaling mechanism from static images. As such, structure-function studies, guided by the new structural advances, will remain an important tool in evaluating GPCR function and the nature of drug-receptor interactions in this family.

In recent years, unnatural amino acid mutagenesis on ion channels and receptors expressed in *Xenopus* oocytes has provided a powerful tool for uncovering crucial drug-receptor interactions and signaling mechanisms (18, 19). The method has been especially successful in highlighting the distinctions among related members of a receptor family and in providing insights into the extent to which structural studies of model systems directly apply to related receptors. GPCRs present an especially attractive target for unnatural amino acid mutagenesis, given the importance of the family, the significant

pharmacological variations among closely related family members, and the central role of structural rearrangements in their biological function.

Incorporating unnatural amino acids into GPCRs, however, presents unique challenges. Most unnatural amino acid mutagenesis studies in eukaryotic cells have focused on ion channels. These studies exploit the exquisite sensitivity of electrophysiology, which allows for detailed characterization even when only small quantities of protein are produced, as is often the case with unnatural amino acid mutagenesis. Because GPCRs are not ion channels and instead produce downstream signals though second messenger systems, a direct readout of GPCR activation during an unnatural amino acid experiment is not possible.

This chapter describes the first general strategy for chemical-scale studies of GPCRs using unnatural amino acid incorporation in a vertebrate cell. Electrophysiology again provides the functional readout, through downstream activation of a K^+ channel. Utilizing this system we investigated several key aromatic amino acids in the agonist-binding region of the D2 dopamine receptor and M_2 muscarinic acetylcholine (ACh) receptor. We find that W6.48, a residue long postulated to play an important role in signaling, makes a cation-π interaction to dopamine in the active state of the D2 receptor. Interestingly, ACh does not make the same interaction to the conserved W6.48 of the M_2 receptor. We also identify F6.51 and F6.52 as critical residues in the activation of the D2 receptor by dopamine.

3.2 Results

Optimization of a GPCR Readout System

We have developed a robust assay for studying GPCRs containing unnatural amino acids expressed in *Xenopus* oocytes. A large portion of the work on assay optimization was done by Dr. Michael Torrice. Key issues are described here; full details can be found elsewhere (20).

We began with an established readout system based on a G-protein-coupled, inward-rectifying K^+ channel (GIRK). Upon activation of a $G_{i/o}$-coupled receptor, $G\beta\gamma$ subunits dissociate from the GPCR, bind to, and activate the GIRK channel; $G\alpha$ subunits also alter channel activation (21-24). This is the least complex known pathway from a GPCR to a channel, providing, in principle, a straightforward electrophysiological assay for GPCR activation.

Figure 3.3 illustrates the basic procedure we used in our GPCR-GIRK1/4 assays. The basal K^+ current ($I_{K,Basal}$) results primarily from the presence of free intracellular $G\beta\gamma$(25,26). The agonist-induced current ($I_{K,Agonist}$) is measured relative to this basal K^+ current. Because GIRKs do not pass significant currents under our standard conditions (ND96 with 2mM KCl), we use a ringer solution with a high (24 mM) potassium concentration. This shifts the equilibrium to favor passage of K^+ ions into the cell, with

current magnitudes sufficient for measurement by voltage-clamp electrophysiology at a
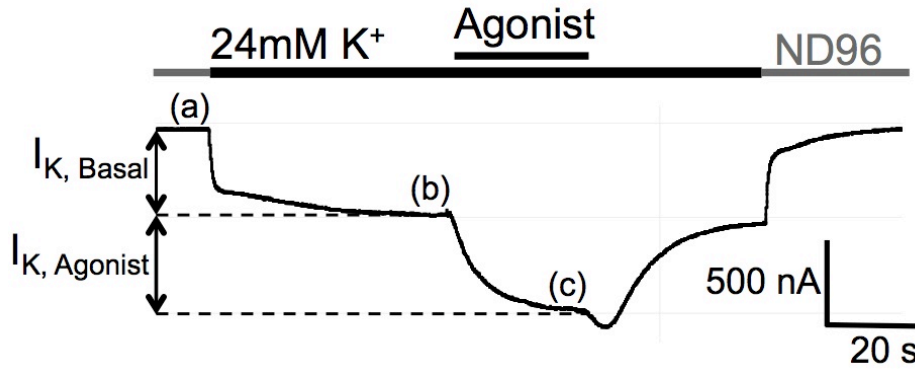
modest holding potential (-60 mV).

Figure 3.3. Example current traces during a GPCR voltage-clamp experiment in a *Xenopus* oocyte. The GIRK1/4 heterotetrameric channel is chosen because it displays relatively low basal activity. The holding potential is -60 mV throughout. ND96 solution at (a) has 2 mM K^+. Introduction of a 24 mM K^+ Ringer solution shifts the ionic equilibrium to favor inward GIRK channel currents (b). 10 mM dopamine ("agonist") is applied to expressed D2 dopamine receptors in the presence of the high- K^+ Ringer, yielding a steady-state current at (c). $I_{K, Basal}$ is defined as the current difference between (b)and (a); subtraction of (b) from (c) yields $I_{K, Agonist}$

The challenge in implementing this system was to ensure that agonist dose-response relationships provided direct assays of GPCR activation. To yield reproducible data, the assay system was first optimized in experiments expressing M_2 receptors, and the findings then accommodated into the D2 receptor system.

RGS4 and Current Trace Kinetics

In order to minimize dose-response variability, we sought uniform current traces that reached a maximum $I_{K,Agonist}$ level quickly (~1s). In previous studies, RGS proteins

were shown to accelerate the deactivation kinetics of GIRK currents via Gα-mediated GTP hydrolysis, while also increasing the activation rates of GIRK currents (26-28). In addition, it has been proposed that RGS4 not only acts as a GAP, but also serves as scaffolding for a signaling complex between the GPCR, G-protein, and GIRK channel. This scaffolding could also accelerate activation kinetics by maintaining the signaling partners in close proximity. In the D2 receptor system, adding RGS4 does indeed result in faster activation kinetics in $I_{K,Agonist}$ traces (figure 3.4). Injection of 10 ng of RGS4 increased activation rates 2.4-fold. Though the faster activation may help in creating reproducible dose-response curves, RGS4 was not included in the injection protocol because it decreased the already low expression of the D2 receptors.

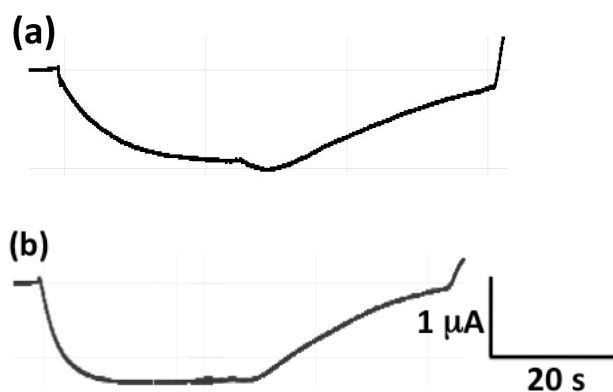**Figure 3.4.** RGS4 increases the activation kinetics of dopamine–induced currents. **(a)** 0ng RGS4 mRNA. **(b)**10 ng RGS4 mRNA.

Variability and Expression Levels

Lower levels of expression are often observed using the nonsense suppression methodology. This was a particular problem when attempting to use this method to express the D2 dopamine receptor, and we often observed agonist-induced GIRK1/4

currents that were too small to measure accurate EC_{50} values. To increase expression levels of the D2 dopamine receptor, we employed two injections of suppressor tRNA. The first injection occurred 48 h prior to recording and included the aminoacyl tRNA, along with the D2 receptor and GIRK mRNAs. The second tRNA-only injection, occurred 24 h before the assay. We evaluated this protocol using nonsense suppression at several sites, including F5.47 and W6.48. In both cases we observed significant increases in $I_{K,Agonist}$ levels with the second tRNA injection.

Considerable variability was seen from oocyte to oocyte in single-cell EC_{50} values (cEC_{50}), as quantified by the coefficient of variation (CV), defined as the ratio of the standard deviation to the mean of a population. Optimization using M_2 receptor system revealed that CV is affected by the ratio of mutant receptor to GIRK1/4 mRNAs used, with smaller ratios producing smaller CVs. At mRNA ratios below 1, expression efficiency of the receptor was quite low and irregular. In the D2 receptor system $I_{K,Agonist}$ levels were consistently lower than those for the M2 receptor, prompting the use of a different mRNA ratio. Adequate expression in the D2 system was achieved by increasing the amount of D2 receptor mRNA and suppressor tRNA 4-fold. Perhaps because of the lower expression levels, including RGS4 affected response waveforms only weakly. Thus, conditions used for D2 receptor experiments were: 40 ng of stop codon mutant D2 receptor mRNA, 10 ng each of GIRK1 and GIRK4 mRNA, and 100 ng of suppressor tRNA 48h prior to recording. Twenty-four hours later, we inject an additional 100 ng of aminoacyl tRNA. These conditions resulted in adequate GIRK currents and cell-to-cell

CVs ranging from 0.21 to 0.46, which are adequate for meaningfully interpreting variations (>3-fold) in EC_{50} among mutants (figure 3.5).
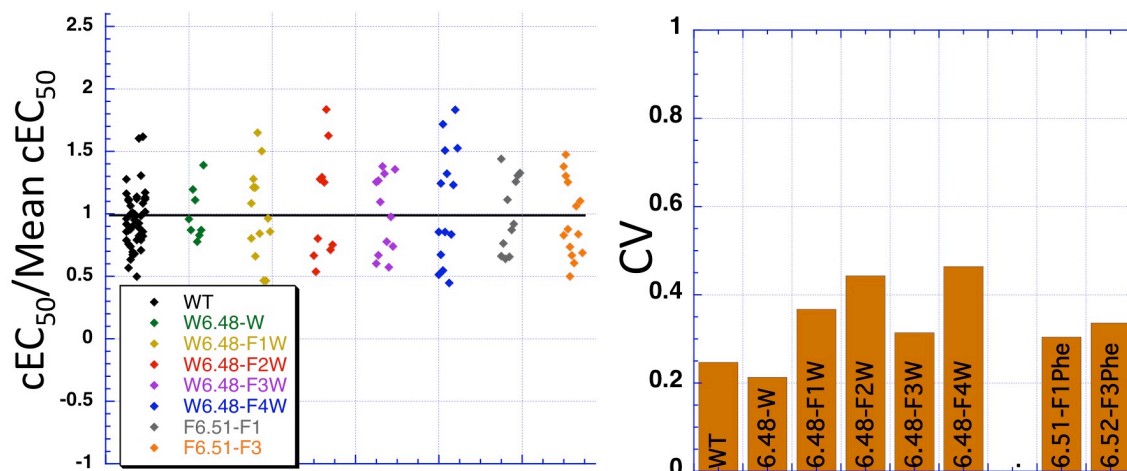
Figure 3.5. Cell-to-cell variability of D2 dopamine receptor suppression data. **(left)** cEC_{50} values normalized to the mean EC_{50} for the condition. **(right)** Bar chart showing the CV values for the Trp fluorination series and the F_1Phe and F_3Phe substitutions at F6.51.

Probing the Aromatic Cluster using Nonsense Expression

The binding region of class A GPCRs such as the M_2 and D2 receptors is rich in aromatic amino acids (figure 3.6) (10-14, 29). Both acetylcholine (ACh) and dopamine have charged ammonium groups, suggesting the possibility of a cation-π interaction (30, 31). In the Cys-loop family of ligand-gated ion channels, ACh and serotonin (which bears structural similarities to dopamine) make cation-π interactions to a conserved Trp in the nicotinic (32, 33) and the 5-HT_3 receptors (34), respectively.

106

a

```
B2 107 (3.26) EFWTSIDVLC VTASIETLCV IAVDRY (3.51)
M2 97         DLWLALDYVV SNASVMNLLI ISFDRY
D2 108        DIFVTLDVMM CTASILNLCA ISIDRY

B2 196 (5.35) NQAYAIASSI VSFYVPLVIM VFVYS (5.59)
M2 183        NAAVTFGTAI AAFYLPVIIM TVLYW
D2 186        NPAFVVYSSI VSFYVPFIVT LLVYI

B2 274 (6.36) TLGIIMGTFT LCWLPFFIVN IV    (6.57)
M2 388        TILAILLAFI ITWAPYNVMV LI
D2 374        MLAIVLGVFI ICWLPFFITH IL

B2 306 (7.33) EVYILLNWIG YVNSGFNPLI YCRS (7.56)
M2 420        TVWTIGYWLC YINSTINPAC YALC
D2 406        VLYSAFTWLG YVNSAVNPII YTTF
```

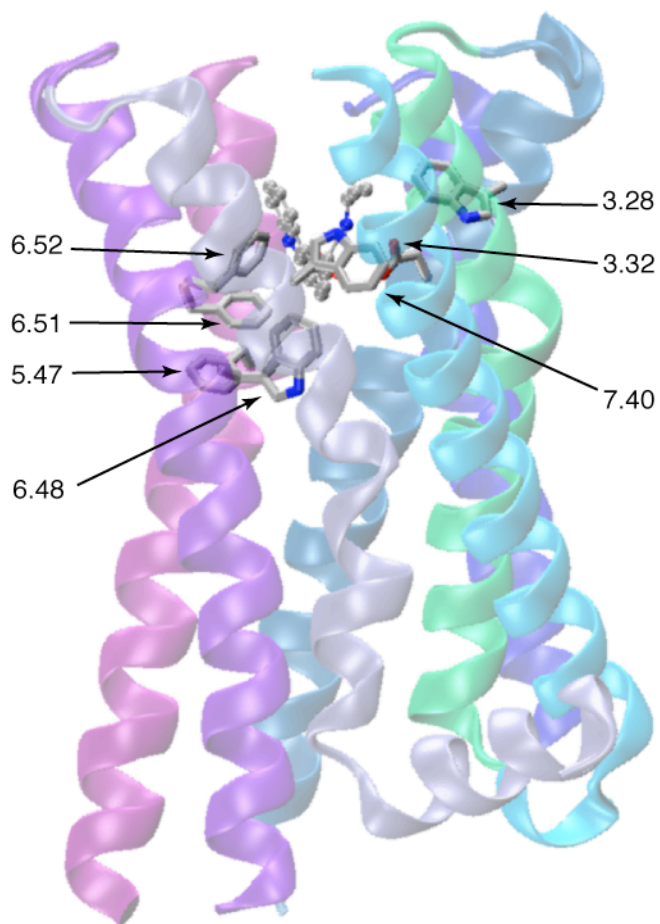**Figure 3.6.** **(a)** Alignment of β_2AR, M$_2$AChR, and D$_2$DR binding site sequences. Residues within 5 Å of the ligand in the β_2AR crystal structure are underlined. Aromatic residues examined in this study are highlighted.

(b) An image of the β_2AR structure with the residues considered here highlighted. The antagonist carazolol is shown as a ball-and-stick model.

b

The nonsense suppression protocol for identifying a cation-π interaction is well established. Progressive fluorination of an aromatic amino acid reduces the electron density in the center of the aromatic ring in a stepwise manner. If a cation-π interaction between the agonist and the particular aromatic is critical to binding, progressive fluorination steadily diminishes the affinity of the drug for the binding site. To probe a potential cation-π interaction at a Trp site, the series of unnatural amino acids; 5-F-Trp (F$_1$Trp), 5,7-F$_2$-Trp (F$_2$Trp), 5,6,7-F$_3$-Trp (F$_3$Trp), 4,5,6,7-F$_4$-Trp (F$_4$Trp), and 1-napthylalanine (Nap) are used (figure 3.7). At a Phe site, the appropriate analogues are 4-F-Phe (F$_1$Phe), 3,5-F-Phe (F$_2$Phe), 3,4,5-F-Phe (F$_3$Phe), 4-methyl-Phe (MePhe), 4-cyano-Phe (CNPhe), 4-bromo-Phe (BrPhe), 3,5-dimethyl-Phe (Me$_2$Phe), and cyclohexylalanine (Cha).

a,b,c,d = H	Trp	a,b = H	Phe	Nap	Cha
b = F	F$_1$Trp	b = F	F$_1$Phe		
b,c = F	F$_2$Trp	a = F	F$_2$Phe		
a,b,c = F	F$_3$Trp	a,b = F	F$_3$Phe		
a,b,c,d = F	F$_4$Trp	b = CH$_3$	MePhe		
		b = CN	CNPhe		
		b = Br	BrPhe		
		a = CH$_3$	Me$_2$Phe		
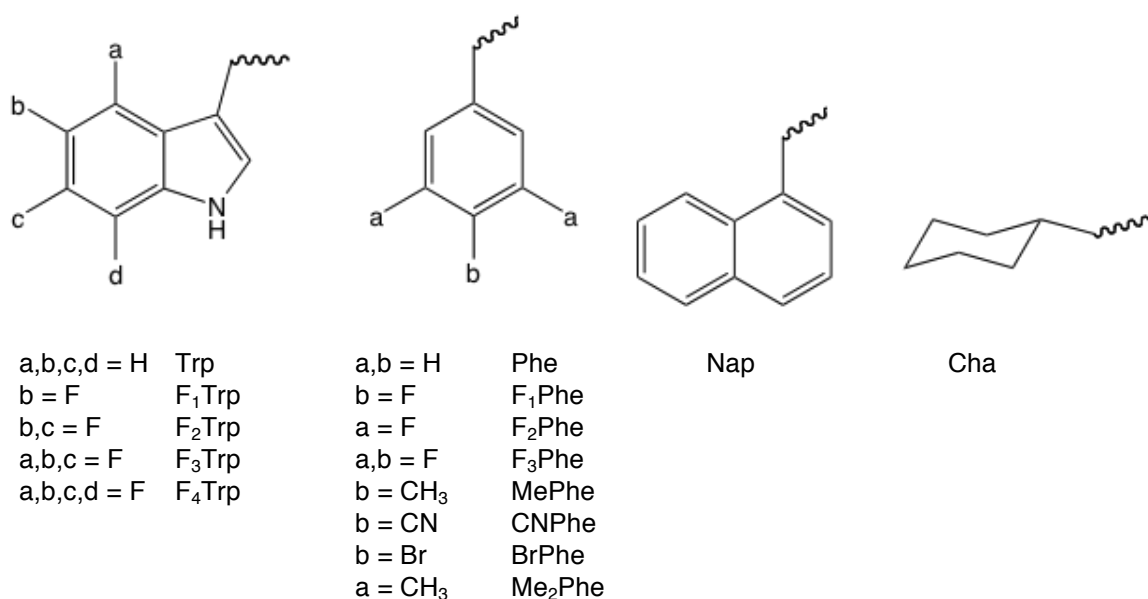
Figure 3.7. Structures of unnatural amino acids used in this study.

In the M_2 receptor, three Trp residues were studied: W3.28, W6.48, and W7.40 (figure 3.6). At W6.48 and W7.40, fluorination studies produce no consistent trends (table 3.1, figure 3.8a). Most importantly, F_3Trp produced an EC_{50} value very near that of wild type at both W6.48 and W7.40. These data strongly indicate that no cation-π interaction exists at these two sites.

Mutation	EC_{50}	n_H[*]	N	Mutation	EC_{50}	n_H[*]	N
WT	59 ± 3	1.06 ± 0.02	44				
F3.28				**F6.52**			
Phe (WT)	55 ± 1	1.13 ± 0.04	5	**Phe (WT)**	45 ± 3	1.04 ± 0.11	6
F₁Phe	140 ± 10	0.84 ± 0.03	4	**F₁Phe**	41 ± 2	1.01 ± 0.11	7
F₂Phe	36 ± 1	1.0 ± 0.1	3	**F₂Phe**	1700 ± 100	1.14 ± 0.03	8
F₃Phe	140 ± 10	0.89 ± 0.14	3	**F₃Phe**	5500 ± 400	1.09 ± 0.03	7
Cha	97 ± 2	1.03 ± 0.04	5	**4-CNPhe**	240 ± 30	1.06 ± 0.05	5
F5.47				**4-BrPhe**	1500 ± 100	1.02 ± 0.04	4
Cha	78 ± 1	1.30 ± 0.14	7	**4-MePhe**	91 ± 6	1.00 ± 0.05	5
W6.48				**3,5-Me₂Phe**	33,000 ± 3000	1.11 ± 0.10	7
Trp (WT)	42 ± 4	0.96 ± 0.05	15	**Conventional**			
F₁Trp	120 ± 10	0.98 ± 0.05	14	**T7.39V**	100 ± 20	0.89 ± 0.12	4
F₂Trp	290 ± 30	0.95 ± 0.06	11	**D3.32E**	50,000 ± 4000	1.07 ± 0.08	9
F₃Trp	840 ± 60	0.85 ± 0.05	13	**D3.32N**	140,000 ± 10,000	1.12 ± 0.03	6
F₄Trp	1800 ± 300	0.84 ± 0.06	16	**D3.32S**	730,000 ± 60,000	1.13 ± 0.09	5
Nap	190 ± 20	1.12 ± 0.06	8				
F6.51							
Phe (WT)	65 ± 4	1.03 ± 0.04	6				
F₁Phe	76 ± 6	0.98 ± 0.03	12				
F₂Phe	4200 ± 350	0.97 ± 0.04	7				
F₃Phe	6200 ± 400	0.095 ± 0.03	18				
Cha	55,000 ± 4000	0.87 ± 0.06	4				
4-CNPhe	1340 ± 160	0.94 ± 0.06	4				
4-MePhe	690 ± 40	1.01 ± 0.02	6				
3,5-Me₂Phe	75,000 ± 5000	0.89 ± 0.05	6				

[a]EC_{50} (nM) and n_H values are ± SEM.

Table 3.1. EC_{50} values (µM), with SEM values in parentheses. Hill coefficients generally range from 0.9 to 1.1; number of cells is generally >7.

Studies of W3.28 in the M_2 receptor were problematic. When we injected mutant mRNA and full-length tRNA without an appended amino acid, we observed $I_{K,Agonist}$ values that were substantially larger than is typically seen in this essential control experiment. As such, W3.28 is presently an uninformative site for studies using nonsense suppression with the amber suppressor THG73 tRNA. We were able to determine an EC_{50} value of 1900 nM for currents created in this experiment, a 10-fold increase over wild type.

Five different aromatic amino acids were evaluated in the D2 receptor (table 1). F3.28 and F5.47 were quite tolerant of substitution. The largest structural perturbation introduced—Cha—gave essentially wild-type behavior. In sharp contrast, F6.51 and F6.52 were very sensitive to substitution. The primary factor appears to be sterics, with larger substituents producing larger effects.

Incorporation of fluorinated tryptophans at W6.48 resulted in systematic increases in EC_{50}, with 2.8-, 6.9-, 20-, and 43-fold shifts in the series from one to four fluorines. The standard plot of the calculated gas-phase cation-π binding energies against the log EC_{50} gave the hallmark linear relationship of a cation-π interaction (figure 3.8b-d).
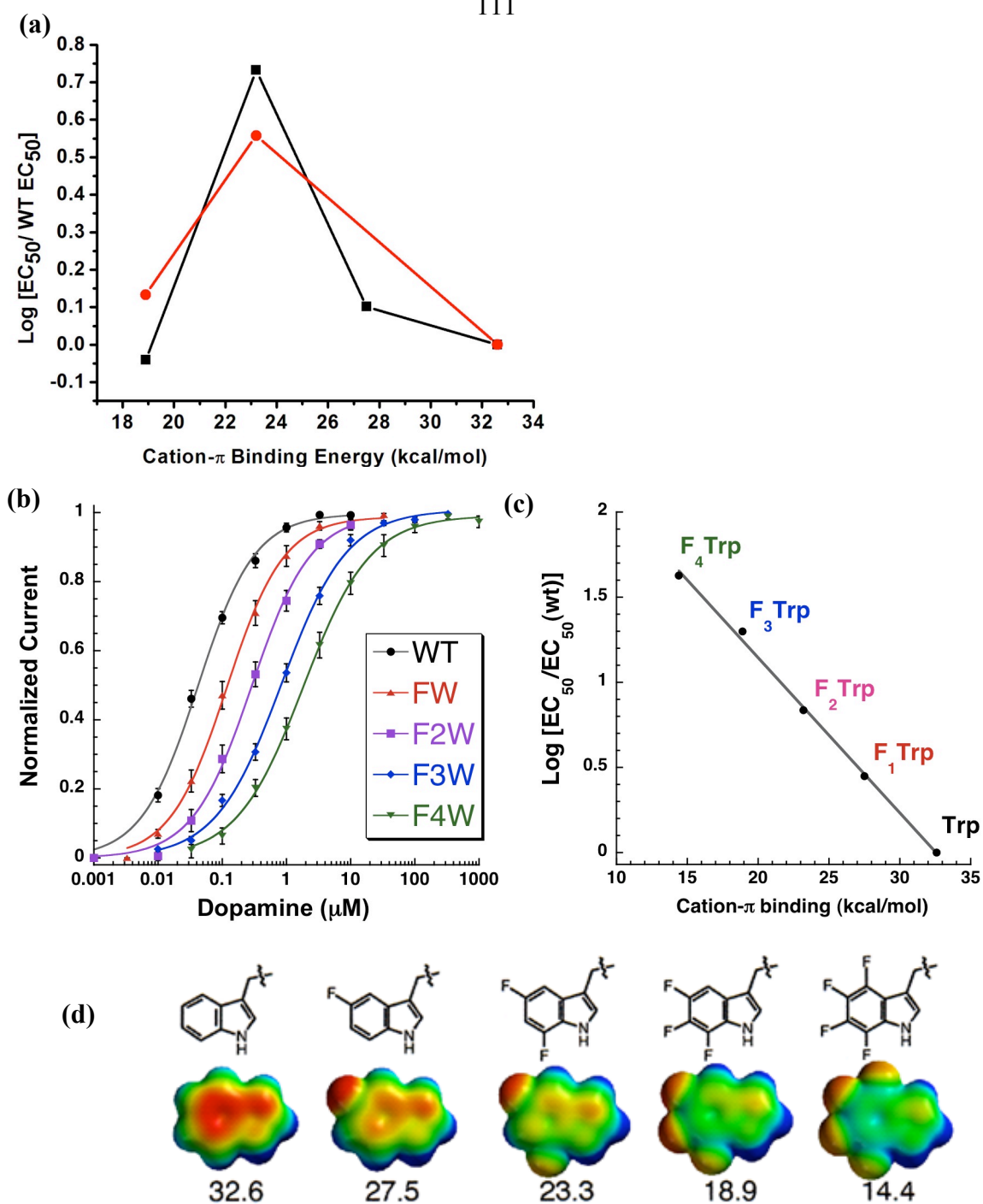
Figure 3.8. (a) F_nTrp data for the M_2 receptor analyzed in terms of gas phase cation-π binding energies of fluorinated indole rings versus the log of the ratio of the F_nTrp EC_{50} and wild-type EC_{50}. Black = W7.40, Red = W6.48. Leftmost point is F_4-Trp; rightmost is wild-type Trp. **(b)** Fluorination of W6.48 in the D2 receptor. Dopamine dose-response relations and fits to the Hill equation. Left to right: D2 receptor suppressed with Trp, F-Trp, F_2-Trp, F_3-Trp, F_4-Trp **(c)** Fluorination plot for W6.48 in D2 receptor. $\log[EC_{50}/EC_{50}(wt)]$ versus calculated cation-π binding ability for the series of fluorinated Trp derivatives). Dopamine data fit the line y = 2.97–0.92x. The correlation for the linear fit is r = 0.9987 **(d)** Electrostatic potential surfaces of the fluorinated tryptophan series calculated using Spartan. Calculated binding energies are included below each molecule.

The electron-withdrawing ability of a fluorine attached to an indole ring would also be expected to diminish the hydrogen bonding ability of the indole NH. If a hydrogen bond to this indole NH were essential to receptor function, a linear fluorination plot could also arise. To test for a hydrogen-binding effect, we removed any possibility of such a hydrogen bond by incorporating the unnatural amino acid Nap, which is sterically very similar to Trp but lacks the NH. The modest shift caused by the Nap mutation (table 3.1) rules out an essential hydrogen bonding role for the indole NH of W6.48, especially in contrast with the much larger 43-fold shift for F_4Trp, which has the indole NH. Note that Nap is a weaker cation-π donor than Trp (32), consistent with the modest rise in EC_{50}.

3.3 Discussion

The studies described in his chapter develop a general protocol to prepare and functionally characterize GPCRs containing unnatural amino acids. Much of the early work of developing this system was done by Dr. Michael Torrice using the M_2 ACh receptor. These protocols were then further optimized for D2 dopamine receptor. In this initial study, we have identified a distinctive cation-π interaction between dopamine and W6.48, a residue that has been proposed to play a key role in receptor function. In addition, we have probed the function of several other aromatic residues in proximity to the agonist binding site.

Unnatural Amino-Acid Mutagenesis at GPCRs

Given the broad range of structures and activities for GPCRs, and their pharmaceutical importance, it has been appreciated for some time that unnatural amino acids could provide a valuable probe of this essential class of membrane receptors. An early study incorporated the fluorescent unnatural amino acid NBD-Dap into the NK2 receptor, and showed that exposure to tachykinin did produce measurable electrophysiological currents in *Xenopus* oocytes (due to opening of Ca^{2+}-activated Cl^- channels that are endogenous to the oocyte) (35). A very recent study used an orthogonal tRNA-synthetase pair to incorporate a benzophenone-containing unnatural amino acid into the Ste2p GPCR (36) and the CCR5 receptor (37). Certainly, extensive conventional mutagenesis studies on GPCRs have provided a wealth of valuable information about which residues are important to receptor function (17). However, the more subtle variations that are possible with the unnatural amino acid methodology can provide additional insights into the precise role of a given residue.

Here we describe the first general application of nonsense suppression methodology to GPCRs, incorporating 13 different unnatural amino acids and developing a reliable readout system that can be used in chemical-scale studies of many GPCRs. Our initial focus has been on the M_2 muscarinic ACh receptor and the D2 dopamine receptor. These are class A GPCRs, a group that also includes adrenergic, serotonin, ordorant, peptide, and glycoprotein hormone receptors. The binding site in this class lies within a crevice formed by several of the transmembrane helices and includes the highly

conserved Asp 3.32 (figure 3.9). In addition, it has long been appreciated that a cluster of aromatic amino acids shapes much of the binding crevice, and recent structural studies position many of them in locations that could be expected to contribute to agonist and antagonist binding.
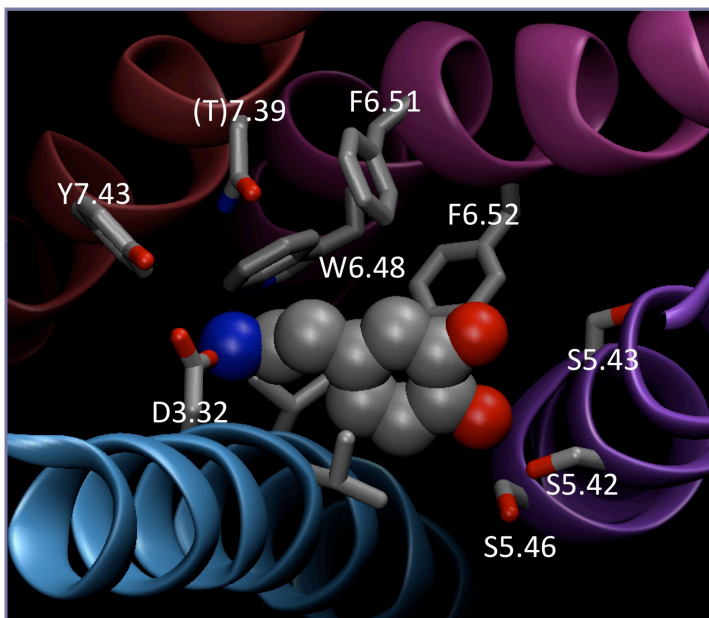

Figure 3.9. Dopamine placed into the binding site of the β2AR structure (2RH1).

We chose the M$_2$ and D2 receptors for this initial study partly because they both couple to the G$_{i/o}$ pathway, which gates G-protein-activated inward rectifying potassium (GIRK) channels, along with inhibiting adenylate cyclase. GIRK channels provide a sensitive readout of GPCR activation, a critical feature given the often-small quantities of protein made by nonsense suppression. However, the use of a downstream signal added significant complications to the process compared to our previous nonsense suppression studies on ion channels. We can readily control the expression levels of some of these proteins, such as GIRK, but it is less straightforward to control others, such as the G-protein and the GPCR itself when incorporating unnatural amino acids. In addition, other cellular pathways can intersect with the desired signaling pathway in unanticipated ways.

Fortunately we found conditions to minimize this variability; variations in EC_{50} reported in this study are meaningful to a confidence level of >99%(20).

After controlling for adequate expression efficiencies and consistent dose-response relationships, we arrived at optimum conditions for the M_2 and D2 receptor systems. RGS4 expression provided faster electrophysiological responses from both receptors, but it was not included in the protocol for the D2 experiments. In addition, relatively low M_2:GIRK1/4 mRNA ratios were necessary. We consider these ratios low, because the typical expression efficiency of the nonsense suppression methodology is roughly 10% that of conventional expression. Thus a 1:1 ratio of M_2:GIRK1/4 mRNA could be considered to be effectively an 0.1:1 ratio of proteins. Presumably the rather low GPCR expression levels minimize the possibility that receptor activation saturates G-proteins, GIRK channels, or other downstream elements in the signaling pathway, which would distort the dose-response relations. Injecting cells with wild-type recovery conditions alongside cells with mutant conditions provided an additional means to assess and control for the variability between batches of cells.

Interactions at GPCR Binding Sites

This initial study focused on several aromatic amino acids in or near the agonist-binding site. W(F)3.28 was chosen due to its position four amino acids—approximately one turn of an α-helix—above the highly conserved D3.32. If the cationic moiety of the agonist makes an electrostatic (ion pair) interaction with D3.32, then W(F)3.28 could be

well positioned to augment agonist binding. W6.48 is highly conserved throughout the class A GPCRs and has been proposed to be in close proximity to the agonist binding site and to play a central role in receptor activation (15, 38). In particular, binding-induced changes in the rotameric state of W6.48 are thought to act as part of a "switch" that is critical to receptor function (10, 15, 38-41) (42). W7.40 is the next most highly conserved residue associated with the aminergic class of GPCRs (43). F6.51 and F6.52 were chosen because the rhodopsin and β_2AR structures place them in close proximity to the agonist. Previous studies on the D2 receptor and other aminergic GPCRs have shown that mutations to these helix 6 residues have substantial effects on agonist affinity (17, 44).

The most compelling results are seen for W6.48 of the D2 receptor. A clear linear correlation is seen in the "fluorination plot" (figure 3.8c), establishing a cation-π interaction. Using the $\beta2$ structure as a guide (11, 13), one finds no cationic residues (Lys/Arg) within 8 Å of W6.48. Thus we propose that dopamine contains the cationic moiety forming the cation-π interaction with W6.48. This establishes an energetically significant cation-π interaction between dopamine and W6.48 of the D2 receptor.

The fluorination strategy employed here has been used previously to identify cation-π interactions in eight different Cys-loop receptors for four different monoamine neurotransmitters (18). These studies have led to the conclusion that the slope of a fluorination plot is related to the energy of the cation-π interaction. Primary ammonium ions (RNH_3^+), such as in serotonin and GABA, produce larger slopes than the quaternary

ammonium ion $(RN(CH_3)_3{}^+)$ of ACh. Studies have established that a cation-π interaction is intrinsically stronger for the smaller, higher-density charge of primary ammonium ions vs. quaternary ammonium ions (45, 46).

In the D2 receptor, the fluorination plot for W6.48 has a slope of 0.092, which is smaller than would be expected for an agonist with a primary ammonium group. For example, the primary ammonium of serotonin interacts with Trp183 in the 5-HT$_3$ receptor with a fluorination slope of 0.17 (34). The value for dopamine is much closer to that measured for the interaction between the quaternary ammonium of ACh and a Trp of the nAChR (0.096) (32). This suggested an alternative type of cation-π interaction for dopamine. Despite the typically employed symbolism (R_4N^+), the positive charge of an alkylated ammonium group is not focused on the nitrogen, but rather on the directly attached hydrogens or alkyl groups. The CH$_2$ group adjacent to the ammonium of dopamine (the β-methylene carbon) carries a significant partial positive charge; one that is similar to that of the methyl groups on the quaternary ammonium of ACh (figure 3.10). Based on the similarity of the slopes for the fluorination plots for dopamine and ACh (in the nAChR), we propose that it is the β-methylene group rather than the ammonium group on dopamine that forms a cation-π interaction with W6.48. Such a cation-π interaction is, in fact, quite common. In a previous survey of cation-π interactions that stabilize protein secondary structure, for energetically significant cation-π interactions involving lysine (i.e., Lys•••[Phe,Tyr,Trp]), most structures involved the ε carbon of lysine contacting the face of the aromatic ring (47).
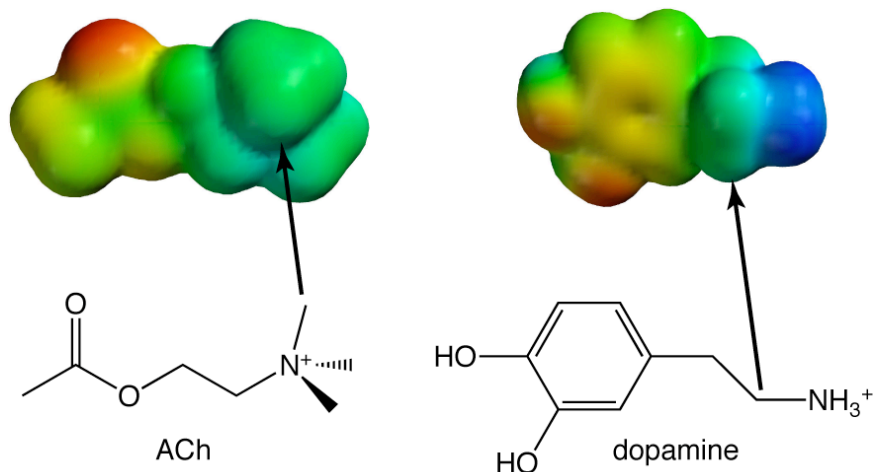
Figure 3.10. Calculated electrostatic potential surfaces (EPS) for ACh and dopamine. Color represents relative electrostatic potential, with red as most negative (limit: 13 kcal/mol) and blue as most positive (limit:178 kcal/mol). Also shown are the structures of each molecule, and arrows from a carbon attached to the ammonium N to the corresponding carbon in the eps, showing the similarities in charge.

A binding orientation in which the β-methylene carbon of dopamine forms a cation-π interaction would leave the ammonium group free to hydrogen bond/ion pair with the highly conserved D3.32. A geometry such as that of figure 3.11 seems quite plausible. A prominent role in binding for D3.32 is well established in several GPCRs (17, 48), and in the present work we find that D3.32E and D3.32N produced 1000- and 3000-fold shifts in dopamine EC_{50}, respectively. Our data thus suggest that helices 3 and 6 jointly interact with the $-CH_2-NH_3^+$ group of dopamine.
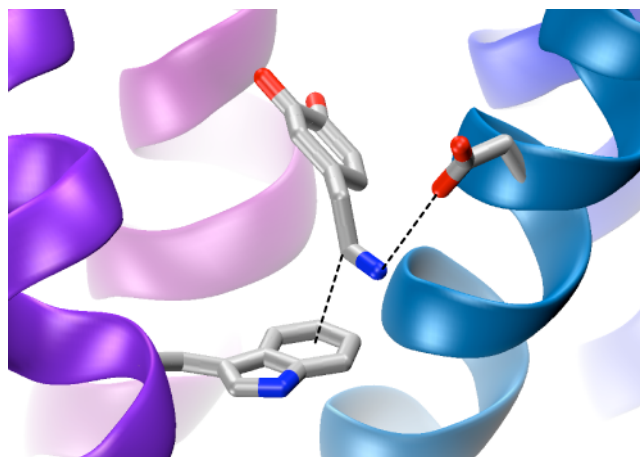
Figure 3.11. A hypothetical docking mode for dopamine in the D2 receptor. Shown are W6.48 (lower left), dopamine (center), and D3.32 (upper right). The view is very similar to that of Figure 3.2b, except the side chain of W6.48 has been rotated as discussed in text. The inverse agonist carazolol from the β_2AR structure has been replaced with dopamine, which has been positioned to allow the hydrogen bond/ion pair interaction between the dopamine ammonium ion (blue) and D3.32 and the cation-π between the dopamine β CH_2 (grey) and W6.48.in an orientation consistent with mutagenesis studies of the D2 receptor. This docking also retains the possibility of hydrogen bonding between the catechol hydroxyls of dopamine and the conserved serines S5.42, S5.43, and S5.46.

Implications for the "Rotamer Switch" Mechanism at W6.48

The joint interaction of the $-CH_2-NH_3^+$ group with helices 3 and 6 agrees with the contemporary model for receptor activation that has the extracellular portion of helix 6 moving toward helix 3. This movement of helix 6 is part of a "rotamer switch" activation mechanism (10, 15, 38-42). A key component of this model is a reorientation of the side chain indole of W6.48, from a perpendicular to a parallel orientation, relative to the plane of the membrane, as the receptor transitions from the inactive to active state. This conformational change is associated with straightening of a proline kink in helix 6 and movement of the extracellular portion of helix 6 toward helix 3 (figure 3.12).
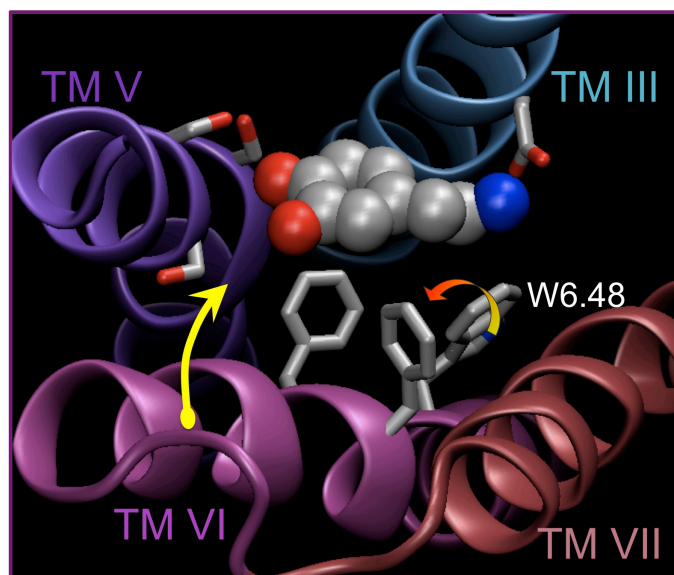
Figure 3.12. Movements of TM helix VI and W6.48 consistent with the 'toggle switch mechanism.'

In a simple docking of dopamine into the β2 receptor structure, it is not possible to make the ion pair interaction to D3.32 and the cation-π interaction to W6.48 simultaneously. In this structure, a presumed inactive form of the receptor (13), the indole side chain is in the perpendicular orientation (figure 3.12). We find that rotation of the indole side chain, with no further relaxation of the structure, does allow formation of both the ion pair and the cation-π interaction, as shown in figure 3.11. Thus, we propose that a key component of the rotamer switch mechanism in the D2 receptor is a reorientation of the side chain of W6.48 so that a cation-π interaction can form to the β carbon on dopamine. This is consistent with the fact that successive fluorination shifts dose-response relationships for receptor function to higher agonist concentrations, suggesting that dopamine and W6.48 interact more strongly while the receptor is in the active, functional state than in the inactive state.

Other Residues

The present data show that two other aromatic amino acids of the D2 receptor—F6.51 and F6.52—do not make a cation-π interaction but are very sensitive to substitution (figure 3.13a-b). Data from the monosubstituted Phe derivatives suggests the sensitivity is at least in part due to a steric interaction more than an electronic effect. For F6.51, F_1Phe is essentially wild type, but MePhe is significantly perturbed. Methyl is sterically larger than fluorine but has essentially no electronic impact when compared to the electron-withdrawing fluorine. For F6.52, an electronic effect can be ruled out, because the magnitude of the EC_{50} shift for the Br analog is larger than that of the cyano analog, which is the reverse of their electron-withdrawing effects. For both F6.51 and F6.52, substitution of fluorine at the 4 position had no significant effect on EC_{50}, but adding fluorine to the 3 and 5 positions resulted in ~100-fold increases. The substitution of methyl groups led to almost 1000-fold increases. Recent structural data for the β-adrenergic receptor are consistent with the steric sensitivity of F6.51 and F6.52: these residues contact each other with a specific geometry (figure 3.12). The high sensitivity to the 3,5 substitutions suggests that these residues participate in an edge-to-face interaction and/or that rotation is highly restricted.

(a)

H F Me CN Br

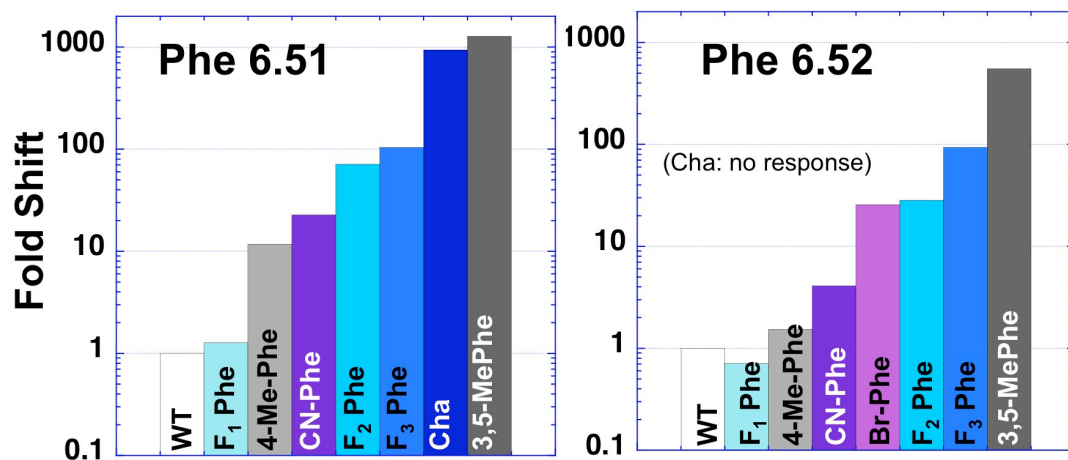F_2 F_3 $(Me)_2$ Cyclohexane
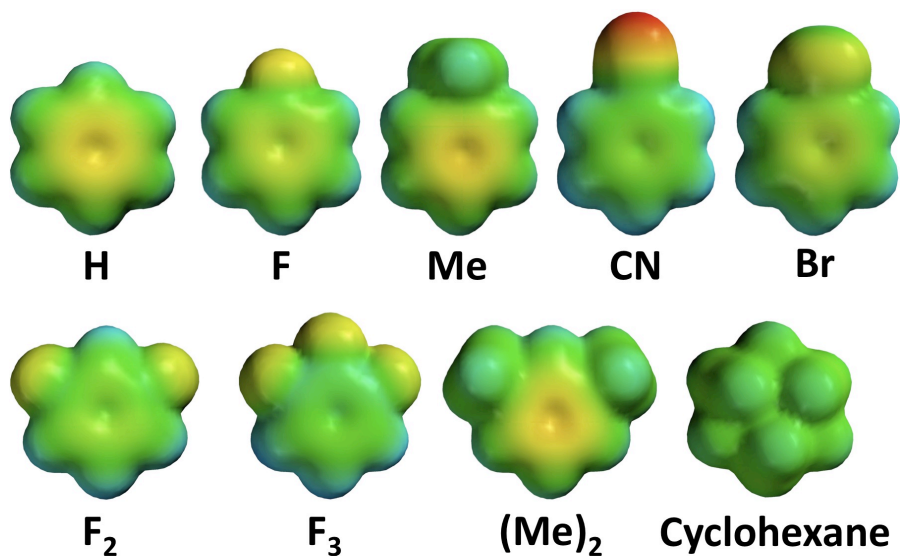
(b)

Figure 3.13. (a) Electric potential surfaces for selected Phe analogues. **(b)** Comparison of fold-shift changes to dopamine EC_{50} induced by incorporation of substituted Phe analogues at F6.51 and F6.52.

A completely different pattern is seen with F3.28 and F5.47 in the D2 receptor. At both sites cyclohexylalanine, Cha, is only minimally different from wild type. Clearly, aromaticity is not a critical feature of the side chains at these sites. Instead, hydrophobicity is probably the key determinant.

Given that a large number of ACh and $R\text{-}N(CH_3)_3^+$ binding sites employ cation-π interactions (30, 49, 50) and the fact that position 6.48 of the M_2 receptor is also a Trp, one might have expected to find a cation-π interaction at W6.48 of the M_2 receptor. However, that is clearly not the case. The data of table 3.1 and figure 3.8a do not support a straightforward cation-π interaction at this site. Mutations at W7.40, another aromatic that is thought to be near the agonist binding site, produced similar data. Given the unusual nature of the "fluorination plots" of Figure 3.8a, we hesitate to ascribe a specific role to these residues.

3.4 Materials and Methods

Molecular Biology

In these experiments, the cDNA for $G\alpha_{oA}$ was in a pCI plasmid, GIRK1 and GIRK4 were in pBSMXT plasmids, D2 receptor (human long form) and RGS4 were in the pcDNA3.1 plasmid, and the human M_2 receptor was in the pGEM3 plasmid. Plasmids were linearized with the appropriate restriction enzymes ($G\alpha_{oA}$ with ClaI, the GIRK plasmids with SalI, D_2DR with XhoI, RGS4 with StuI, and the M_2AChR with HindIII). mRNA was prepared by *in vitro* runoff transcription using the Ambion (Austin, TX) T7 mMessage mMachine kit for all of the constructs except for GIRK1 and GIRK4, which required the T3 kits. For unnatural amino acid mutants, the site of interest was mutated to the TAG stop codon by standard means, verified by sequencing through both strands.

Oocyte Preparation and RNA Injection (51)

Stage V-VI oocytes of *Xenopus laevis* were harvested and injected with RNAs as described in text. Typical oocyte injection volumes were 50 nL per cell for M_2 receptor and 100 nL for D2 receptor experiments; doubly injected oocytes received 50 and 100 nL injections respectively at each injection session. Synthetic amino acids, which were conjugated to the dinucleotide dCA and ligated to truncated 74 nt tRNA as previously described, were deprotected via a 1 kW xenon lamp for 5 minutes, using WG-335 and UG-11 filters to remove the NVOC protecting group. Injection mixture concentrations were typically made such that a 1:1 combination of an mRNA mixture solution and a volume of deprotected tRNA yielded the appropriate concentrations. Wild-type recovery

conditions (injecting tRNA with the native amino acid) were injected alongside mutant conditions to control for data variability. Misacylation was assessed at every site of unnatural amino acid incorporation through the injection of 74 nt THG73 ligated to dCA (THG73-dCA).

Electrophysiology

Oocyte recordings were made in two-electrode voltage clamp mode using the OpusXpress 6000A (Axon Instruments, Union City, California). Recording buffers were ND96 (96 mM NaCl, 2 mM KCl, 1 mM $MgCl_2$, 5 mM HEPES, 1.8 mM $CaCl_2$, pH 7.5) and high K ringer (96 mM NaCl, 24 mM KCl, 1 mM $MgCl_2$, 5 mM HEPES, 1.8 mM $CaCl_2$, pH 7.5). Solution flow rates without drugs were 2 ml/min; drug application flow rates were 4 ml/min for the M_2 receptor and 2.5 ml/min for the D2 receptor experiments. Initial holding potential was -60 mV. Data were sampled at 125 Hz and filtered at 50 Hz. The ND96 pre-wash lasted 10 s; the high K application for basal currents lasted 50 s; drug applications were 15 s in duration for the M_2 receptor and 25 s for the D2 receptor; the high potassium and ND96 washings were 45 and 90 s in duration, respectively. Acetylcholine chloride and dopamine were purchased from Sigma/Aldrich/RBI. All drugs were prepared in sterile double distilled water for dilution into high-K ringer. Dose-response relations were fitted to the Hill equation, $I_{Norm} = 1/(1+(EC_{50}/A))^{\wedge}n_H$, where I_{Norm} is the normalized current peak at [agonist] = A, EC_{50} is the concentration of agonist that elicits a half-maximum response, and n_H is the Hill coefficient. cEC_{50} values were obtained by fitting a single cell's I_{Norm} data to the Hill equation, while EC_{50} values were obtained by averaging the I_{Norm} values for each cell at a given dose and fitting those

average I_{Norm} data to the Hill equation. Statistical calculations were performed using Origin 7.0 (Origin Lab, Northhampton, MA), MiniTab (MiniTab, State College, PA), or Excel (Microsoft).

3.5 References

1. Torrice, M. M., Bower, K. S., Lester, H. A., and Dougherty, D. A. (2009) *Proc Natl Acad Sci U S A* **106**(29), 11919-11924

2. Hopkins, A. L., and Groom, C. R. (2002) *Nat Rev Drug Discov* **1**(9), 727-730

3. Klabunde, T., and Hessler, G. (2002) *ChemBioChem* **3**(10), 928-944

4. Lagerstrom, M. C., and Schioth, H. B. (2008) *Nat Rev Drug Discov* **7**(4), 339-357

5. (2007) Market Opportunity in the G-Protein Coupled Receptors GPCRs Target Space. In., Drug and Market Development Publishing

6. Lefkowitz, R. J., and Shenoy, S. K. (2005) *Science* **308**(5721), 512-517

7. Pierce, K. L., Premont, R. T., and Lefkowitz, R. J. (2002) *Nat Rev Mol Cell Biol* **3**(9), 639-650

8. Kobilka, B. K. (2007) *Biochimica et Biophysica Acta (BBA) - Biomembranes* **1768**(4), 794-807

9. Offermanns, S. (2003) *Progress in Biophysics and Molecular Biology* **83**(2), 101-130

10. Rosenbaum, D. M., Cherezov, V., Hanson, M. A., Rasmussen, S. G. F., Thian, F. S., Kobilka, T. S., Choi, H.-J., Yao, X.-J., Weis, W. I., Stevens, R. C., and Kobilka, B. K. (2007) *Science* **318**(5854), 1266-1273

11. Rasmussen, S. G. F., Choi, H.-J., Rosenbaum, D. M., Kobilka, T. S., Thian, F. S., Edwards, P. C., Burghammer, M., Ratnala, V. R. P., Sanishvili, R., Fischetti, R. F., Schertler, G. F. X., Weis, W. I., and Kobilka, B. K. (2007) *Nature* **450**(7168), 383-387

12. Warne, T., Serrano-Vega, M. J., Baker, J. G., Moukhametzianov, R., Edwards, P. C., Henderson, R., Leslie, A. G., Tate, C. G., and Schertler, G. F. (2008) *Nature* **454**(7203), 486-491

13. Cherezov, V., Rosenbaum, D. M., Hanson, M. A., Rasmussen, S. G. F., Thian, F. S., Kobilka, T. S., Choi, H.-J., Kuhn, P., Weis, W. I., Kobilka, B. K., and Stevens, R. C. (2007) *Science* **318**(5854), 1258-1265

14. Jaakola, V. P., Griffith, M. T., Hanson, M. A., Cherezov, V., Chien, E. Y., Lane, J. R., Ijzerman, A. P., and Stevens, R. C. (2008) *Science* **322**(5905), 1211-1217

15. Palczewski, K., Kumasaka, T., Hori, T., Behnke, C. A., Motoshima, H., Fox, B. A., Trong, I. L., Teller, D. C., Okada, T., Stenkamp, R. E., Yamamoto, M., and Miyano, M. (2000) *Science* **289**(5480), 739-745

16. Filipek, S., Teller, D. C., Palczewski, K., and Stenkamp, R. (2003) *Annual Review of Biophysics and Biomolecular Structure* **32**(1), 375-397

17. Shi, L., and Javitch, J. A. (2002) *Annual Review of Pharmacology and Toxicology* **42**(1), 437-467

18. Dougherty, D. A. (2008) *Chem. Rev.* **108**(5), 1642-1653

19. Dougherty, D. A. (2008) *J Org Chem* **73**(10), 3667-3673

20. Torrice, M. M. (2009) Chemical-Scale Studies of the NIcotinic and Muscarinic Acetylcholine Receptors. In. *Chemistry*, California Institute of Technology, Pasadena

21. Ivanina, T., Rishal, I., Varon, D., Mullner, C., Frohnwieser-Steinecke, B., Schreibmayer, W., Dessauer, C. W., and Dascal, N. (2003) *J. Biol. Chem.* **278**(31), 29174-29183

22. Kofuji, P., Davidson, N., and Lester, H. A. (1995) *Proceedings of the National Academy of Sciences* **92**(14), 6542-6546

23. Krapivinsky, G., Krapivinsky, L., Wickman, K., and Clapham, D. E. (1995) *J. Biol. Chem.* **270**(49), 29059-29062

24. Mark, M. D., and Herlitze, S. (2000) *European Journal of Biochemistry* **267**(19), 5830-5836

25. Rishal, I., Porozov, Y., Yakubovich, D., Varon, D., and Dascal, N. (2005) *J. Biol. Chem.* **280**(17), 16685-16694

26. Zhang, Q. L., Pacheco, M. A., and Doupnik, C. A. (2002) *Journal of Physiology-London* **545**(2), 355-373

27. Doupnik, C. A., Davidson, N., Lester, H. A., and Kofuji, P. (1997) *Proceedings of the National Academy of Sciences* **94**(19), 10461-10466

28. Sadja, R., Alagem, N., and Reuveny, E. (2003) *Neuron* **39**(1), 9-12

29. Hibert, M. F., Trumpp-Kallmeyer, S., Bruinvels, A., and Hoflack, J. (1991) *Mol Pharmacol* **40**(1), 8-15

30. Dougherty, D. A. (1996) *Science* **271**(5246), 163-168

31. Ma, J. C., and Dougherty, D. A. (1997) *Chem. Rev.* **97**(5), 1303-1324

32.   Zhong, W. G., Gallivan, J. P., Zhang, Y. O., Li, L. T., Lester, H. A., and Dougherty, D. A. (1998) *Proceedings of the National Academy of Sciences of the United States of America* **95**(21), 12088-12093

33.   Xiu, X., Puskar, N. L., Shanata, J. A. P., Lester, H. A., and Dougherty, D. A. (2009) *Nature* **in press.**

34.   Beene, D. L., Brandt, G. S., Zhong, W., Zacharias, N. M., Lester, H. A., and Dougherty, D. A. (2002) *Biochemistry* **41**(32), 10262-10269

35.   Turcatti, G., Nemeth, K., Edgerton, M. D., Meseth, U., Talabot, F., Peitsch, M., Knowles, J., Vogel, H., and Chollet, A. (1996) *J Biol Chem* **271**(33), 19991-19998

36.   Huang, L. Y., Umanah, G., Hauser, M., Son, C., Arshava, B., Naider, F., and Becker, J. M. (2008) *Biochemistry* **47**(20), 5638-5648

37.   Ye, S. X., Kohrer, C., Huber, T., Kazmi, M., Sachdev, P., Yan, E. C. Y., Bhagat, A., RajBhandary, U. L., and Sakmar, T. P. (2008) *Journal of Biological Chemistry* **283**(3), 1525-1533

38.   Lu, Z.-L., Saldanha, J. W., and Hulme, E. C. (2002) *Trends in Pharmacological Sciences* **23**(3), 140-146

39.   Shi, L., Liapakis, G., Xu, R., Guarnieri, F., Ballesteros, J. A., and Javitch, J. A. (2002) *J Biol Chem* **277**(43), 40989-40996

40.   Schwartz, T. W., and Rosenkilde, M. M. (1996) *Trends Pharmacol Sci* **17**(6), 213-216

41.   Lin, S. W., and Sakmar, T. P. (1996) *Biochemistry* **35**(34), 11149-11159

42.   Schwartz, T. W., Frimurer, T. M., Holst, B., Rosenkilde, M. M., and Elling, C. E. (2006) *Annu Rev Pharmacol Toxicol* **46**, 481-519

43.   Huang, E. S. (2003) *Protein Sci* **12**(7), 1360-1367

44.   Cho, W., Taylor, L. P., Mansour, A., and Akil, H. (1995) *J Neurochem* **65**(5), 2105-2115

45.   Deakyne, C. A., and Meot-Ner (Mautner), M. (1985) *J. Am. Chem. Soc.* **107**, 474-479

46.   Meot-Ner (Mautner), M., and Deakyne, C. A. (1985) *J. Am. Chem. Soc.* **107**, 469-474

47.   Gallivan, J. P., and Dougherty, D. A. (1999) *Proceedings of the National Academy of Sciences of the United States of America* **96**(17), 9459-9464

48.   Lu, Z.-L., and Hulme, E. C. (1999) *J. Biol. Chem.* **274**(11), 7309-7315

49.   Ma, J. C., and Dougherty, D. A. (1997) *Chem. Rev.* **97**(5), 1303-1324

50.   Zacharias, N., and Dougherty, D. A. (2002) *Trends in Pharmacological Sciences* **23**(6), 281-287

51.   Nowak, M. W., Gallivan, J. P., Silverman, S. K., Labarca, C. G., Dougherty, D. A., Lester, H. A., and Conn, P. M. (1998) In vivo incorporation of unnatural amino acids into ion channels in Xenopus oocyte expression system. In. *Methods in Enzymology*, Academic Press

Chapter 4

Developing Methods for Unnatural Amino Acid Mutagenesis in Mammalian Cells

4.1 Introduction

Unnatural amino acid incorporation into proteins by nonsense suppression has been proven as a valuable tool for the study of ion channel structure-function (1-3). The *in vivo* nonsense suppression methodology (4) is particularly useful for the study of ion channels, but until recently, these studies have been limited to the *Xenopus* oocyte heterologous expression system. While the *Xenopus* system is robust, easy to work with, and a useful tool for many studies, there are clear benefits to expanding this technology to a mammalian expression system. In general such a system would provide a more relevant environment for many of the proteins we study, because many of them are of mammalian origin. More specifically, when we wish to study receptor biology, we will be looking at processes such as signal transduction pathways, which are cell specific and must be studied in a mammalian system.

Methods have now been developed that can successfully incorporate unnatural amino acids into channels expressed in mammalian cells (5). While this was important progress, they use relatively large amounts of precious reagents compared to the *Xenopus* system, and the methods are not yet robust enough for many studies we would like to pursue. This chapter describes efforts to further develop these methods and use them to study the function of NMDA receptors in mammalian cells.

The NMDA Receptor

The NMDA receptor (NMDAR) is a ligand gated ion channel gated by the simultaneous binding of both glutamate and glycine (6). Because the physiological

concentration of glycine is thought to be sufficient such that the glycine site remains occupied, this co-agonist will be ignored for the time being.

Glutamate is a major excitatory neurotransmitter in the central nervous system, and its function is critical in learning and memory. Two different glutamate receptors, NMDA and AMPA (α-amino-3-hydroxyl-5-methyl-4-isoxazole-propionic acid) receptors are often found side by side in the synapse. AMPA receptors have fast kinetics and a greater ability to depolarize the post-synaptic membrane. Thus they are responsible for most of the excitatory post-synaptic potential (EPSP) and for the depolarization that may sum and trigger an action potential in the post-synaptic cell (7). NMDA receptors have slower kinetics and do not contribute as significantly to the electrical changes in the synapse, but do serve a very important function.

One of the key aspects of NMDAR function is related to its ability to conduct Ca^{2+}, which in turn facilitates dynamic changes in synaptic characteristics. While this regulated movement of Ca^{2+} is a key aspect of NMDAR function in learning and memory, excessive levels of Ca^{2+} are cytotoxic. There are numerous diseases that are believed to involve excitotoxicity and to have an underlying mechanism involving NMDARs (figure 4.1).
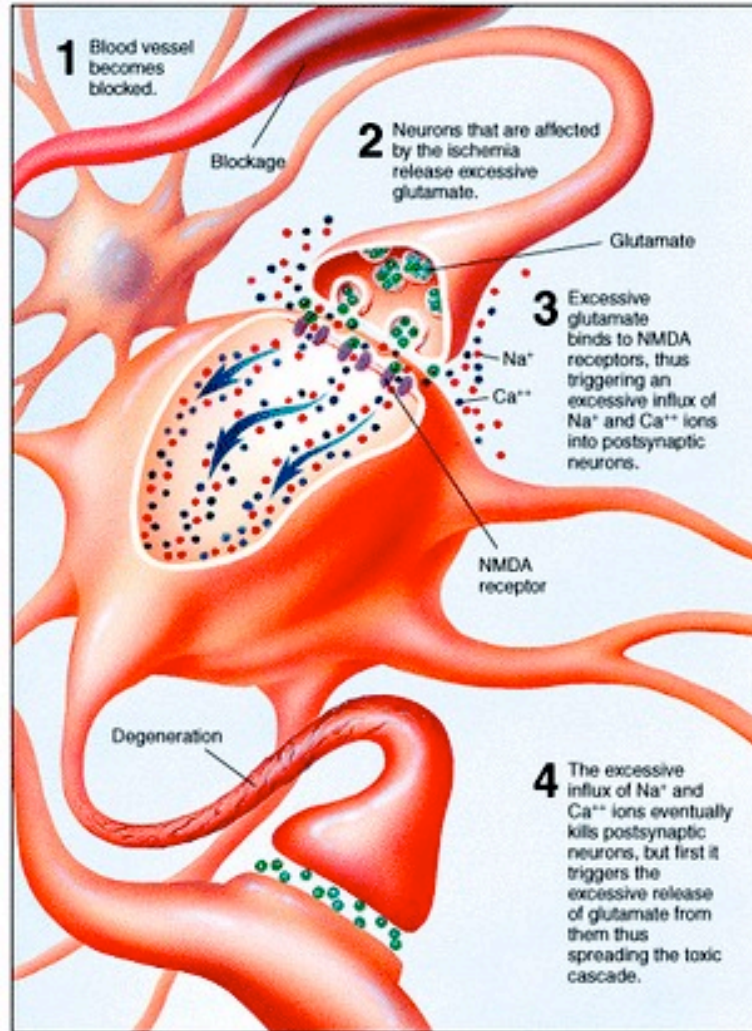
Figure 4.1. Mechanism of NMDAR excitotoxicity during acute CNS trauma.

Stroke is one of the most common diseases associated with NMDAR function. During a stroke, a block in blood flow causes nerve cells to be deprived of oxygen. Without a way to produce ATP, these cells can no longer maintain their ion concentration gradients, and the membrane begins to depolarize. This depolarization increases the firing rate of action potentials, which causes a subsequent release of excessive glutamate at the axon terminals. Glutamate release activates NMDARs in postsynaptic neurons, and this leads to excessive calcium influx in these cells. The presence of excessive calcium in a cell for an extended period of time is toxic, and leads eventually to the death of the cell.

As the cell begins to die, excessive glutamate release is triggered and activates downstream nerve cells. Thus a cascade occurs that can spread from the original site of damage and injure areas of the brain not deprived of oxygen (reviewed in (8,9)).

Treatment of these conditions by targeting the NMDAR is challenging, because it is an endogenous protein with critical functions in the CNS. The most effective drugs targeting this receptor will be those that act very specifically to modulate its function. Thus, developing these therapies will require an understanding of subtle aspects of NMDAR structure and function.

The particularly unique characteristic of this receptor is the third condition that must be met before ions can pass through the channel. At resting membrane potentials Mg^{2+} ions sit in the channel pore and block the flow of ions. Ion conduction is blocked even if both agonists are bound to the receptor. Removal of this blockade requires a depolarizing shift in the membrane potential (figure 4.2) (10)
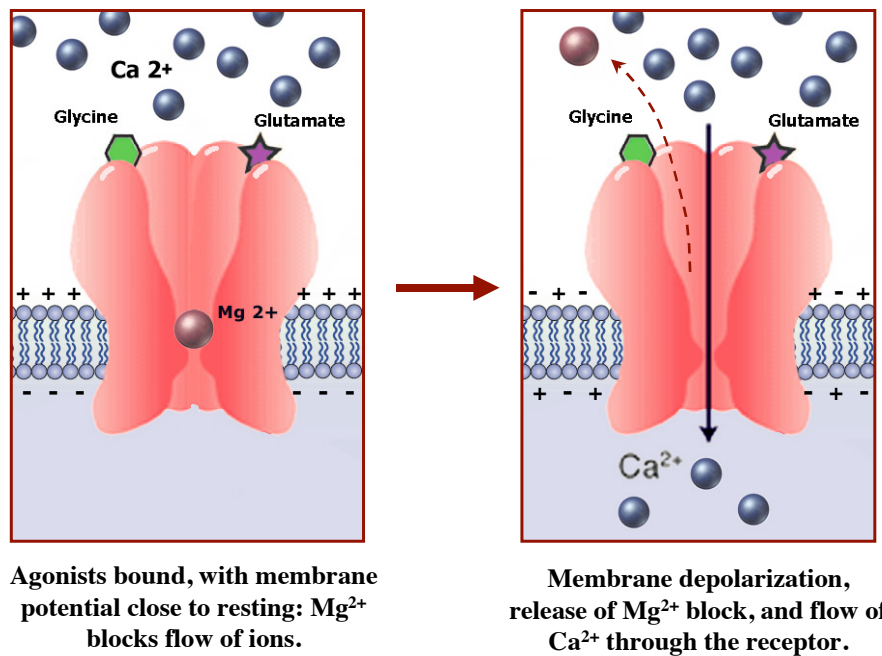
Figure 4.2. Mechanism of Mg^{2+} block in the NMDA receptor.

Agonists bound, with membrane potential close to resting: Mg^{2+} blocks flow of ions.

Membrane depolarization, release of Mg^{2+} block, and flow of Ca^{2+} through the receptor.

The NMDA receptor is permeable to sodium, potassium, and calcium, but it is calcium that plays the most important role in the function of this receptor. The Ca^{2+} permeability is quite high, approximately 10-fold higher than the permeability of the monovalent ions. Thus, even though the physiological concentration of Ca^{2+} is ~100-fold lower than Na^+, it is responsible for about 10% of the current passing through the channel.

The NMDA receptor is essential for many aspects of learning and memory, and some of the characteristics described above relate directly to this function. First, the necessity for both agonist binding and membrane depolarization makes this receptor a coincidence detector (11,12). The first condition that must be met is the presence of glutamate, which is released from the presynaptic cell. This condition is the result of activity at the local synapse. The second requirement of membrane depolarization

however, provides a means for the receptor to detect the activity of the neuron as a whole. This is because it is sensitive to depolarization, which results both from the opening of other channels such as AMPAR, but also from back-propagating action potentials (13).

The resulting influx of Ca^{2+} leads to the localized activation of kinases, and alters numerous cellular processes including the activity of AMPA receptors. These changes are the basis of long-term potentiation (LTP), which is a strengthening of the synaptic connections as a result of simultaneous firing of the pre and post synapse (14,15). LTP is thought to be a key step in memory formation. Figure 4.3 is a scaled cartoon that illustrates some of the components that are associated with this system.
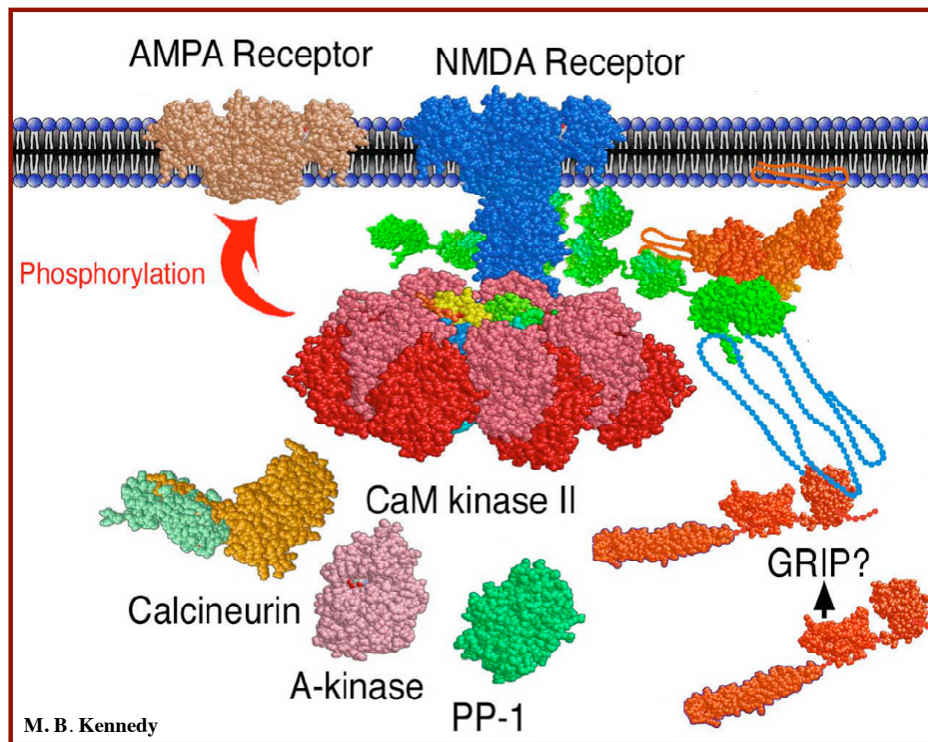

Figure 4.3. Cartoon illustration of some of the components involved in NMDA regulation and LTP.

NMDAR Structure

In the presently accepted structural model, the NMDA receptor is composed of two NR1, and two NR2 subunits. Each subunit of this tetramer has three transmembrane domains and a reentrant loop, M2, which is reminiscent of the P-loop in voltage-gated channels (figure 4.4) (14,15). Mutagenesis studies have revealed that several residues on this loop are important for Mg binding (16). S1 and S2 form the ligand-binding domain S1S2.
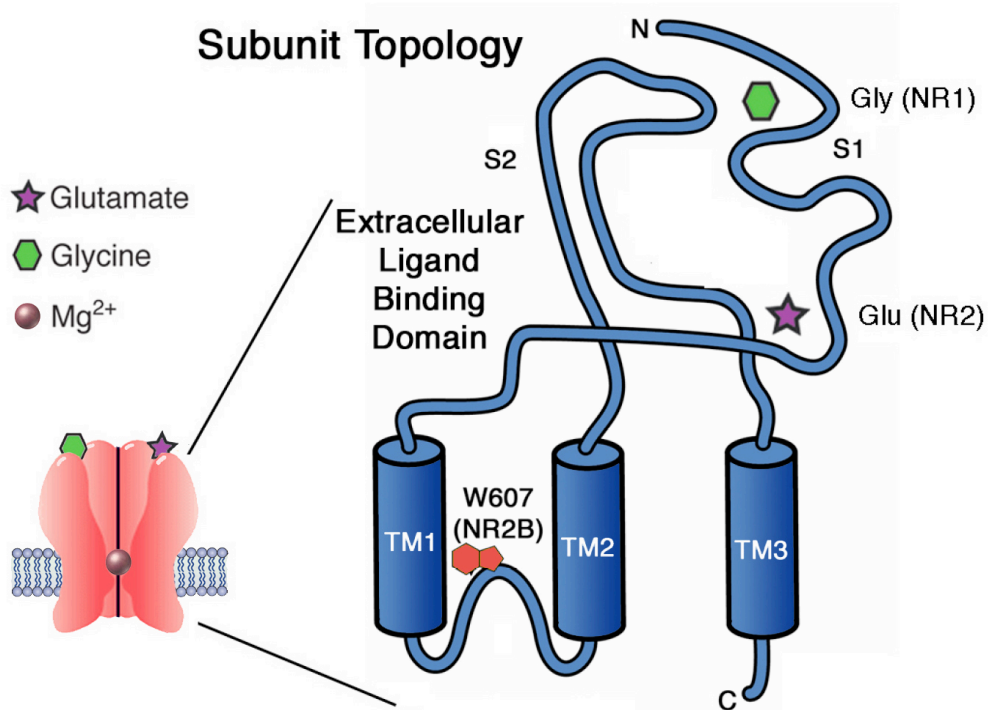

Figure 4.4. Subunit topology of the NMDA receptor.

The soluble S1S2 domain of the NR1 subunit (glycine binding domain) has been recently crystallized (17). This structure is a great source of information from which to begin studies of specific ligand-binding interactions.

The Mg^{2+} binding site is interesting, from a chemical perspective, because unlike all other known Mg^{2+} binding sites, which have a highly negative character, this site is made of hydrophobic and polar amino acids. One can see how this would facilitate easy unblocking with a simple voltage shift. The binding site is within the voltage field and is directly voltage dependant so block is stronger at hyperpolarized voltages. Mg^{2+} is able to move past the block site and, especially at very hyperpolarized voltages, will pass through the channel (15).

A study by Williams et al. in 1998 (16) suggested that the block site may be formed by tryptophan 607, and these findings were the rational for the choice of this site as the subject of our initial investigations. They had shown that substitution of non-aromatic hydrophobic residues such as leucine at tryptophan 607 increased the IC_{50} from 19 µM to greater than 300 µM (16). IC_{50} is the concentration at half-maximal inhibition, therefore a larger value means that a higher concentration of Mg^{2+} is required to cause the same degree of inhibition. If the tryptophan is replaced with another aromatic residue such as tyrosine, the change in Mg^{2+} binding was minimal (16). This suggests that the tryptophan may bind to the Mg^{2+} through a cation-π interaction. In this type of interaction, a cation favorably interacts with the electrons from the delocalized π system of an aromatic ring.

The most conclusive way we have to identify this putative cation-π interaction is through the incorporation of a series of fluorinated tryptophan unnaturals. If Mg^{2+} interacts with the π electrons of the aromatic ring, it should be possible to attenuate the

strength of binding by reducing the availability of these electrons. Decreasing the electron availability in the π system can be done using fluorinated tryptophan analogues as discussed in section 1.2 (figure 1.3).

It was expected that incorporation of this fluorinated tryptophan series at Trp 607 would be an ideal means to verify the success of unnatural amino acid incorporation into the NMDA receptor. Subsequent studies however have indicated that there is not a cation-π interaction at this position (18), so a different site will need to be selected if this project is continued.

Unnatural Amino Acid Incorporation in Mammalian Cells

We are interested in understanding structure-function relationships in ion channels, and the powerful tool we have to study this is unnatural amino acid mutagenesis. This technique allows us probe the structures of the channels with chemical-scale precision, and to make more subtle changes than is possible with traditional mutagenesis. We are interested in extending this method for use in a mammalian cell culture system for several reasons.

There are many interesting questions regarding receptor biology that unnatural amino acid mutagenesis is well suited to address. However, to study a process such as a cell-specific signal transduction pathway, we must work within a compatible system that contains the relevant components and regulatory elements. For example, some of the most interesting questions about the NMDAR and memory involve its interaction with

other cellular proteins, many of which do not function in an oocyte. Many of the receptors we are interested in are mammalian in origin, therefore our projects would benefit from an ability to study receptor function in a more relevant biological context. There are also receptors that we would like to study, but which do not express well in *Xenopus* oocytes. It is likely mammalian cells will also facilitate better expression of at least some of these difficult receptors.

Important progress has been made toward our goal of expressing unnaturals in mammalian cells. The first demonstration of unnatural expression was in the Nicotinic Acetylcholine receptor (5). This was an exciting and promising development, but the NMDAR was a more appropriate choice for the project. Earlier work by Sarah Monahan (5) demonstrated wild-type recovery nonsense suppression of the NMDAR channels in mammalian cells. Another study used a serine amber suppressor tRNA to recover wild-type function in a hERG channel (19). Such accomplishments demonstrated that we are able to use this methodology in mammalian cells. What remained was to expand the method to include more cell types, and receptors, and to make the procedures more efficient and robust.

4.2 Methods

Molecular Biology

The genes for NR1a, NR2A, and NR2B were subcloned from pBluescript into pcDNA3.1 to facilitate expression in a mammalian system. Primers were designed to

include sequences complimentary to the 5' and 3' ends of each gene, as well as overhang regions containing the appropriate restriction site. The NR1a and NR2A contain HindIII and BamHI restriction sites, while NR2B contains NheI and BamHI. These primers were used to amplify the coding sequence using the gene in pBluescript as a template. The PCR products were then cut with appropriate enzymes and subsequently ligated into the pcDNA3.1 vector (figure 4.5). The 5' region of each gene was sequenced, and restriction tests performed to confirm correct incorporation.
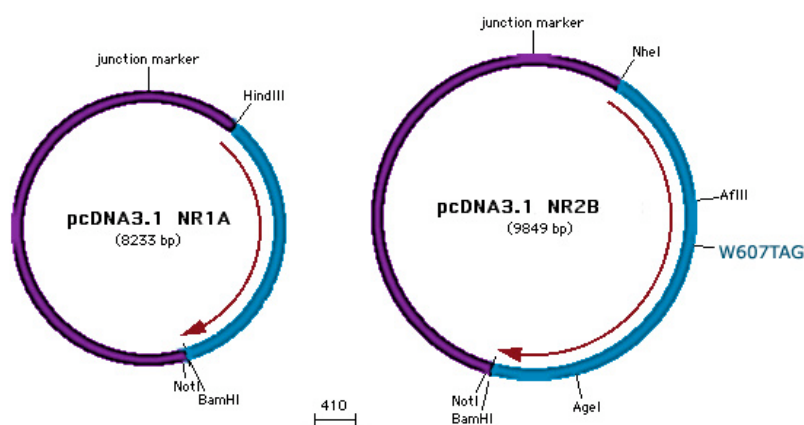

Figure 4.5. Maps of two NMDAR constructs. NR1a and NR2B were placed in pcDNA3.1 to enhance expression in a mammalian system.

Quikchange mutagenesis (Stratagene) was used to incorporate a TAG stop codon at the Trp607 position in NR2B. To help with expression of the NR1a construct quickchange was also used to insert a Kozak sequence immediately upstream of the translation start site. Because it was determined sufficient to transfect cells with DNA, mRNA transcription was unnecessary. Thus, DNA was simply purified and quantitated, and the circular plasmid used for transfection.

General Method for Nonsense Suppression in Mammalian Cells

Mammalian cells use similar translation machinery as oocytes, and the molecular mechanism is basically the same, so figure 1.4 accurately describes both systems. The

methods used to express channels in mammalian cells are different than those used in oocytes, but they are conceptually similar. Figure 4.6 illustrates the process in mammalian cells. Along with the gene of interest and charged tRNA, a small amount of plasmid containing EGFP is included in the transfection mix. This reporter gene allows the identification of cells that have been successfully transfected. mRNA is included in the figure, but when using mammalian cells, it is sometimes sufficient to transfect DNA and allow the cell to transcribe its own mRNA.
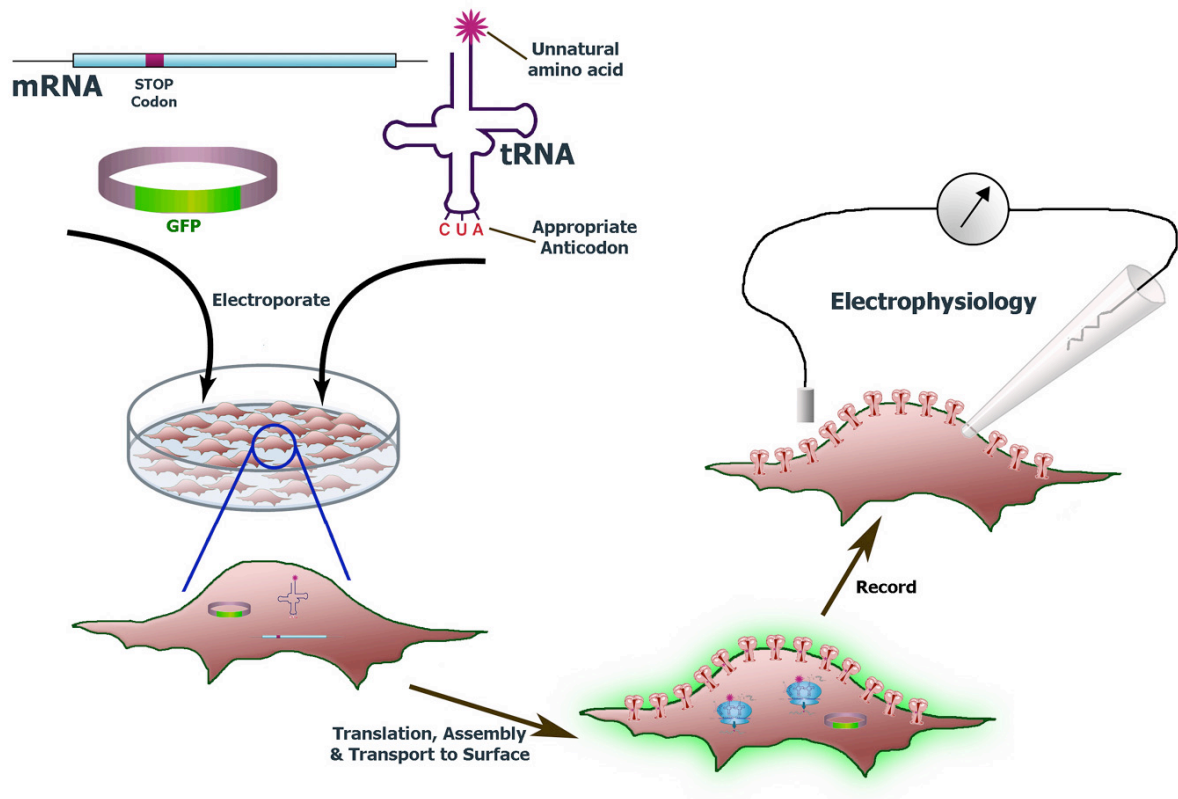

Figure 4.6. Method of nonsense suppression in mammalian cells. The process is similar to that in oocytes. Some differences include transfection via electroporation, use of GFP reporter gene, recording done using patch-clamp setup.

Several transfection techniques were investigated in our lab, and it was determined that electroporation was the most effective method. This now published method was developed by Sarah May (5). Using a custom-made microelectroporator, brief pulses of 120V are applied to adherent cells bathed in a concentrated mix of nucleic acid. Transfection efficiency is about 80% (figure 4.7), and it can deliver amounts of tRNA into the cells that are sufficient for our suppression experiments and single-cell recording.

Figure 4.7. (left) Microelectroporator used to transfect adherent mammalian cells. **(right top)** Phase contrast image of transfected cells. **(right bottom)** EGFP fluorescence same field of view. Comparison of the two images can estimate the transfection efficiency (~80%).
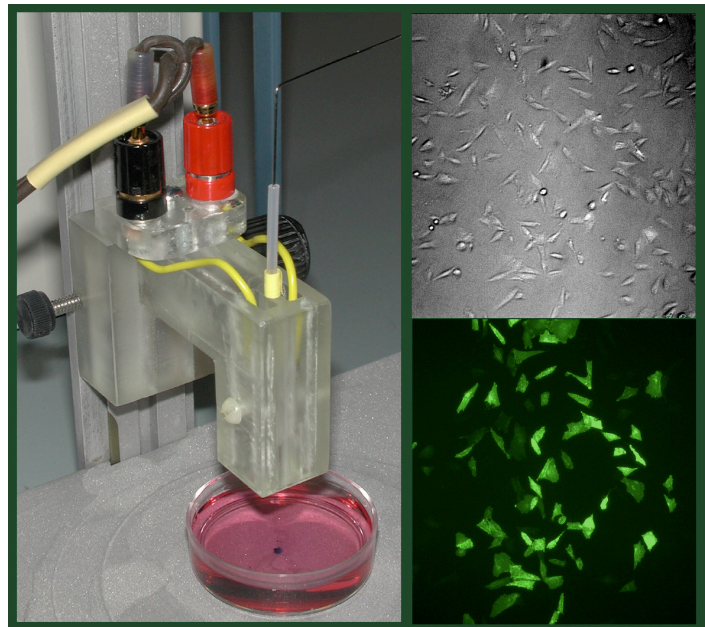
Variations in Transfection Protocols

- Withdraw pipette piston when over cells.

<u>Toward More Efficiency</u>

- Transfect with smaller volume (just more efficient).

- Repeat use of reagents.

Spot, Transfect, and Split Protocol

<u>Day 1: Passage and Spot</u>

- Allow CHO cells to reach 90% confluency in a 25 cm^2 flask.

    - Passage as usual, leaving all harvested cells in a final volume of 2 ml of F-12 media.

    - Use remainder to make dilution(s) for spotting.

- On dishes intended for newly plated cells, mark a dashed circle to indicate approximate area to be covered by media.

- Dilute harvested cells in media and spot ~200 µl onto the marked area of each dish, utilizing surface tension to minimize the spread of solution.

    - If transfection will be done in ~24 hours dilute cells to 1:8.

    - If transfection will be done in ~48 hours dilute cells to 1:16.

Note: To maximize humidity and minimize evaporation from the droplet, it may be helpful to place other drops of fresh media around the edge of the dish.

- Carefully place dishes in incubator and wait 60-90 minutes to allow cells to adhere to the bottom of the dish.

- Gently add ~2 ml of pre-warmed F-12 media to each dish.

Day 2: Transfect Cells

- Transfect as normal, being sure to center foot of electroporator over the marked area where cells are present.

- Allow cells to recover for 2 hours in the incubator.

Split Transfected Cells to Multiple Dishes

- On dishes intended for split cells, mark a dashed circle to indicate approximate area to be covered by media.

- Treat the spot of transfected cells with PBS and a 20 sec application of trypsin.

  - You should be able to see the opaque spot cleared away.

- Suspend the spot of cells in 800 μl of F-12 media.

  - Leave dish at an angle so that media drains to one side (this minimizes evaporation and maximizes amount of solution recovered).

- Spot 180 μl cells onto each of 4 dishes.

- Place dishes in incubator for 60-90 minutes to allow cells to adhere.

- Add 2.5 mL warm F-12.

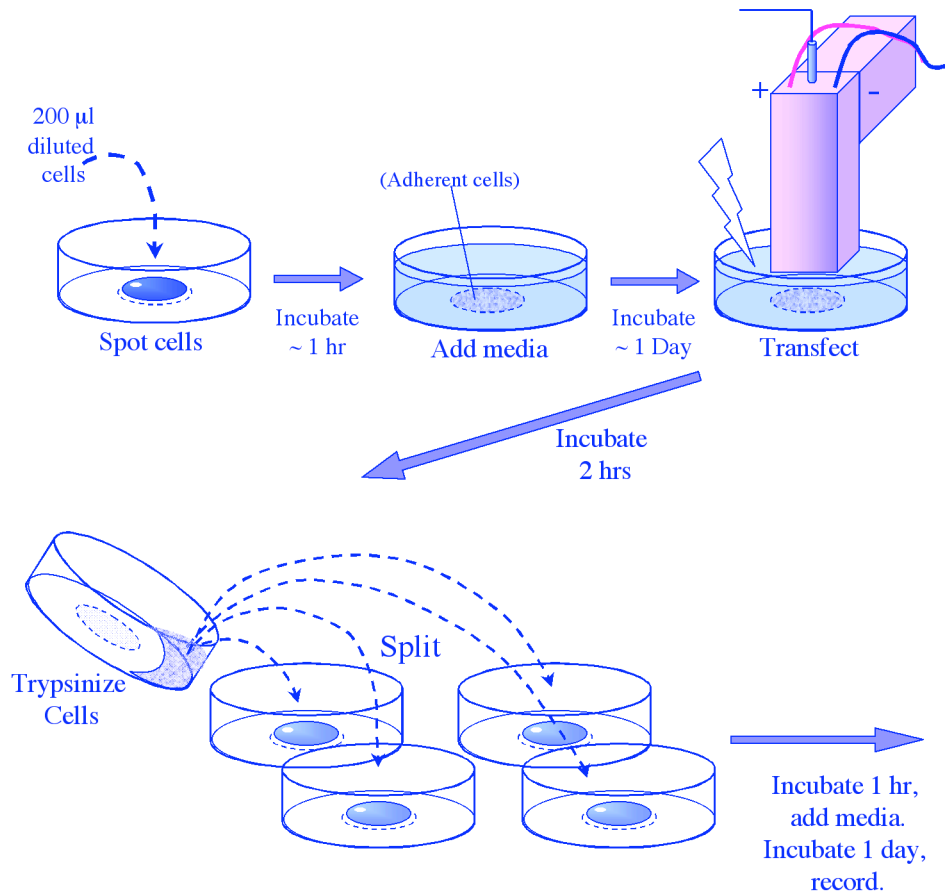Day 3: Record

- Replace media on the morning of recording.

Figure 4.8. Protocol developed to help minimize the quantity of valuable reagents used for each nonsense suppression experiment in mammalian cells. The number of dishes each transfection is split into can be varied.

Tissue Culture

CHO cells were grown in Ham's F12 media enriched with glutamine, 10% fetal bovine serum, penicillin, and streptomycin. The incubator was held at 37°C and 5% CO_2. 1 to 2 days prior to electroporation, cells were plated onto culture dishes such that confluency was 30%–50% at the time of transfection.

To minimize NMDAR-induced cytotoxicity after transfection:

- Antagonist and channel blocker were added to culture media:

    1 mM APV
    2 mM Mg^{2+}.

- Transfections were also optimized with reduced concentrations of NR2B.

Electrophysiology

Whole-cell recordings were performed on EGFP-expressing cells using an Axopatch 1-D amplifier. Cells were visualized using an inverted microscope and a GFP filter set with an excitation band pass of 450 to 490 nm, and an emission band pass of 500 to 550 nm. The setup is shown in figure 4.9. A patch-clamp pipette technique is used to gain electrical access to the cell. Patch electrodes were pulled to give a final resistance of 2-4 MΩ. The membrane potential was held at -60 mV. Once the correct compensation has been carried out, whole cell currents are recorded in voltage-clamp mode.
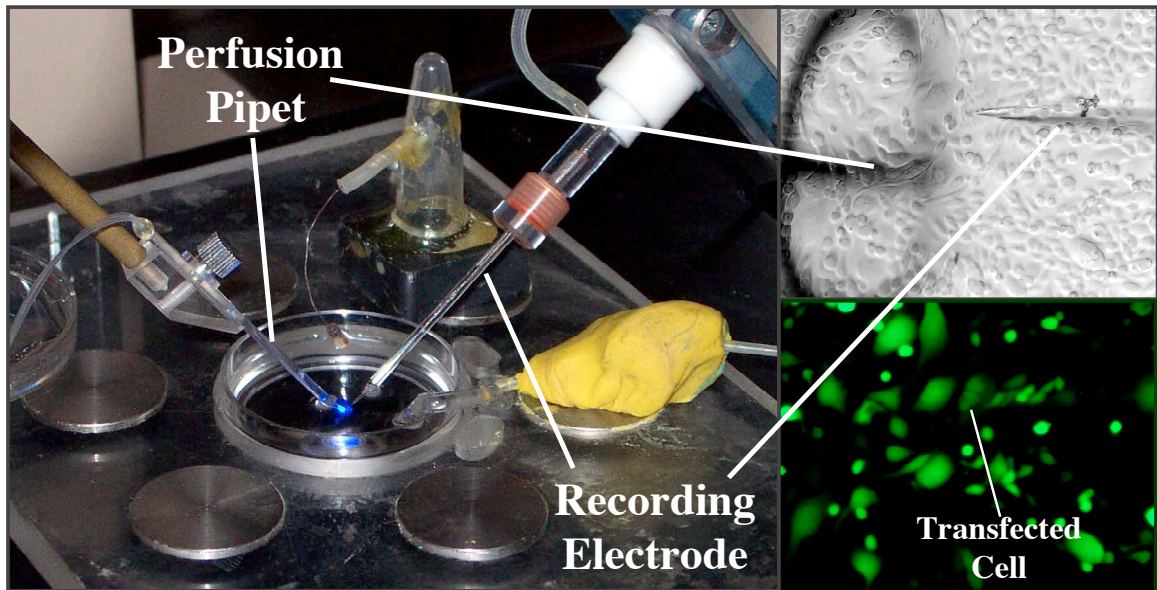
Figure 4.9. Setup for electrophysiology recoding of mammalian cells. Cells are patched with the recording electrode. The double-barreled perfusion pipette continuously passes solution over the cell. Brief movement of this pipette exposes the cell to the solution flowing from the other barrel, usually the solution containing agonist.

Solutions of glutamate, glycine and Mg^{2+} were delivered using a two-barrel glass theta tube connected to a peizoelectric translator. Each barrel is connected to a 12-way manifold, which allows up to 12 different solutions to be fed into either barrel. Agonists were usually applied for 1 second.

4.3 Results and Discussion

Optimization of NMDAR Expression

The goal of this project was to work towards the optimization of the nonsense suppression methodology in mammalian cells, and more specifically, to develop such methods using the NMDA receptor. To make this method accessible to our experiments, it must develop to the point where it is dependable, efficient, and minimizes tedium.

After a handle was gained on the technique of patch-clamp electrophysiology, we were able to observe glutamate-induced NMDAR currents in CHO cells, as well as the
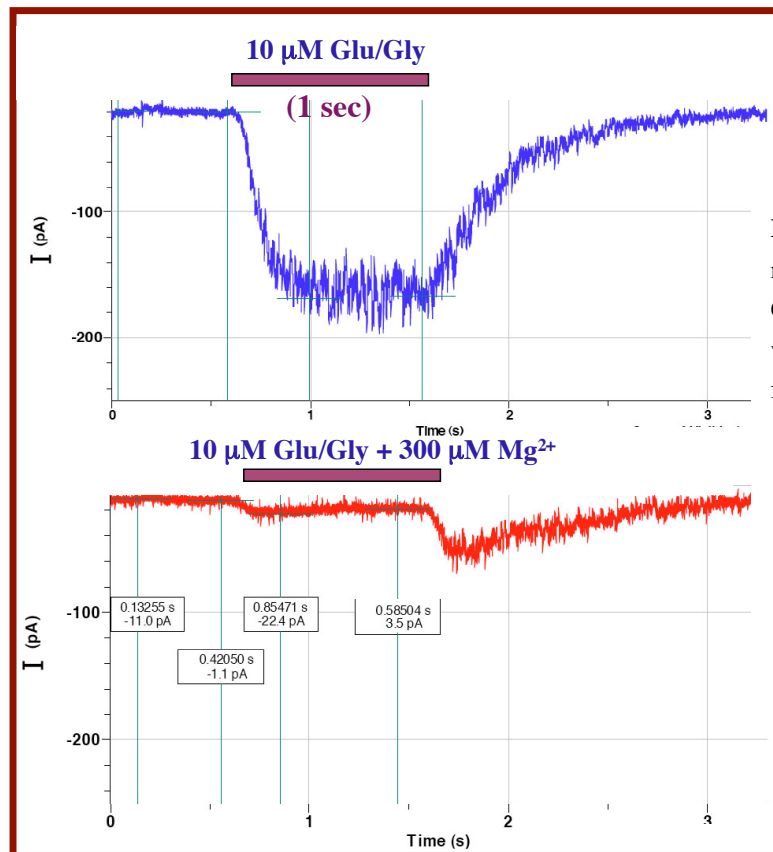

Figure 4.10. Mg^{2+} block recorded in CHO cells. Currents were ~200 pA, which is relatively low for our purposes.

effect of Mg^{2+} block (Figure 4.10). This was encouraging, but additional steps are needed to demonstrate efficient incorporation of unnatural amino acids. One difficulty we experienced working with this channel is its toxicity to cells. Figure 4.11 illustrates differences in cell health under different conditions and levels of NMDAR expression. We found that even in the presence of antagonist, high expression levels of this receptor caused cell death. Some of this is due to the receptor's permeability to calcium, and some of it seems to be due to the presence of the receptor itself. To reduce this toxicity, cells were incubated in high concentrations of Mg^{2+} and antagonist, and lower concentration of DNA were used in the transfection mix.
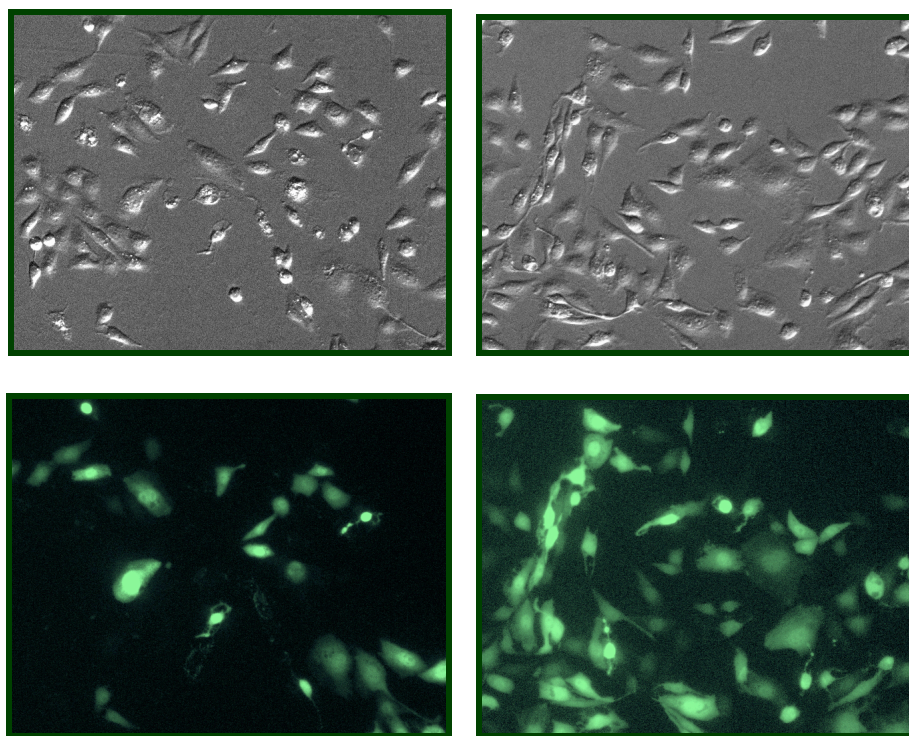

Figure 4.11. Transfection with smaller quantities of NMDAR DNA reduced cell toxicity and is notable by the higher percentage of surviving transfected cells. Bottom panels are the same field as upper panel but image GFP fluorescence. Left 2 panels: 4 µg NR1a/2B. Right 2 panels: 0.5 mg NR1a/2B.

Efficiency Optimization

One of the significant issues we would like to address is the excessive consumption of reagents. Aminoacylated tRNA is a stoichiometric reagent, and its production requires substantial investment of both time and money. When used for nonsense suppression in mammalian cells, this cost becomes a more significant consideration because transfection consumes up to 100 times more tRNA per recordable cell produced.

One source of this inefficiency is the nature of the transfection device and cell recording setup. Each electroporation performed on a dish of cells actually transfects more than 100 cells at the same time, but because the cells are adherent, they all remain on the dish during recording. Due to requirements of the experimental setup, the cells other than the one being recorded are unavoidably exposed to the agonist for an extended period and become unusable.

To address this issue, methods were explored that divided the population of transfected cells so that recording could be performed on multiple cells originating from the same transfection event. The method we developed that was most effective used special plating techniques to divide the transfected cells, but kept them at sufficient density to remain healthy and easy to detect and record from. This method is outlined above as the "Spot, Transfect, and Split Protocol" (figure 4.8).

The large difference in delivery efficiency between oocytes and mammalian cells is due to the completely different method used to deliver nucleic acid to the cells. While oocytes are injected with the nucleic acid mix directly, mammalian cells are subjected to electroporation while bathed in a solution of concentrated nucleic acid. Only a small fraction of the nucleic acid actually enters the cells during the electroporation step and the majority of the reagents are wasted.

This loss of reagent is difficult to address, while adhering to the standard electroporation device, but one method change was tested. We found that if the micropipette was aspirated very carefully, it could recover a significant amount of the nucleic acid solution, which could then be used in further transfections. Reuse of the solution produced visible fluorescence of the GFP marker in cells that had been transfected with solution that had been used in as many as four rounds of transfection. This suggests that significant quantities of DNA are carried over during subsequent transfections. However, GFP fluorescence is not a quantitative assay of transfection efficiency, so further studies would be useful to determine the effectiveness when using a stoichiometric reagent such as tRNA.

4.4 Conclusions and Future Directions

This report describes the development of techniques that successfully conserve the precious reagents used for nonsense suppression. While electroporation was found to be effective, improvements can still be made if we wish to approach the efficiency of the oocyte method. Other methods of transfection are also being considered that may further enhance the efficiency of our mammalian transfections.

Single cell electroporation is probably the most efficient method available because a very small volume of reagent is needed for each cell and little is wasted. The other advantage is the minimal disruption to the cell health and integrity. Electroporation is performed on adherent cells, which are robust. Additionally, only a small section of the membrane is exposed to the electric field. The disadvantage of this method is the tedious nature of the method, which requires working under a microscope and maneuvering the pipette to the cells one at a time.

Use of microfluidics is another method that could possibly be used effectively for transfection. This technique would allow cells and reagents to be mixed in small volumes before electroporation. Alternatively the system could be set up to allow for the electroporation of one cell at a time. If such a system could be implemented successfully, it has the potential to be the ideal solution.

Though improvements were made in the transfection and expression of NMDA receptors in CHO cells, robust and reproducible incorporation of unnatural amino acids was not demonstrated. In principle, this should be achievable once technical obstacles are overcome. Because recent work in oocytes has ruled out a cation-π at Trp 607, another site will need to be selected that can conclusively demonstrate unnatural incorporation in mammalian cells.

Possible Directions for the NMDA Receptor

There is now sufficient molecular data available to study agonist binding sites, channel gating, phosphorylation, Zn^{2+} inhibition, redox modulation, and nitric oxide modulation (14,15). Unnatural amino acid mutagenesis will be a very useful tool for these types of studies.

One powerful demonstration of unnatural amino acid utility would be the incorporation of photosensitive caged compounds that can undergo deprotection of the caged group to unmask a phosphate or a phosphorylation site. Such compounds would facilitate precise control of the phosphorylation state of the NMDAR, which is believed to be a significant modulatory mechanism of this receptor. These receptors have long intracellular C-termini, especially in NR2 subunits (15), and this domain is involved in linking intracellular signaling pathways to NMDA receptors by harboring kinase phosphorylation sites (15).

Using traditional biochemical methods, it would not be easy to isolate the effects

of each of the many phosphorylation states of these domains, but the caged molecules would give us a powerful tool with which to do this. They will allow us to control the phosphorylation state of specific sites on the receptor, and will also allow control over the time at which the phosphorylation and dephosphorylation events occur, giving us a $t = 0$. We can insert a caged phospho-amino acid, decage it using visible light, and measure the resulting change in activity or surface expression. Alternatively, we could begin with an amino acid protected from phosphorylation, decage it, and see if it is then phosphorylated by a kinase, and what effects this has on the system.

Figure 4.12. Photocleavable caged serine and phosphoserine.
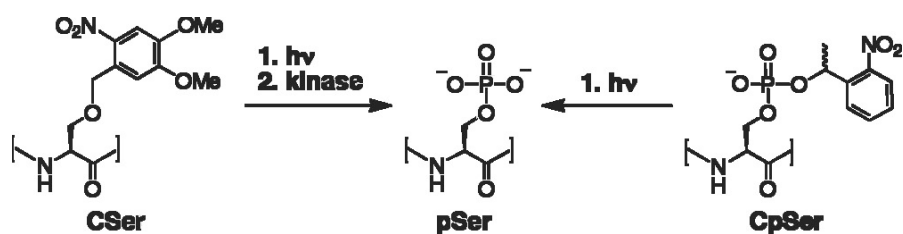
These experiments would require the use of a mammalian expression system, because the effects measured would be the result of cell-specific interactions. By not being limited to using the *Xenopus* oocyte system, we will be able to expand the study of structure-function relationships of proteins in cell-specific signaling cascades. Once fully developed, the techniques will permit the investigation of many more neuronal receptors, and we will be able to study them in the context of a more native environment.

4.5 References

1.	Beene, D. L., Dougherty, D. A., and Lester, H. A. (2003) *Curr Opin Neurobiol* **13**(3), 264-270

2.	Cornish, V. W., Benson, D. R., Altenbach, C. A., Hideg, K., Hubbell, W. L., and Schultz, P. G. (1994) *Proc Natl Acad Sci U S A* **91**(8), 2910-2914

3.	Dougherty, D. A. (2000) *Curr Opin Chem Biol* **4**(6), 645-652

4.	Steward, L. E., and Chamberlin, A. R. (1998) *Methods Mol Biol* **77**, 325-354

5.	Monahan, S. L., Lester, H. A., and Dougherty, D. A. (2003) *Chem Biol* **10**(6), 573-580

6.	Kleckner, N. W., and Dingledine, R. (1988) *Science* **241**(4867), 835-837

7.	Hill, B. (2001) *Ion Channels of Excitable Membranes*, 3rd Edition Ed., Sinauer Associates

8.	Gagliardi, R. J. (2000) *Arq Neuropsiquiatr* **58**(2B), 583-588

9.	Janardhan, V., and Qureshi, A. I. (2004) *Curr Cardiol Rep* **6**(2), 117-123

10.	McBain, C. J., and Mayer, M. L. (1994) *Physiol Rev* **74**(3), 723-760

11.	Mayer, M. L., Westbrook, G. L., and Guthrie, P. B. (1984) *Nature* **309**(5965), 261-263

12.	Nowak, L., Bregestovski, P., Ascher, P., Herbet, A., and Prochiantz, A. (1984) *Nature* **307**(5950), 462-465

13.	Kennedy, M. B. (2004) Personal Communication. In.

14.	Carroll, R. C., and Zukin, R. S. (2002) *Trends Neurosci* **25**(11), 571-577

15.	Dingledine, R., Borges, K., Bowie, D., and Traynelis, S. F. (1999) *Pharmacol Rev* **51**(1), 7-61

16.	Williams, K., Pahk, A. J., Kashiwagi, K., Masuko, T., Nguyen, N. D., and Igarashi, K. (1998) *Mol Pharmacol* **53**(5), 933-941

17.	Furukawa, H., and Gouaux, E. (2003) *Embo J* **22**(12), 2873-2885

18.	McMenimen, K. A. (2006) *Chem Biol* **1**(4), 227-234

19.	Moss, F. (2005) Personal Communication. In.